PROCESSING VERTICALLY ALIGNED CARBON NANOTUBES

FOR HEAT TRANSFER APPLICATIONS

A Thesis
Presented to
The Academic Faculty

by

Robert Cross

In Partial Fulfillment
of the Requirements for the Degree
Masters of Science in Mechanical Engineering in the
George W. Woodruff School of Mechanical Engineering

Georgia Institute of Technology
December 2008

PROCESSING VERTICALLY ALIGNED CARBON NANOTUBES

FOR HEAT TRANSFER APPLICATIONS

Approved by:

Dr. Samuel Graham, Advisor
School of Mechanical Engineering
Georgia Institute of Technology

Dr. Yogendra Joshi
School of Mechanical Engineering
Georgia Institute of Technology

Dr. Suman Das
School of Mechanical Engineering
Georgia Institute of Technology

Date Approved: August 4, 2008

ACKNOWLEDGEMENTS

I wish to express my sincere gratitude to my thesis advisor, Dr. Graham for all of his help and patience throughout my graduate studies. He taught me a great deal about conducting research and problem solving, and I know I am a better engineer because of him. I would also like to thank my other committee members, Dr. Joshi and Dr. Das for their guidance and expertise.

Next, I would like to thank my fellow graduate students for their sustained support and advice. One faces many challenges as a graduate student, both scholastic and personal. It was a tremendous asset to have a group of friends to lean on and confide. Specifically I would like to thank, in no particular order, Adam Christensen, Abe Greenstein, Thomas Beechem, Roderick Jackson, Minseok Ha, Namsu Kim, Carter Dietz, Fabian Goericke and Mark Gleva.

My family has also been a great help for me throughout my Georgia Tech career. I have been very lucky to have parents that are interested in my research and fantastic researchers in their own right. Their guidance has been priceless. My brothers, Richard and David, have helped me by being a great support system. Finally, I would like to thank my wife, Laura. Her unwavering support and encouragement has meant everything to me. I am so blessed to have such a smart and caring companion with whom to share my life.

TABLE OF CONTENTS

LIST OF TABLES

LIST OF FIGURES

SUMMARY

The development of wide band gap semiconductors for power and RF electronics as well as high power silicon microelectronics has pushed the need for advanced thermal management techniques to ensure device reliability. While many techniques to remove large heat fluxes from devices have been developed, fewer advancements have been made in the development of new materials which can be integrated into the packaging architecture. This is especially true in the development of thermal interface materials. Conventional solders are currently being used for interface materials in the most demanding applications, but have issues of high cost, long term reliability and inducing negative thermomechanical effects in active die.

Because of the mismatches in thermal expansion coefficients between the solder and semiconductors, large thermal stresses are created during operation. This, along with other manufacturing limitations such as surface wettability and internal voids (which act as large thermal resistors within the solder) creates a need for advanced material solutions. Carbon nanotubes have been suggested as a possible thermal interface material which can challenge solders because of their good thermal properties and 1-D structure which can enhance mechanical compliance between surfaces. Recently, experiments by several researchers have shown that a dense array of vertically aligned carbon nanotubes grown on silicon and copper substrates can provide thermal resistance values which are less than 20 mm^2K/W *[1-6]*. For perspective, with such a resistance, a 1 mm^2 device operating at 1 watt of power would increase in temperature 20 ºC. Comparatively, lead free solders on the market process thermal resistances from 7 to 28 mm^2K/W *[7]*. Figure 1 shows the thermal resistance values of common thermal interface materials and how current CNT thermal interfaces relate. Such resistance values make them attractive for

use in semiconductor devices. However, the direct growth of CNTs on microprocessors or bulk metal heat sinks make the implementation of this technology still a challenge of CNT integration. Moreover, the contact resistance between the CNTs and the parts to which they are attached control the overall thermal resistance of the CNT thermal interface material and must be addressed.

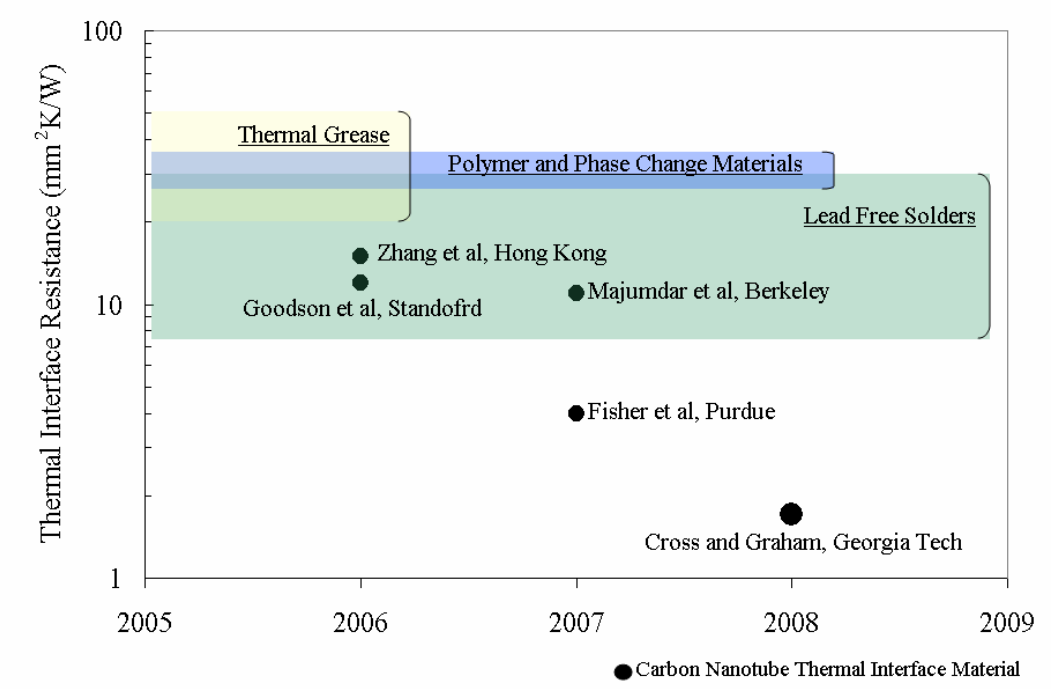

Figure 1. Outline of thermal resistances for market based thermal interface materials and vertically aligned CNT thermal interfaces *[2, 4-6]*.

In this work, we have developed a novel growth and transfer printing method to manufacture vertically aligned CNTs for thermal interface applications. This method follows the nanomaterial transfer printing methods pioneered in our research group over the past several years. The nanomaterial transfer process is attractive as it separates the high growth synthesis temperatures from the lower temperatures needed during device

integration. For this thesis, CNTs were grown using a standard process on oxidized Si substrates which allowed us to produce high quality vertically aligned CNTs with specific lengths. Through the development of a water vapor assisted etch process, which takes place immediately after CNT synthesis, control over the adhesion of the nanotubes to the growth surface was achieved. By controlling the adhesion we were able to demonstrate the capability to transfer arrays of vertically aligned CNTs to polyimide tape. The CNTs were then printed onto substrates like Si and Cu using a unique gold bonding process. The thermal resistances of the CNTs and the bonded interfaces were measured using the photoacoustic method, and the strength of the CNT interface was measured through tensile tests. Finally, the heat dissipation capabilities of the vertically aligned CNTs were demonstrated through incorporation with high brightness LEDs. A comparison of LED junction temperatures for devices using a CNT and lead free solder thermal interface was made.

CHAPTER 1

INTRODUCTION

Motivation of Research

For more than a decade, carbon nanotubes (CNTs) have received much attention from the scientific world. Since their discovery in 1991 *[8]*, CNTs have shown extraordinary thermal, electrical, and mechanical properties *[9, 10]*. However, limitations with performance in bulk materials, manufacturing, handling, and cost have stalled their introduction into consumer microelectronics. The microelectronics industry has consistently been striving for faster and more powerful devices with greater functionality. Albeit, such devices often come at the cost of higher heat generation density and the potential for higher operational temperatures. With these trends comes the need to improve the thermal transport within the system to ensure device reliability. The motivation of this research is to investigate the effectiveness of carbon nanotubes as a thermal interface material from a manufacturing and performance perspective.

Microelectronics Cooling

Development of wide band gap semiconductors such as gallium nitride (GaN) and silicon carbide (SiC) for power and RF applications have propelled the need for advanced thermal management techniques. These materials are being used in such high power applications because of their ability to handle higher switching frequencies and higher junction temperatures. Additionally, silicon based microelectronic devices are being used in multiple core and higher power applications. In each case, thermal management is crucial to ensure device reliability. Trends toward multiple core modules (MCM) have increased the heat fluxes produced to levels above 50 W/cm^2. Asymmetric hotspots in some dual core processors have been predicted as high as 1500 W/cm^2 *[11]*. With such

high heat fluxes, increases in thermal resistance of 1 mm^2K/W can cause the hot spot temperature to increase 15 degrees.

Thermal interface materials (TIM) bridge the gap thermally and mechanically between a heat producing element and a heat spreader or heat sink. The thermal resistance of the TIM is a function of its contact resistance with the two surfaces, its thermal conductivity, and thickness. Conventional interface materials in use today include solders, thermal greases, thermal pads, polymer composites, and phase change materials. Thermal greases and pads are most often used between heat spreaders and heat sinks because of their re-workability and the large contact area. These materials may not be suitable for direct chip contact because of their low conductivity and susceptibility to pump out. For high-performance devices, metallic alloys such as solders are used as the thermal interface to the heat spreader because of their high thermal conductivity *[12]*. Challenges with surface wetting, unintended voids formed during the reflow process, and mechanical durability exist with solders. Solder selection can also be a laborious exercise when considering a bevy of specific properties. Additionally, the movement toward lead free solders for environmental reasons has thrown another level of complexity into the process. Thermal resistances for lead-free solder interfaces can range from 7 mm^2K/W for pure indium, to 28 mm^2K/W for a tin/bismuth combination *[7]*. However, such lead free solders with low melting point temperatures are difficult to handle in that they are susceptible to oxidation and have poor retention of mechanical properties. These solders, which melt at temperatures below 200°C (156.7°C for pure indium) also operate at high homologous temperatures ($T_{operational}/T_{melt}$). Operation at high homologous temperatures is associated with fast diffusion kinetics and many changes in the material which makes their stability and long term durability an issue. On the other, polymer TIMs may be desired because of cost and simplicity of implementation. Polymer interfaces, aside from being less thermally conductive than solder, can also degrade over time due to high temperatures. Thus, most polymer based TIMs can not address the most critical TIM

applications near the die level where the highest heat fluxes exists. In general, the increase in device performance and power has pushed the electronics industry to primarily consider solder based TIMs for the most critical applications, although, with much caution due to long term reliability concerns.

A need for newer advance material solutions is evident to address the challenges presented by current day TIM materials. A material with high conductivity and conformity that is easily integrated is required. Vertically aligned carbon nanotube arrays have shown measured conductivities greater than 70 W/mK *[1]* which is greater than typical solders of today *[13]*. However, overall thermal resistances for CNT interfaces of 15 mm^2W/K have been observed; greater than some commercially available solders *[14]*. The higher resistance values for CNT thermal interfaces can be attributed to the contact resistances between the tips of the CNTs and the mating surfaces. The mechanical integrity of the bond between the CNTs and the mating surface is critical for lowering contact resistance. The typical thermal path that will be referenced in this study is depicted in Figure 2.

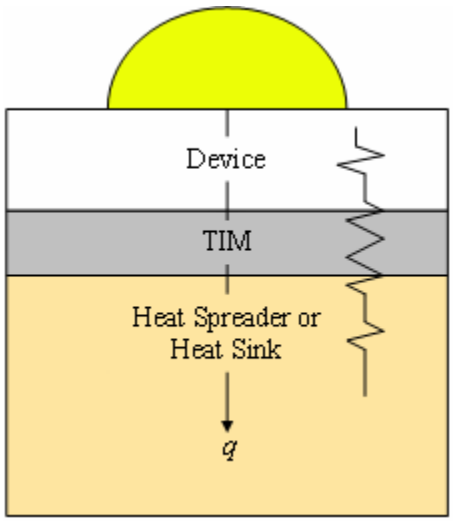

Figure 2. Schematic for a typical thermal path of device to heat sink has several thermal resistances to take into account.

To address the issue of CNT bond strength, one of two paths can be taken; direct synthesis onto the device or heat spreader, or transfer onto these surfaces. Achieving substantial adhesion between the CNTs and the growth surface is commonly done by employing sublayers on which the CNT catalyst can adhere. However, direct growth of CNTs onto heat spreading materials such as bulk copper can be quite difficult and complicated. Furthermore, because of high synthesis temperatures, growth onto the device or other precious materials could be detrimental. For these reasons transfer techniques are being researched. Currently, CNT transfer has only been accomplished with the aid of an adhesive filler material. Transfer printing of vertically aligned CNTs into thermal adhesives, solders, and polymers has been accomplished *[15-25]*. These composites have shown relatively significant increases in thermal conductivity. However, the introduction of CNTs has not adequately addressed their respective thermal interface challenges. Publications concerning the transfer of vertically aligned CNTs without the assistance of a filler material has been scarce. Chai et. al. has published a technique in which the oxide sublayer of the growth surface is etched away leaving behind the vertically aligned CNT array *[26]*. This technique has not demonstrated the ability to transfer the tubes to another surface with any meaningful adhesion. Therefore, a procedure for transferring CNT with good adhesion to foreign surfaces would be a tremendous contribution.

Initial results are promising for future exploration into the role of CNTs as high performance thermal interfaces. The ability to transfer patterned CNT arrays with controlled properties onto other materials could prove to be a tremendous advantage in stabilizing hotspots. In order for CNTs to be a viable interface material strides must be made to reduce interface resistance, and reliable printing techniques must be developed.

Carbon Nanotube Synthesis

For CNTs to be an effective thermal interface material, bond line thickness, thermal conductivity, and contact resistance must be considered. Each of these properties can be addressed through specific growth techniques. Bond line thickness (length of the CNTs) and thermal conductivity of the CNT array can be controlled through adjustments in growth parameters. For this study, thermal CVD was used instead of other synthesis methods such as arc discharge and laser ablation because of its low cost, simplicity and flexibility *[9]*. Such apparatuses can be created using common lab equipment and the process is easily scaled up for higher production quantities. Variations in precursor flow rates, catalyst composition, and temperature can yield carbon nanotubes with a myriad of different properties such as diameter, length, purity, and adhesion to the substrate. Since the primary heat transfer pathway of CNTs is down the axis of the tubes, this makes the thermal conductivity highly anisotropic *[27, 28]*. Thus, the alignment of the tubes is critical for thermal transport. Vertically aligned CNT arrays have been produced using many different catalysts and CVD techniques *[15, 27, 29-34]*. Vertical alignment can be created with the assistance of an electric field *[35]*, or naturally by the van der Waals forces between the tubes. These intermolecular forces elicit globally aligned structure with shorter range entanglements when there is a high density of catalyst. Carbon nanotubes synthesized with a free floating catalyst fail to have such an alignment.

One aspect which must be considered in either the direct growth or transfer of CNT TIMs to other substrates is the adhesion between the CNTs and the growth substrate. Adhesion of the CNTs can be changed based on the catalyst and sublayer combinations or through transfer. The adhesion of the nanotubes to the growth substrate is a combination of the catalyst/substrate and catalyst/CNT interactions. Thin films of titanium or titanium and aluminum beneath the catalyst layer are often used to increase catalyst/substrate adhesion. On the other hand, using Fe particles provides relatively weak adhesion which can assist in CNT transfer during printing processes.

Another area of concern is the high CNT synthesis temperatures (>700 ºC) which can prevent direct growth onto sensitive microelectronic devices. Efforts have been made to produce nanotubes at low temperatures *[36]*. However, at lower temperatures the quality of the tubes is compromised. Also, the direct growth of CNTs onto bulk copper and other heat spreading materials has proven very difficult.

In order to circumvent the issues with high processing temperature, transfer techniques must be developed. For transfer to take place, the adhesion of the CNTs to the growth surface must be addressed. Neglecting adhesive sublayers such as titanium is often done to produce CNTs with weak substrate adhesion. Water vapor or H_2O_2 etching has often been used for the synthesis of long stacks of vertically aligned CNTs *[33, 34, 37]*. In addition to weakening the CNT/catalyst interface, this technique also eliminates the end caps of the CNTs and helps remove unreacted amorphous carbon *[34]*. With these tactics in mind, vertically aligned CNT arrays with weak growth substrate adhesion can be produced.

As previously discussed, several procedures have been developed to transfer CNTs to other surfaces, but most employ the assistance of a filler material. Techniques that do not use a filler *[26]* have been shown to have fairly weak adhesion. Methods must be developed to directly transfer vertically aligned CNTs to other surfaces with a secure mechanical connection.

Thesis Overview

The goal of this study was to develop synthesis and transfer procedures to facilitate the integration of carbon nanotubes into microelectronics. Specifically, this work addressed the following:

- Repeatable growth of CNTs with controlled lengths
- Decreasing the adhesion between the CNTs and growth surface in order to facilitate transfer

- Transferring vertically aligned CNT arrays to polyimide tape for storage purposes
- Bonding vertically aligned CNT arrays to semiconducting and heat spreading surfaces to produce a thermal interface material with low thermal resistance and excellent mechanical strength

Chapter 2 discusses the background behind the thermal challenges facing microelectronic devices. It includes details concerning the state of heat fluxes being generated and an in depth breakdown of the thermal interface materials currently being used. Chapter 3 dives into the background of carbon nanotubes. Structural, electrical, mechanical and thermal properties are discussed. Additionally, thermal measurement techniques, printing methods, and their role in TIMs are outlined. Chapter 4 details the experiments and results conducted in an effort to grow and transfer vertically aligned CNTs with strong adhesion. Chapter 5 discusses the thermal measurements of the CNT interfaces using a photoacoustic method and their affect on LED junction temperature. Finally, Chapter 6 concludes the study and proposes future work to further develop this technology.

CHAPTER 2

BACKGROUND OF THERMAL CHALLENGES FACING MICROELECTRONIC DEVICES

The desire consumers have for faster and more powerful microelectronic devices with increased functionality is undeniable. Sales in personal computers, cellular phones, and music listening devices such as mp3 players and ipods have exploded over the past 15 years. Each of these technologies has become increasingly popular because of their performance and accessibility. Exemplifying the boost in popularity for consumer electronics are cellular phones. According to the Gartner Group, annual cellular phone sales are expected to reach 1 billion by 2009. With sales of such magnitudes, vendors such as Nokia and Samsung are predicted to reach combined revenues of over $1.7 billion dollars.

The Pentium processor is a prototypical example of the trends toward smaller, faster and more powerful devices. With each evolution of the Pentium chip, (386, 486, Pentium I, Pentium II, etc.) the power and speed has increased exponentially. In 2007, the Intel Core 2 chip was released, boasting a seven times increase in number of transistors and 70% the size of the 2002 edition of the Pentium 4 *[38]*. Figure 3 is a chart of the upward trends in power density over the past 20 years.

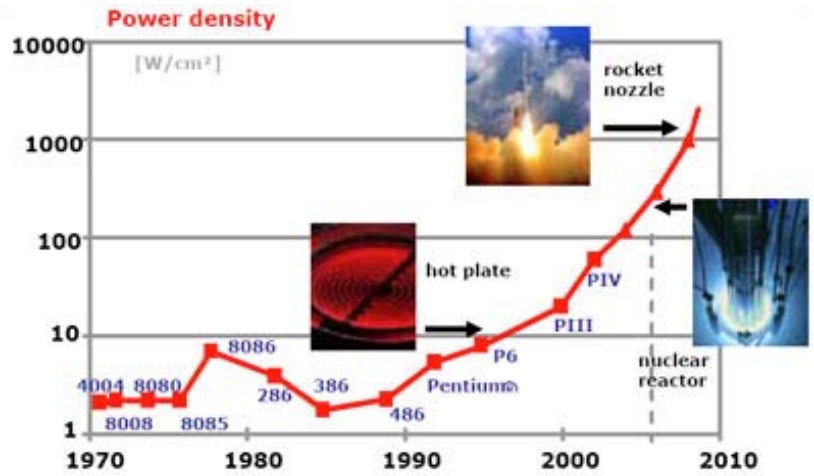

Figure 3. Trend in power densities for microelectronic devices is rapid increasing (Intel) *[39]*.

Because of basic physical limitations, the trend as predicted by Moore's Law of number of transistors in a given area cannot perpetuate. Therefore, a transition toward multiple core modules (MCM) is underway. MCMs such as the Intel Core 2 Extreme QX9650 Quad Core Processor have 4 cores and operating powers of 130W, but a maximum operating temperature of 64.5 ºC. Other companies such as IBM, AMD, and Fujitsu are also developing and marketing MCMs for personal computing and server applications.

Light emitting diodes are receiving an increased amount of attention because of their potential to replace fluorescent and incandescent lighting. LEDs have superior efficiency and operating lifetimes to conventional light sources used today. Currently, solid state lighting outperforms incandescent and fluorescent lighting in most metrics except for cost. The standard for high brightness LEDs today are a 1mm^2 die producing between one and three watts, or a 4 mm^2 die producing 5 watts. According to such specifications, HB-LEDs can produce heat fluxes as high as 300 W/cm^2. Figure 4 is the roadmap for SSL-LED technology as introduced by the Department of Energy in 2002 which as of 2008 is on schedule.

TECHNOLOGY	SSL-LED 2002	SSL-LED 2007	SSL-LED 2012	SSL-LED 2020	Incande-scent	Fluore-scent
Luminous Efficacy (lm/W)	25	75	150	200	16	85
Lifetime (hr)	20,000	>20,000	>100,000	>100,000	1,000	10,000
Flux (lm/lamp)	25	200	1,000	1,500	1,200	3,400
Input Power (W/lamp)	1	2.7	6.7	7.5	75	40
Lumens Cost ($/klm)	200	20	<5	<2	0.4	1.5
Lamp Cost ($/lamp)	5	<5	<5	<3	0.5	5
Color Rendering Index (CRI)	75	80	>80	>80	95	75

Figure 4. DOE roadmap for SSL-LED technology published in 2002.

With these drastic increases in power density come substantial increases in unwanted heat, specifically local hot spots. The life time and performance of a device, as described by the Arrhenius relationship, is adversely effected by increasing temperature. This relationship states that the mean time to failure (*MTF*) of a electronic device can be described in the following equation

$$MTF = MTF_{ref} e^{E/K_B T} \tag{1}$$

where MTF_{ref} is the reference mean time to failure, E is the device activation energy (eV), K_B is the botzman constant, and T is the steady state temperature *[40]*.

Thermal management solutions have been focused in several areas. Thermal conductivity of the semiconducting layer could be increased to facilitate heat transfer to the surface. However, with this methodology compromises must be made between electrical performance, thermal performance, and cost. Wide band gap semiconductors such as GaN and SiC (thermal conductivity ~180 W/mK *[41]* and 340 W/mK respectively) are being developed for power electronics applications. However, silicon is firmly entrenched as the market standard for semiconductors in conventional microelectronics, and a wholesale replacement would be incredibly expensive and impractical.

Heat removal technologies as shown in Figure 5, such as heat pipes, thermo-electric coolers, water cooling solutions, and refrigerant systems, are continually being

developed to address the issue of heat removal. These systems are more effective when a large heat flux between the source and the ambient is applied. If the thermal resistance between the device and the heat sink is too high, the temperature seen by the heat sink will be close to the ambient. In this case, even the most expensive heat sinks and fan combinations can be rendered ineffective. Therefore, the thermal path, shown in Figure 6, from the source to the heat sink must have as little resistance as possible.

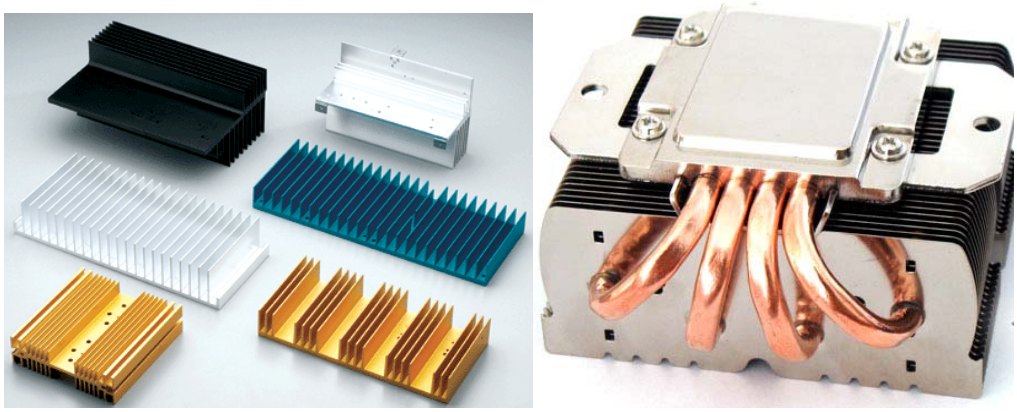

Figure 5. Examples of passive heat sinks (left) and actively cooled heat sink (right) such as the OCZ Tempest CPU Cooler (OCZ Technologies).

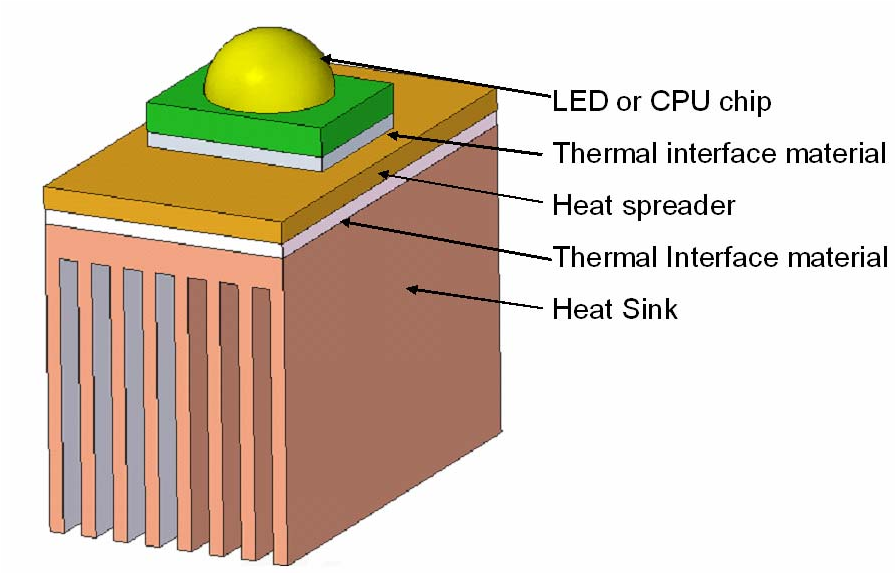

Figure 6. Typical schematic of thermal path for a microelectronic device.

The dominant form of heat transfer for LEDs and microelectronics is through conduction. Following the thermal path of an LED from the die, to the first thermal interface material, to the heat spreader, then to a second thermal interface material, and finally the heat sink, it becomes clear that significant resistance can form before the heat sink. Figure 7 is the result of a finite element analysis of a HB-LED with a thermal path similar to that in Figure 6. For this experiment a heat flux of 300 W/cm^2 was applied at the SiC die, and a convection coefficient of 70 W/m^{2}K was used. Examining the graph, the steepest drops in temperature occur in the thinnest regions of the thermal path. This reveals that the largest areas of thermal resistance exist at the thermal interface materials (Au-20Sn lead free solder). The thermal resistance in these layers is a function of the thermal conductivity (57 W/mK) of the material and its thickness (50 μm). The following relationship is used to quantify thermal resistance within a material

$$R_{material} = \frac{BLT}{k \cdot Area} \tag{2}$$

where *BLT* is the bond line thickness or thickness of the material, and *k* is the thermal conductivity of the material. Therefore, to decrease thermal resistance, thermal conductivity should be maximized while minimizing layer thickness.

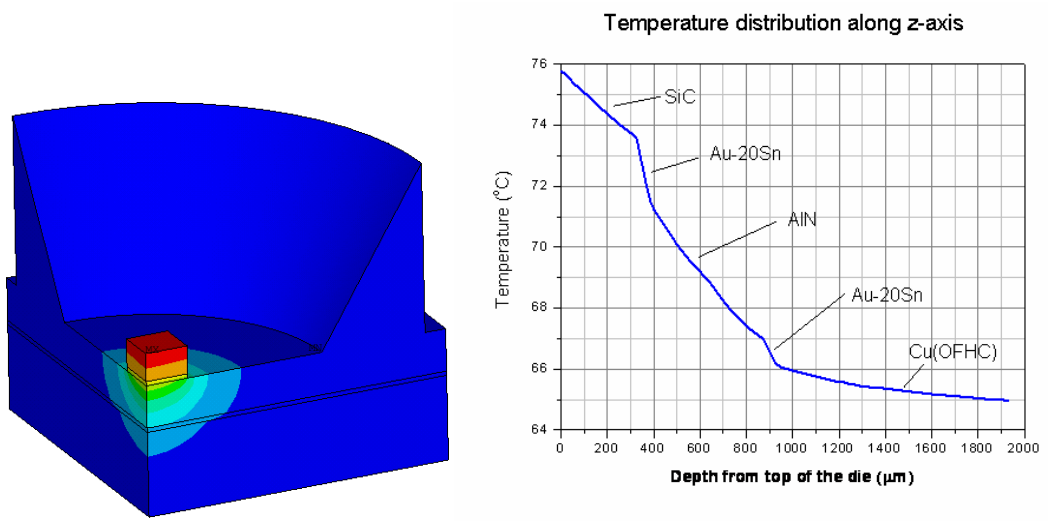

Figure 7. Thermal path from SiC die, solder TIM, aluminum nitride substrate, solder TIM, and copper heat sink.

A major contributor to thermal resistance, however, is the contact resistance between the TIM and the mating surfaces. Contact resistance is a result of imperfect mating between two rough surfaces *[42, 43]*. Small asperities are formed and therefore the area for conductive heat transfer is cut down. The regions void of material act like large thermal resistors and can be quite detrimental to the performance of the device. Figure 8 is an enlarged view of an physical interface between two imperfect materials.

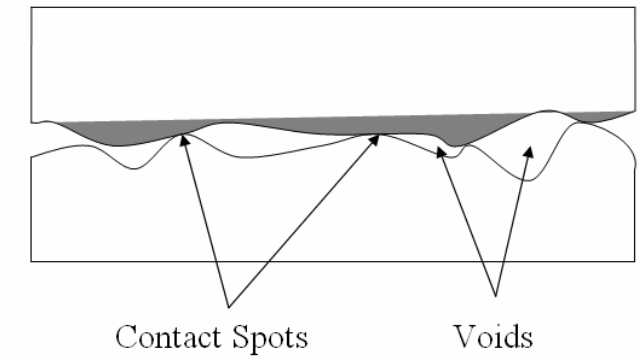

Figure 8. Enlarged view of an interface between two surfaces. Microgaps formed between the two surfaces act as thermal resistors.

When selecting a thermal interface material several considerations must be made. First is thermal conductivity. The conductivity of the material, as mentioned before, will help to characterize the resistance within the layer. In conjunction with thermal conductivity, reducing the thickness of the layer is important to decrease thermal resistance. With regards to contact resistance, the compliance of the interface material is of great interest. The TIM should have the ability to conform to imperfections of the mating surfaces to create more conducting paths. By conforming to the roughness of the mating surface, the voids (Figure 8) are filled with conductive material. In many cases to fill such gaps, pressure is applied to the joint. The thermal contact resistance responds proportionally to the inverse of applied pressure *[44]*. Therefore, more pressure leads to less contact resistance. Differences in thermal expansion coefficients between the package layers will induce an appreciable amount of stress in the interface and device. Silicon possesses a CTE of 2.6 x 10^{-6}/ ºC while most lead based solders have a CTE an order of magnitude higher. Reducing the discrepancy in CTE between joining materials will help to lower the shear stresses created during device operation.

The following sections will outline the different thermal interface materials currently being employed and how each addresses the previously listed considerations.

Thermal Interface Materials

Polymer and Phase Change Materials

The ability of a thermal interface material to conform to the undulations of a mating surface is paramount to limiting air pockets in the interface. These pockets of air (k=0.0285 W/mK at 60 ºC *[42]*) act like resistors in the thermal circuit. Phase change materials (PCM) have the ability to change from a solid to a liquid state with an increase in temperature. Specific materials that are chosen have liquidus temperatures at or around the operating temperature of the device. By transforming to a liquid, the interface

material gains the ability to fill the areas of the interface that are not in direct contact. Furthermore, the absorption of the latent heat of fusion throughout the melting process provides another form of heat dissipation *[45]*. Some PCMs being used today are polyolefins, polyesters, paraffin wax, and acrylics *[46, 47]*. PCM are an attractive alternative to greases or gels because they can be applied easily to a surface. As a film, these materials can be cut and patterned to fit the desired region. The ability to apply and reapply these materials is also an attractive attribute. Commonly used PCMs on the market today, such as Chromerics T725 and Berquist HiFlow, have thermal resistance values between 25 and 32 mm^2K/W, as shown in Table 1.

Sacrifices in material thermal conductivity must be made to use current phase change materials. To increase the conductivity of organic phase change materials, inorganic fillers such as boron nitride (BN), carbon, alumina (Al_2O_3), and zinc oxide (ZnO) can be used *[45]*. The particulate fillers do not change phase, but will effect the thermal capacitance and liquidus temperature of the material *[48]*. Organic polymers such as silicone (polydimethylsiloxane) *[49]* and polymethylmethacrylate (PMMA) *[50]* have been used in conjunction with the aforementioned conductive particles to form thermal interface materials with increased thermal conductivity. The volume percentage of conductive particles is called the loading of the matrix.

In addition to low conductivity (0.5-1 W/mK *[46]*), PCMs have issues with migration while in the liquid phase. Similar to thermal greases, thermally induced expansions can cause the interface material to be evacuated from junction. To reduce these effects, the wetting of the material can be controlled by introducing wetting and coupling agents. Mesh materials and adhesive tapes have also been employed to alleviate the migration issue, but the stresses translated to the die with these solutions can not be ignored *[46]*.

Thermal Grease

Thermal greases are typically comprised of silicone oil and particulate filler materials such as ceramics like ZnO, or more recently metallics like silver. While relatively inexpensive, thermal greases offer good wetting ability and conformability. Thermal greases can be used on any surface with direct application. Furthermore, post processing is unnecessary. The bulk thermal conductivity of thermal greases is typically around 3-5 W/mK which is quite competitive with other similar materials that do not require curing *[46]*. The conductivity of the grease is positively correlated with increasing loading percentages of filler material. Typical bond line thicknesses of thermal greases are between 25 and 50 microns.

The reliability of thermal greases under cyclic loading is a concern. Temperature cycling, which induces substantial stress to the interface because of CTE discrepancies between the mating materials, can cause grease migration. Grease migration, also known as pump out, occurs when the interface material is expelled from the junction. This drastically reduces the effectiveness of the interface and may cause device failure. Pump out is a phenomenon dependent on mechanical stresses, package geometry, and material chemistry *[51]*.

With consideration to these advantages and limitations, thermal greases are typically employed in low performance systems. High bulk thermal conductivity, conformability, and ability to be reworked make thermal greases an attractive solution as TIMs between heat spreaders and heat sinks, or other interfaces with large contact areas. But insufficient adhesion and the issue of pump out make thermal greases less apt for direct device contact.

Table 1. Manufacture specifications of commonly used thermal greases and PCMs *[51]*.

	R_{int} cm^{2}K/W	Pressure MPa	Conductivity W/mK
Thermal Grease			
Arctic Silver	0.018	0.083	4.50
ShinEtsu G751	0.101	-	2.89
Berquist TIC-7500	0.226	-	7.50
Phase Change Materials (PCM)			
Chromerics T725	0.258	0.345	0.60
Berquist HiFlow	0.323	0.276	1.00
Berquist 200U	0.258	0.069	1.60

Solder

Solders are used as thermal interface materials because of their high thermal conductivity and the strong mechanical bond they form. Because of environmental concerns, a shift to lead free solders is underway. Lead free solders, such has SAC (tin/silver/copper), SnBi, SnAg, SnCu have thermal conductivities on the order of 30-50 W/mK *[7, 14]* which is much greater than other TIMs previously discussed. High thermal conductivity and superior adhesion make solder interfaces an attractive solution for thermal management. However, solder selection can be a very difficult and tedious process. Factors such as thermal conductivity, mechanical properties (tensile strength, shear strength, and coefficient of thermal expansion), and wettability must be considered. CTE mismatches of an order of magnitude between semiconducting and electronic materials and lead free solders can lead to significant shear stress during operation. Most lead free solders have CTEs on the order of 2 x 10^{-5}/ºC

Another category of solder is the low melt alloys that have considerably low thermal resistances *[13, 52]*. LMAs typically consist of combinations of Ga, In, Bi, and Sn to name of few. Resistance values for LMAs range from 1.5 to 6 mm^{2}K/W *[52]*. Such low values for LMAs are very attractive, but significant deficiencies in reliability

caused by oxidation/corrosion, intermetallic formation, drip-out, or dewetting make them difficult to employ. Figure 9 shows a comparison of thermal resistances for several categories of thermal interface materials including LMAs. Resistance values for several (lead based and lead free) solders are outlined in Table 2.

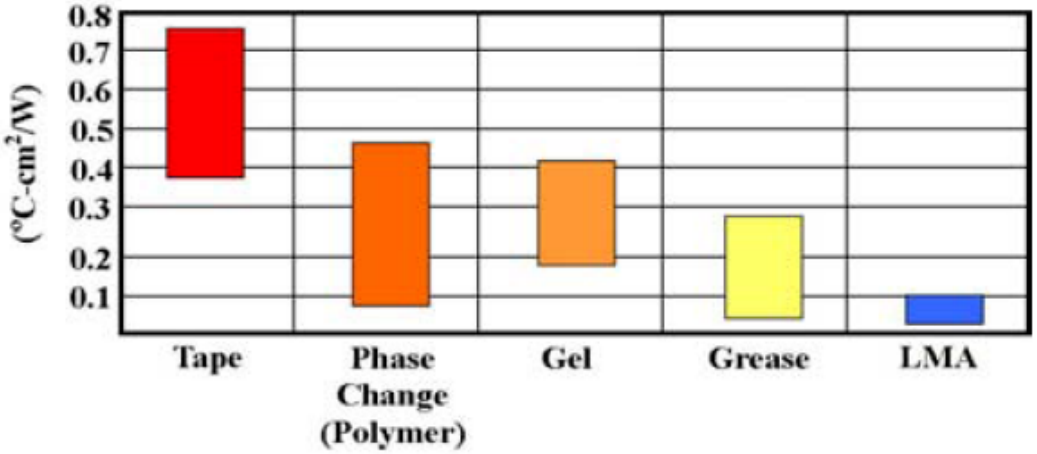

Figure 9. Comparison of thermal resistance for several thermal interface material categories *[52]*.

Solders, above all other TIMs discussed, provide the best mechanical connection as well as the highest thermal conductivity. Limitations of solder thermal interfaces include stress due to thermal cycling and voids in the interface layer. The shear stresses observed by the solder as a result of different expansion rates of the mating surfaces must be considered *[53]*. The drastic discrepancy between the CTEs of semiconducting materials and lead free solders is illustrated in Table 2. Finite element analyses of heat producing SiC on Sn – 3.5Ag solder have provided insight to the operating stress levels in the device. Studies conducted at the Naval Research Laboratory have produced models of a 380 μm SiC die attached with 50 μm of Sn – 3.5Ag solder to a two part closed channel copper cooler *[54]*. Operating stresses as high as 240 MPa were observed in the SiC at the solder interface (Figure 10).

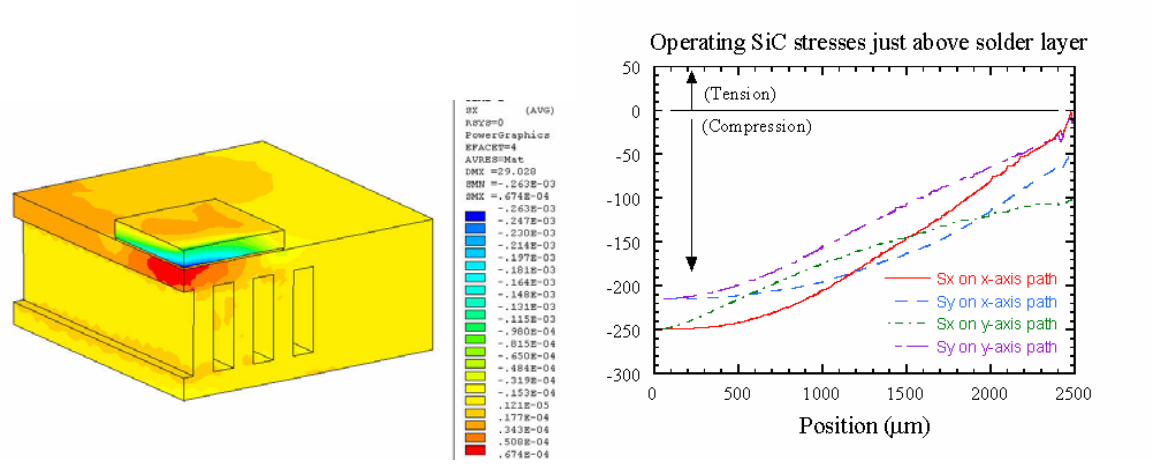

Figure 10. Finite element anaylsis of operating stress in SiC device attached to a copper heat sink with a 50 μm thick layer of Sn – 3.5Ag solder *[54]*.

Table 2. Coefficients of thermal expansion and thermal conductivities for semiconducting and lead free solder materials *[7, 14]*.

Material	CTE ($x10^{-6}$/K)	Thermal Conductivity (W/mK)	Thermal Resistance (mm^2K/W)
Lead free Solders			
Bi-42 Sn	15	21	28.4
In-48 Sn	20	34	16.5
Sn-3.5 Ag	22	33	7.5
In	33	84	7.6
Semiconductor and Electronic Materials			
Si	2.6	150	
SiC	4.3	385	
GaN	3.2	225	
Cu	16	400	
Au	14.4	301	

For applications where high stresses may occur, a soft solder such as Au/Sn would be acceptable. Bismuth solders tend to be more brittle and have lower thermal conductivity, but offer significantly lower reflow temperatures (140 ºC EFD Inc.) which is attractive for devices with increased temperature sensitivity. Voids are areas within the solder film where no material exists. They are created by shrinkage of the solder during

the solidification phase *[53, 55]*. These zones create a large amount of thermal resistance, as is expected, but because of the solid state of the solder, they do not propagate due to pump out or migration. Moreover, they can have devastating effects on bond strength. These voids can be eliminated with an iterative reflow process.

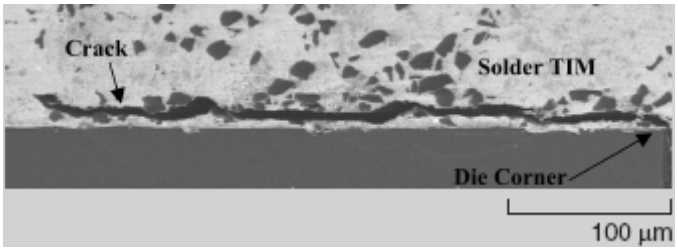

Figure 11. Crack formation of solder thermal interface material at the corner of a die *[56]*.

The ability of the solder to wet a surface is of critical importance. The oxide layer that inherently forms around the reflowed solder can be difficult to penetrate without the proper surface chemistry. Many solders will wet gold or copper surfaces, but this material property is not the same for each solder mixture. Lead free solders have a higher surface tension than lead based solders which creates difficulties in wettability and spreadability *[57, 58]*. In cases where the solder is unable to wet the substrate a flux may be used. The purpose of the solder flux is to remove oxides from the substrate, and prevent reoxidation of the solder and substrate during reflow *[59]*.

Understanding the current state of microelectronics and the trend toward increasing power density, the issue of thermal management is of great importance. The reliability of the device is predicated on the ability of the system to remove heat from the local hot spots. It has been shown that the effectiveness of a heat sink, regardless of size and cost, is directly related to the ability of the thermal interface material to facilitate heat transfer away from the device. Reduction in thermal interface resistance by increasing

TIM conductivity, decreasing bond line thickness, and reducing contact resistance remains a common goal for all microsystems engineers. The following chapter focuses on the properties, synthesis, characterization, and manufacturing techniques of carbon nanotubes. Furthermore, the state of carbon nanotubes as a TIM is discussed.

CHAPTER 3

BACKGROUND AND LITERATURE REVIEW OF CARBON NANOTUBES

Carbon Nanotube Properties

Structure

Carbon can take several crystalline forms as shown by the phenomenon of electronic hybridization *[60]*. Each crystalline form; diamonds, graphites, carbines, and fullerenes/nanotubes, have different electrical, thermal, and mechanical properties. The bonds formed in CNTs are essentially sp^2, similar to graphite, but the π orbital is more delocalized outside of the tube. This structure makes the CNT more electrically and thermally conductive, and mechanically stronger *[10]*.

Table 3. Classification information for the different forms of carbon *[60]*.

Crystalline Form	Diamonds	Graphites	Carbynes*	Fullerenes, Nanotubes
Hybridization	sp^3	sp^2	sp^1	$sp^{2+\epsilon}$
Coordinance z	4	3	2	3
Physical dimensionality D	3	2	1	0 and 1
Bond length (Å)	1.54	1.40	1.21	1.33 to 1.40
Bond energy (eV/mole)	15	25	35	> 25

* Also mixed sp^1 and sp^3 hybridizations (α form)

Single wall carbon nanotubes (SWNT) are seamless cylinders of graphene sheets and are considered to be one dimensional systems. When the graphene sheet is rolled into the tube, a chirality is induced which can be described by a set of (n, m) integers. These integers form the chiral vector. Three forms of nanotubes, chiral (n, m), armchair

(*n*, *n*), and zig zag (*n*,0), can be formed based on the chirality of the tube. Figure 12 shows a schematic of a graphene sheet which is rolled to form a SWNT. The chirality determines the structure and electrical properties of the individual tubes *[10]*. The ability to grow single wall carbon nanotubes with controlled chirality has not been achieved. However, recent studies has demonstrated the capability to separate SWNT based on their electronic behavior and diameter through processes such as selective chemistry, selective destruction, electrophoretic separation, chromatography, and ultracentrifugation *[61]*.

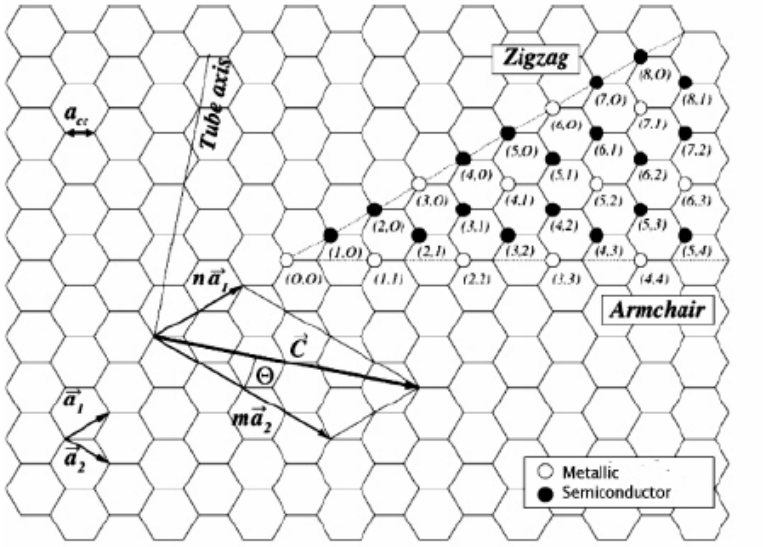

Figure 12. Chiral vector schematic taken from *[62]*.

In addition to SWNT, other forms of CNTs such as double-walled carbon nanotubes (DWNT) and multi-walled carbon nanotubes (MWNT) exist. As their names suggest, these derivatives have multiple coaxial single wall tubes comprising their structure. Diameter ranges for SWNT, DWNT, and MWNT are 0.4 - 4 nm, 2 – 5 nm, and 5 – 100 nm respectively. SWNT as long as 4 cm (Figure 13) have been grown *[63]*.

Vertically aligned arrays of MWNT have been grown to lengths exceeding 4 mm (Figure 14) at the University of Cincinnati (Shulz et. al.).

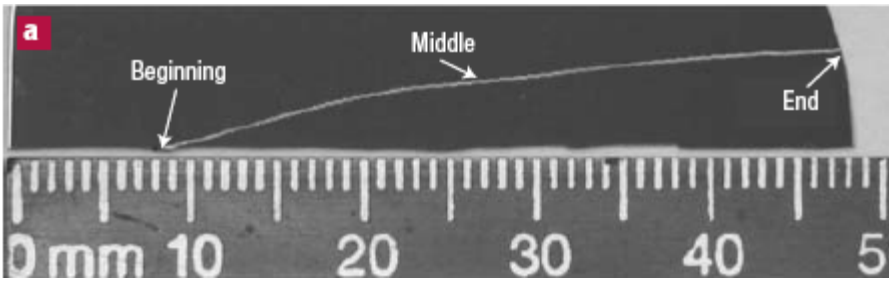

Figure 13. 4 cm long SWNT synthesized using catalytic chemical vapor deposition *[63]*.

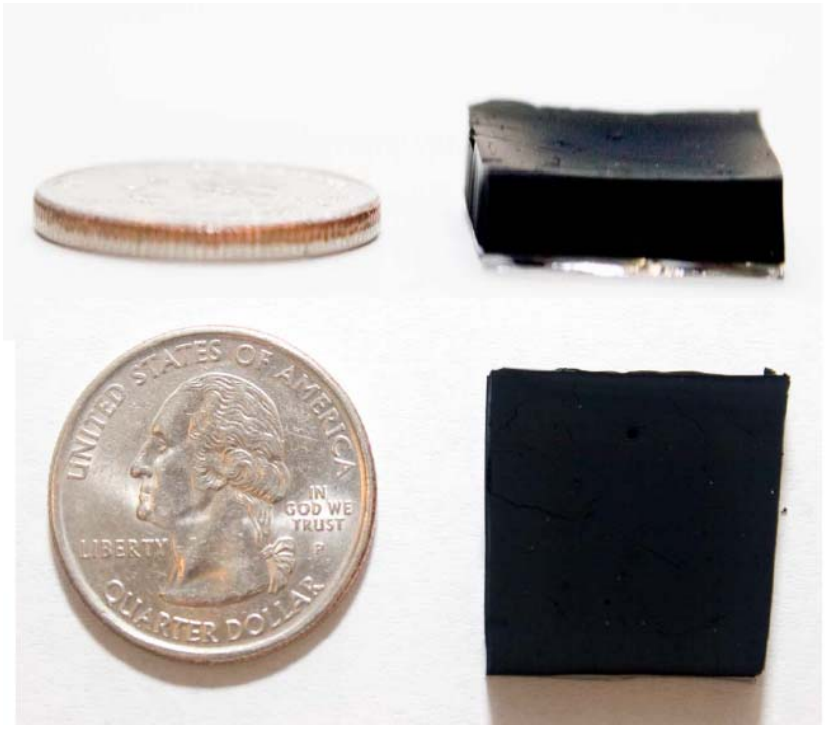

Figure 14. 4 mm long vertically aligned MWNT stacks grown at the University of Cincinnati *[37]*.

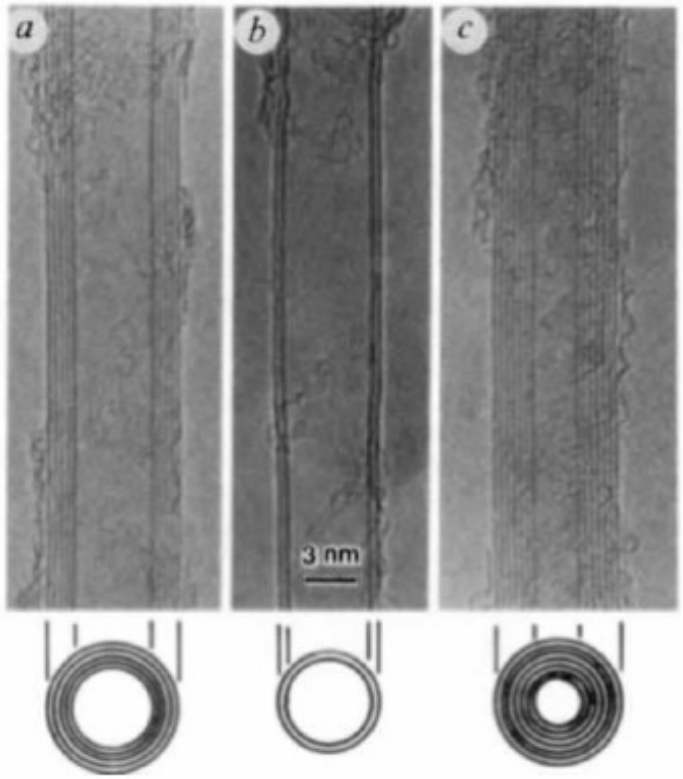

Figure 15. Cross sections of MWNT (a, c) and DWNT (b) imaged with TEM *[10]*.

Thermal Properties

It can be expected that since other forms of carbon such as graphite and diamond have superb thermal conductivities that CNTs will perform similarly. Unlike metals where heat is typically carried by electrons, in graphite heat is almost exclusively transported through lattice vibrations known as phonons *[27, 28]*. This form of conduction is highly anisotropic along the tube axis. Defects in the tube lattice such as holes, functionalities, or bends can cause perturbations in the atomic geometry which negatively affect the flow of heat. Experiments have shown *[64, 65]* and theoretical simulations have verified *[66]* that individual MWNTs have thermal conductivities of 3000 W/mK. Although thermal conductivity measurements of individual nanotubes can be quite difficult and results can vary, theoretical calculations and experimental data have

shown the thermal conductivity of individual SWNTs (diameter ~ 1-1.4 nm) can range between 1800 and 6000 W/mK *[64, 65]*.

For large areas arrays of CNTs, the experimental bulk thermal conductivity is lower by orders of magnitude *[2, 5, 66]* from that of a single nanotube. Reasons for such a dramatic drop off in performance include the presence of uncontrollable defects, build up of amorphous carbon during growth, and thermal resistances created by tube-to-tube interactions *[66]*. Defects such as holes can lead to an increase in phonon scattering which in turn reduces the thermal conductivity of the array. Amorphous carbon often present in MWNT arrays can serve as a physical boundary between the tubes and the contact surface. When carbon nanotubes grow they tend to bundle together due to the van der Waals forces between them. As dimensionality of the CNT array increases, the population of tube-to-tube contact points increases. Therefore, phonon-phonon scattering, also known as Umklapp scattering, is suppressed resulting in a significant decrease in thermal conductivity. At temperatures below 300K, the thermal conductivity of a single CNT decreases with 1/T due to the reduction in mean free path *[67]*.

The transverse conductivity of carbon nanotubes has been qualified as 10 to 20 times less than the axial conductivity *[68, 69]*. In the latter experiment, the axial conductivity was measured using the pulsed photothermal reflection technique. And the ratio between transverse and axial thermal conductivity was assumed to be equal to the ratio of transverse and axial electrical conductivity *[64]*. Molecular dynamics simulations have produced results suggesting that the discrepancy in thermal conductivity between the axial and transverse directions may be as much as three orders of magnitude *[70]*. According to the previous study, the transverse thermal conductivity is similar to the thermal conductivity of out-of-plane graphite. Qualifying carbon nanotubes as vertically aligned can be misleading. The alignment mentioned refers to the overall alignment of the array. Individually, and in smaller groups called bundles, the CNTs tend to bend and curve around one another as shown in Figure 16. The curvature and wave

nature of carbon nanotubes is not accounted for in theoretical calculations which could help to explain the aforementioned discrepancies.

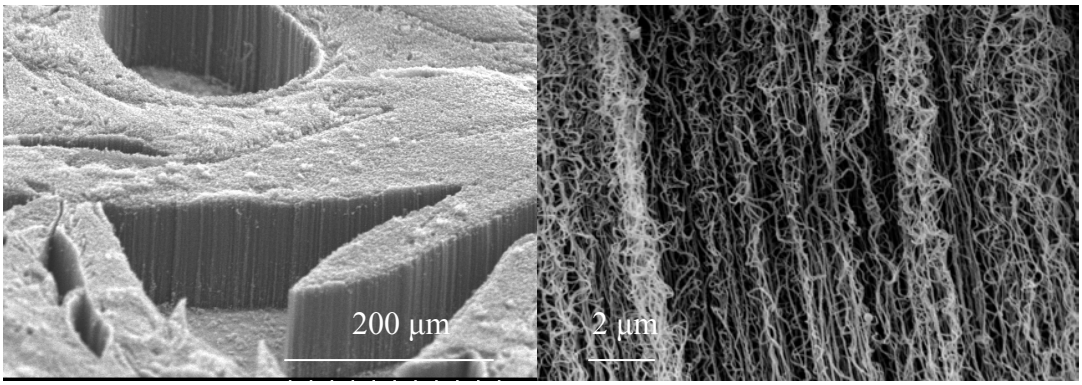

Figure 16. SEM images of vertically aligned CNTs. Image a) shows the clear vertical alignment of the nanotubes, while image b) shows the entangling nature of the tubes as caused by van der Waals forces.

The stability of carbon nanotubes at high temperatures must be accounted for when considering potential applications. Thermogravimetric analysis (TGA) has shown a dramatic degradation of CNTs at temperatures above 450 ºC (Figure 17) *[71]*. For many conventional applications, this threshold temperature does not factor. However, for extreme conditions that may occur in space exploration, automotive, or aeronautical applications, thermal stability can be an issue.

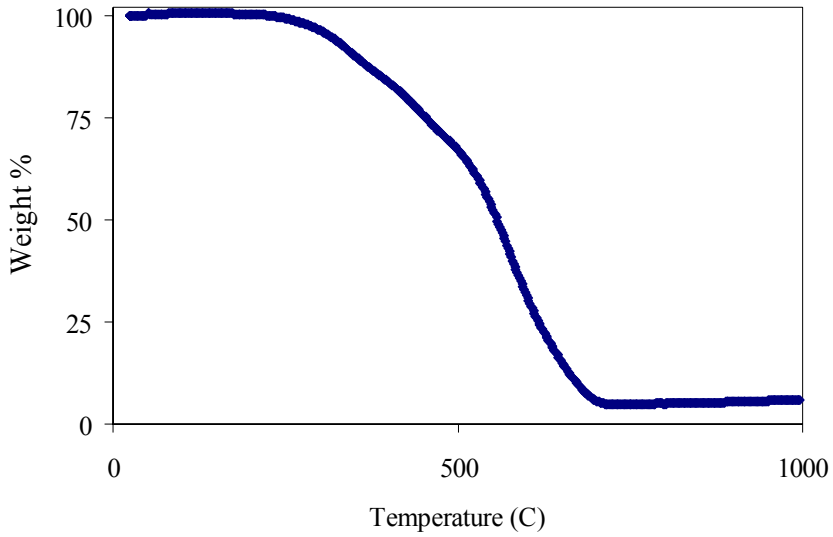

Figure 17. Thermo gravimetric analysis of single wall carbon nanotubes in air.

At room temperature and above all forms of carbon nanotubes, SWNT and MWNT, possess specific heat values of 700 mJ/gK, which is in close agreement with graphite. However, at temperatures below 100 K, nanotubes have shown quantum confinement effects *[10]*. At low temperatures SWNT bundles and graphite have a heat capacity around 0, for MWNT it is between 2 and 10 mJ/gK, and approximately 0.3 for a (10,10) individual SWNT *[65]*. These values were found using a self heating 3ω technique. Voltage contacts are secured on the sample and an AC current of the form $I_0 sin\omega_f$ is passed through the sample. This creates a temperature response at 2ω which in turn creates a 3ω voltage harmonics. Using this signal, thermal conductivity and specific heat can be solved explicitly with the following equations

$$V_{3\omega} = \frac{2I_0^3 LR(dR/dT)}{\pi^4 \kappa S \sqrt{1+(2\omega\gamma)^2}} \sin(3\omega t - \phi_0) \tag{3}$$

$$\tan\phi_0 = 2\omega\gamma \tag{4}$$

where $\gamma = L2/\pi^2 a^2$, $a^2 = k/C_p\rho_m$ is the diffusivity of the sample, k is the thermal conductivity, C_p is the specific heat, ρ_m is the densitiy, L is the length of the sample, R is the resistance, and S is the cross-sectional area of the sample *[65]*.

Electrical Properties

CNTs are also being investigated for their potential electrical applications. Based on the chirality of the individual tube, the CNT can be considered metallic or semiconducting. Metallic conductance occurs when the following equation is satisfied

$$(n - m) = 3q \tag{5}$$

where q is an integer and n and m are the graphite vectors mentioned previously. According to this equation, it can be considered that one third of the CNTs are metallically conductive, and the others semiconducting. In addition to chirality, the diameter of the nanotube affects its conductivity *[9, 60]*. The 1-D nature of the SWNT band structure elicits profound peaks in their density of state diagram as shown in Figure 18.

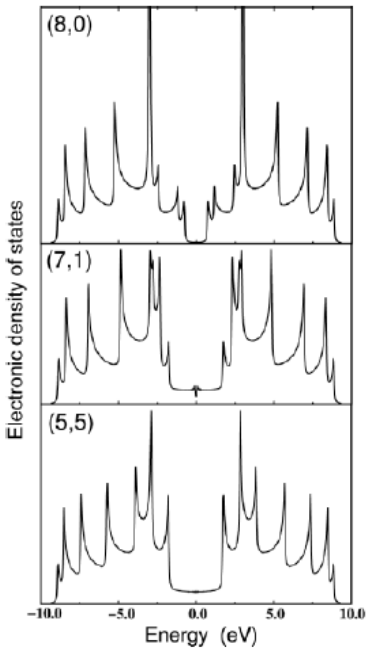

Figure 18. Density of state (DOS) diagram for zigzag (8,0), chiral (7,1), and armchair (5,5) SWNTs *[60]*.

The band gap for semiconducting nanotubes correlates approximately with the inverse of tube tube diameter *[72]*, and can be found using the following equation

$$E_g = \frac{2d_{cc}\gamma}{D} \tag{6}$$

where d_{cc} is the interatomic distance (0.144 nm for carbon), γ is the interaction energy between nearest neighbors (2.95 eV) *[9]*, and D is the diameter of the particular nanotube. Single carbon nanotubes can have electron mobilities as high as 100,000 cm^2/Vs *[73]*, and current carrying capacities of 10^9 A/cm^2 *[74]*. The band gap of a carbon nanotube decreases with increasing diameter *[75]*. An empirical fitting formula for the band gap of semiconducting nanotubes is

$$E_g = 1(eV)/d \tag{7}$$

where d is the diameter of the nanotube.

The fact that CNTs can exist as a semiconducting or metallic material lends them to microelectronic applications as electrical interconnects or active devices respectively.

For instance, in 2000 at Harvard University, nonvolatile random access memory and logic function tables with a density of 10^{12} elements/cm^2 operating at a frequency greater than 100 GHz were created using SWNTs *[76]*.

Mechanical Properties

Along with superior electrical and thermal properties, carbon nanotubes have shown promise for their mechanical attributes. Experimental results align closely with theoretical calculations *[77, 78]* to reveal Young's moduli in excess of five times that of AISI 4000 steel *[79, 80]*. Theoretical estimates of the Young's modulus for single wall nanotubes suggests no meaningful dependence on diameter *[78]*. For MWNT, the Young's modulus is a combination of the highest valued SWNT and the coaxial Van der Waals forces. Therefore, MWNTs have a higher modulus, usually on the order of 1.1 to 1.3 TPa *[81]*. Molecular dynamic simulations have shown the ability of a SWNT to endure over 15% tensile strain before fracture *[10, 82]*. However, through experimental research, tensile strains as high as 5.8% have been observed *[83]*. Measurements for which were done using an atomic force microscope (AFM) to depress a single wall nanotube secured on both ends. Figure 19 is an example of a force deflection curved created by Salvetat et al. This data was acquired by deflecting a cantilevered SWNT using a Si_3N_4 AFM tip. The linearity and reversibility of the curve suggests the deflection of the nanotube was linear and elastic in that particular force range.

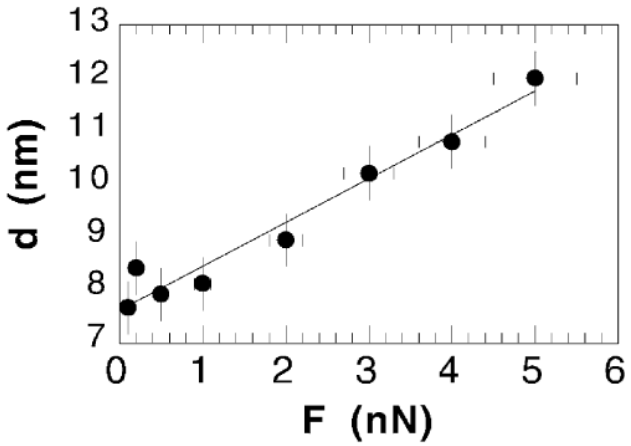

Figure 19. Typical force-deflection curve of SWNT bundle *[84]*.

Composite materials with carbon nanotubes have been created to harness the superior mechanical properties of the nanomaterial. Fibers of polyacrylonitrile (PAN) with 5 wt% carbon nanotubes (SWNT, MWNT, and DWNT) have shown to increase such mechanical properties as strength to breaking, strain to failure and toughness while reducing thermal expansion *[85]*. For the MWNT composites, increases of 70% tensile strength, 110% strain to failure and 230% toughness were observed. In addition to polymer fibers, CNT reinforcements have been integrated into ceramics *[86-88]* and various metallic materials *[32, 89, 90]*.

Carbon Nanotube Growth Techniques

Carbon nanotubes are grown using a vapor-liquid-solid (VLS) technique. VLS describes the action of liquid catalyst particles becoming super saturated with a vapor and the subsequent forming a solid crystal structure *[91]*. Specifically, growth occurs via a process of diffusion of the precursor into the catalyst particle, adsorption of reactive species onto the catalyst surface, and subsequent surface reactions with the precursors to create the nanotube *[92]*. This process is illustrated in Figure 20. Typically, transition metals such as Fe, Ni, Co, or Mo are used as catalysts for carbon nanotube synthesis. These metals have proven effective because of their ability to absorb the carbon based

reactant gases. The adhesion of the CNT to its growth surface is a function of the catalyst's adhesion to the substrate and the CNT's adhesion to the catalyst *[92]*.

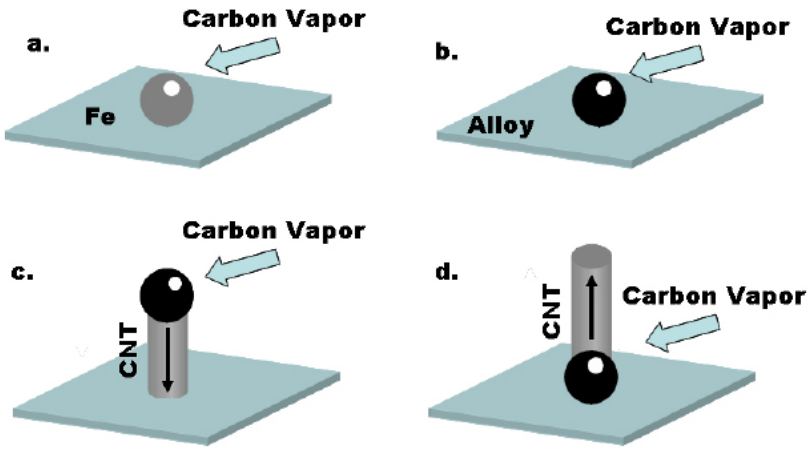

Figure 20. Steps of CNT growth via CVD; (a) precursor diffuses into catalyst particle, (b) adsorption onto catalyst surface, (c) base growth of CNT, or (d) tip growth of CNT.

Chemical Vapor Deposition

Chemical vapor deposition is widely used in labs today to grow carbon nanotubes. CVD processes are characterized by their energy source. Conventional energy sources such as resistive heaters or furnaces are considered thermal CVD. When a plasma source is used to create a glow discharge, it is referred to as plasma enhanced chemical vapor deposition (PECVD).

Thermal CVD utilizes a quartz tube and a tube furnace with good temperature control capabilities. It is important that the temperature during the growth phase remain constant. In many cases, this technique is performed at atmospheric pressure so a vacuum apparatus is unnecessary. The substrate is placed near the middle of the tube radially *[93]* and directly under the thermocouple to ensure temperature control. While

elevating the temperature in the furnace, inert gasses are sourced (Argon or Nitrogen) to create an inert atmosphere throughout the tube. Once the growth temperature has been achieved various hydrocarbon gases are introduced at specific flow rates to begin nanotube growth. Hydrocarbons typically used include methane, ethane, acetylene, ethylene, and ferrocene *[15, 32, 62, 94-98]*. This list, however, is not comprehensive. After the growth phase, the furnace is cooled in an inert atmosphere to temperatures below 300 °C to avoid oxidation effects. Figure 21 shows a schematic of a thermal CVD apparatus and Figure 34 is a picture of the thermal CVD system used for this study.

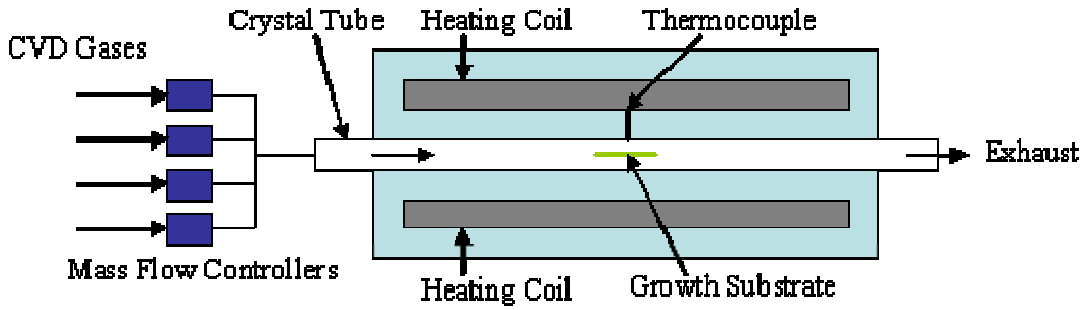

Figure 21. Thermal CVD schematic.

Lower temperature operation is possible with PECVD because the precursor dissolution that is necessary can be achieved with high energy electrons *[99]*. However, there is a minimum temperature (~500 ºC) required to activate the catalyst on the substrate to facilitate nanotube growth *[29]*. PECVD systems will therefore utilize a local heat source for the substrate and catalyst. This allows for faster processing because less time is required to completely cool the chamber. Figure 22 is an example of a PECVD setup. PECVD systems may be preferred by some users because vertical alignment of the CNTs is a result of the electric field present in the plasma during synthesis *[29]*. Thermal CVD achieves the vertical alignment through a crowding effect

as a result of the density of the catalyst. Therefore, to grow shorter (< 10 μm) vertically aligned CNTs, PECVD would be preferred.

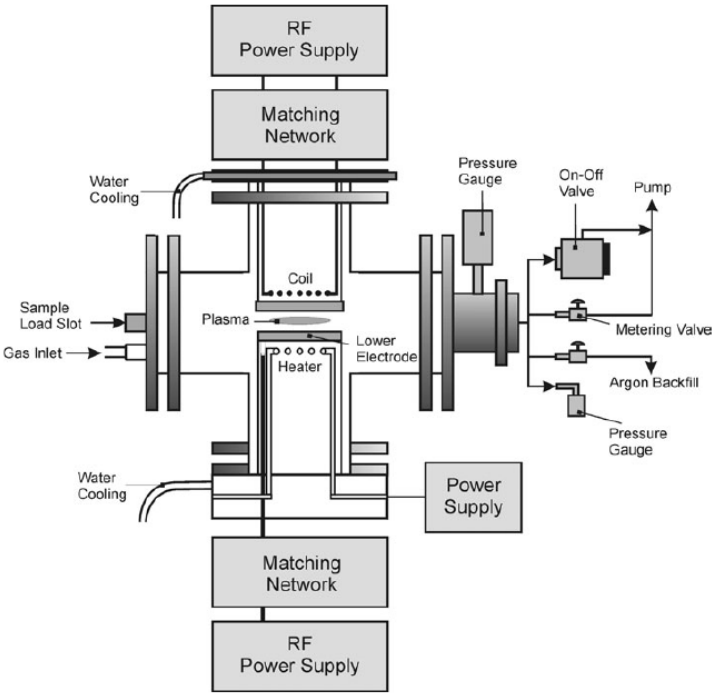

Figure 22. PECVD setup *[29]*.

Arc Discharge

The arc discharge method of CNT growth relies on a direct current arc operating between two graphite electrodes in a water-cooled chamber of helium at low pressures *[100]*. In this technique, the anode is consumed and the cathode is grown upon. The combination of carbon vapor, catalyst particles, inert atmosphere, and DC plasma makes it possible for CNT growth *[101]*. By maintaining a constant cathode feed rate, the arc current can remain constant thereby producing a high yield and stable process *[100]*. There are two methods of catalyst delivery, drilled hole and uniform dispersion. The catalyst and graphite powder for the drilled hole method are placed inside a recessed hole

in the anode. Alternatively, the catalyst is deposited uniformly in the anode rod during production *[9]*. Figure 23 shows a typical arc discharge setup.

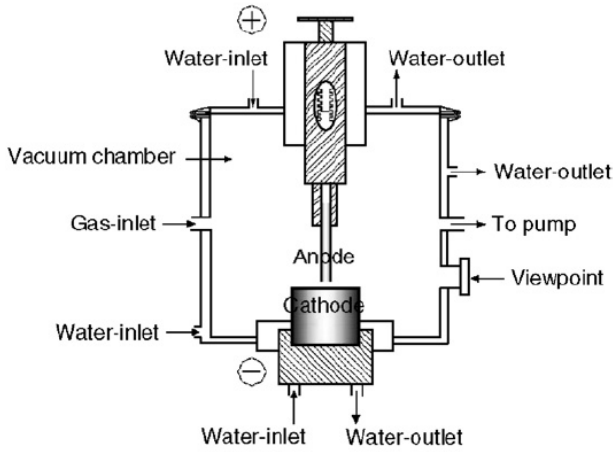

Figure 23 Arc discharge setup *[9]*.

Arc discharge, due to its high temperature synthesis of at least 1200 ºC *[102]* can produce very high quality tubes with superior properties. However, this technique has not shown the economic flexibility *[23]* to scale up production like thermal CVD.

Thermal Characterization Methods

The small size and high conductivity of carbon nanotubes makes it difficult to measure their thermal properties. Common thermal measurement techniques such as the guarded heat plate method may not be suitable. This method, in addition to large uncertainty, is more apt for materials that have low thermal conductivity (< 10 W/mK) *[103]*. The techniques highlighted in this section are ones that are more suited for highly conductive thin films.

Photoacoustic Method

The photoacoustic effect is observed when photons are converted into kinetic energy thereby creating pressure fluctuations *[104]*. This phenomenon was first observed by Alexander Graham Bell *[105]* and revisited decades later with emphasis on its role in solids. Locally heating a surface with a laser will cause pressure changes on the back side of the sample which can be recorded with the aid of a microphone. Based on the phase change and amplitude of the signal *[106]*, thermal conductivity and diffusivity properties can be deduced.

This method has the advantage of being noninvasive. By not physically contacting the substrate, the integrity of the experimental conditions is maintained. It can also be used to analyze multiple layer systems *[1]*. Figure 24 shows and example of a photoacoustic measurement setup.

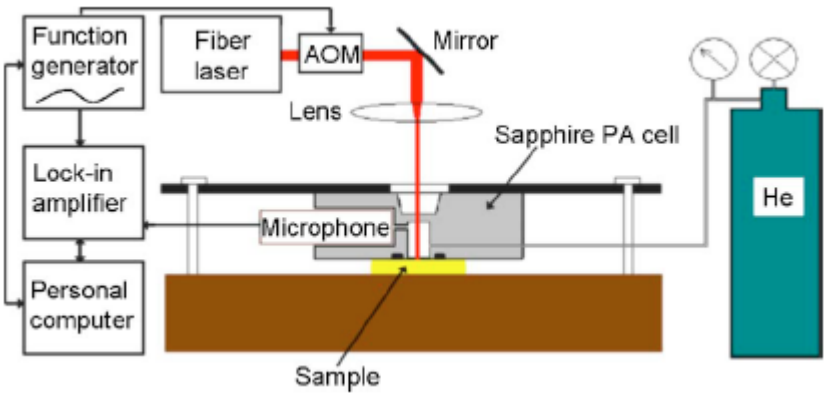

Figure 24. Photoacoustic measurement set up from *[1]*.

The PA measurements consist of any number of arbitrary layers (1,2,…*N*) and a base material (0) heated periodically by a laser with a frequency ω and intensity $1/2I_0[1+\cos(\omega t)]$. Absorption of the laser beam is permissible in any number of layers. The base layer (0) and the gas surrounding (*N*+1) are assumed to be thermally thick.

Because the thermal diffusion length in gas is much less than the chamber radius, the PA signal can be considered independent of the energy distribution of the laser . The complex solution for the temperature distribution in the surrounding medium θ_{N+1} can be expressed as

$$\theta_{N+1} = (1-\rho)\cdot B_{N+1} e^{-\sigma_{N+1}x} e^{j\omega t}, \tag{8}$$

where

$$B_{N+1} = -\frac{[0\ 1]\sum_{m=0}^{N}\left(\prod_{i=0}^{m-1} U_i\right) V_m \begin{bmatrix} E_m \\ E_{m+1} \end{bmatrix}}{[0\ 1]\left(\prod_{i=0}^{N} U_i\right)\begin{bmatrix} 0 \\ 1 \end{bmatrix}}, \tag{9}$$

$$U_i = \frac{1}{2}\begin{bmatrix} u_{11,i} & u_{12,i} \\ u_{21,i} & u_{22,i} \end{bmatrix}, \quad V_i = \frac{1}{2}\begin{bmatrix} \nu_{11,i} & \nu_{12,i} \\ \nu_{21,i} & \nu_{22,i} \end{bmatrix}, \tag{10}$$

$$u_{1n,i} = (1 \pm k_{i+1}\sigma_{i+1}/k_i\sigma_i \mp k_{i+1} \times \sigma_{i+1}R_{i,i+1}) \times \exp(\mp\sigma_{i+1}l_{i+1}), \quad n = 1,2, \tag{11}$$

$$u_{2n,i} = (1 \mp k_{i+1}\sigma_{i+1}/k_i\sigma_i \mp k_{i+1} \times \sigma_{i+1}R_{i,i+1}) \times \exp(\mp\sigma_{i+1}l_{i+1}), \quad n = 1,2, \tag{12}$$

$$\nu_{n1,i} = 1 \pm \beta_i/\sigma_i, \quad n = 1,2, \tag{13}$$

$$\nu_{n2,i} = (-1 \mp k_{i+1}\beta_{i+1}/k_i\sigma_i + k_{i+1} \times \beta_{i+1}R_{i,i+1}) \times \exp(-\beta_{i+1}l_{i+1}), \quad n = 1,2, \tag{14}$$

$$E_m = \frac{G_m}{\beta_m^2 - \sigma_m^2}, \tag{15}$$

$$G_m = \begin{cases} \dfrac{\beta_m I_0}{2k_m} e^{-\sum_{i=m+1}^{N} \beta_i l_i} & \text{for } m < N \\ \dfrac{\beta_m I_0}{2k_m} & \text{for } m = N \\ 0 \quad \text{for } m = N+1. \end{cases} \tag{16}$$

For this series of equations, $\sigma_i=(1+j)a_i$ with $j=I$ and $a_i=(\pi f/a_i)^{1/2}$. The thermal diffusivity of layer i is a_i, f is the modulation frequency, k_i is the thermal conductivity of the layer, ρ is the surface reflectivity of the sample, β is the optical absorption coefficient and $R_{i,i+1}$ is the thermal contact resistance between layer i and i+1. The temperature in the gas layer is correlated to the phase shift and amplitude of the PA signal. This phase shift is calculated as $Arg(B_{N+1})$-π/4 and the amplitude is found by Abs[(1-ρ)·$B_{N+1}P_0$/sqrt(2)$l_{N+1}a_{N+1}T_0$], where P_0 and T_0 are the ambient temperature and pressure respectively *[107]*.

The photoacoustic apparatus as shown in Figure 24 employs a cylindrical sapphire PA cell. Sapphire is used because it has a low reflectance and high transmittance for the particular laser wavelength used. Meaning, most of the energy from the laser that is reflected from the sample is then transmitted out of the cell. The microphone is planted near the inside wall of the cell to maximize signal strength. It senses the acoustic signal and transmits it to a lock in amplifier for amplitude and phase measurements. A personal computer that is synced via GPIB controller to the amplifier and signal generator is used for control and data acquisition.

Flash Diffusivity

Flash diffusivity is another noninvasive system used to measure thermal conductivity and diffusivity. This method is similar to the photoacoustic technique, but instead of recording pressure waves, it measures backside temperature. A focused heat source (typically a laser) is targeted at the sample while an infrared (IR) camera measures

the backside temperature. By monitoring the change in temperature over time, thermal properties of the sample can be concluded. This method has been used to measure the conductivity of carbon nanotube arrays *[108]*. The flash diffusivity technique is well suited for planar subjects *[109]*.

The thermal diffusivity, α, of the sample can be found using a simple expression where L is the thickness of the specimen and $t_{0.5}$ is the time required to reach half of the maximum temperature.

$$\alpha = \frac{1.38L^2}{\pi^2 t_{0.5}} \tag{17}$$

According to this equation, it is assumed that all of the energy induced into the system is absorbed at the surface. Thermal conductivity is then equal to the thermal diffusivity times density and specific heat of the sample. Flash pulses are typically on the order of a millisecond and measurement are made over a several seconds to minimize the effects of heat loss *[110]*. While the method has been applied to CNT arrays, care must be taken in applying this method to short vertically aligned arrays. This is due to the fact that the CNTs are a porous mat and thus the assumption of all energy being absorbed at an infinitesimal depth at the surface of the sample may be invalid.

Laser Thermo Reflectance

Laser thermo reflectance is a transient form of thermal measurement. It requires a high speed laser that can produce pulses on the pico and femtosecond level. A laser is sourced and subsequently split into two beams. One beam, the pulse beam, is reflected directly to the surface of the test specimen while the other is rerouted through a longer path (to control delay time). After traveling the longer route, the second beam hits the target and is reflected into a photo-detector. The change in reflectivity is then correlated to the change in temperature of the sample. By recording this change over several hundred picoseconds, one can deduce certain thermal properties of the given sample.

Figure 25 is an example of how the pulse and probe lasers interact with the test subject. The probe laser is the beam that is redirected in order to create a time delay. Figure 26 is an example of the thermo reflectance response for Pyrex glass.

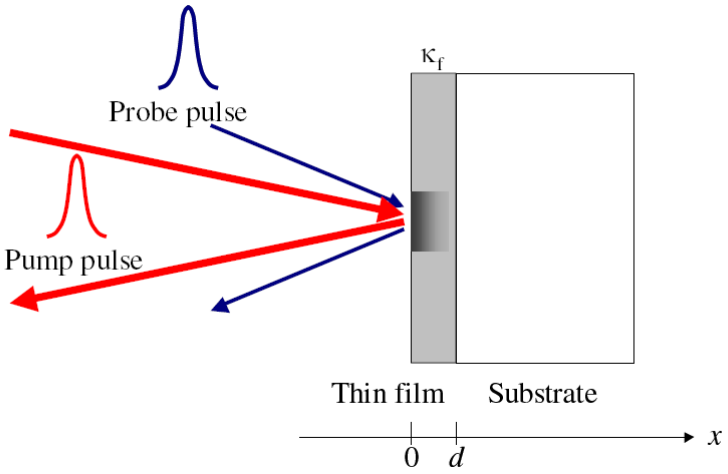

Figure 25. Diagram of pump and pulse probe used in the laser thermo reflectance thermal measurement technique *[111]*

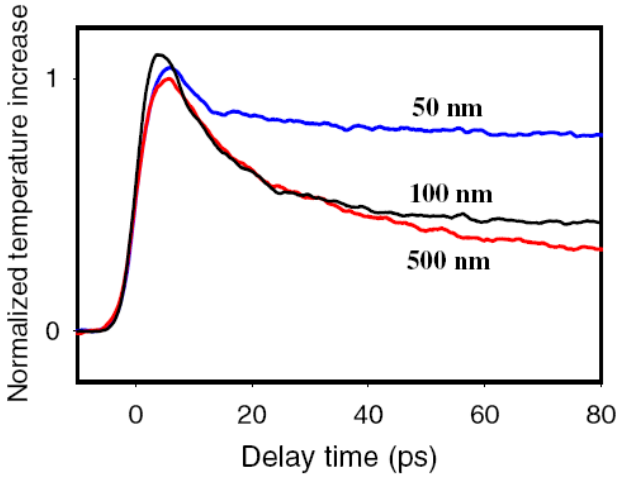

Figure 26. Thermo reflectance response of Pyrex glass *[111]*

Manufacturing and Printing

The ability to integrate carbon nanotubes into various systems is not a trivial capability. Manufacturing techniques must be developed and perfected to deliver such a small material into device with a high level of precision. Concerns such as temperature, bond strength, and nanotube alignment must be addressed when developing a printing technique. Direct growth of CNTs onto devices, while producing excellent adhesion and alignment, is not a practical solution because of high process temperatures. Additionally, direct growth of nanotubes onto any surface can not be assumed because of surface chemistry issues. With such limitations it becomes necessary to create procedures to integrate carbon nanotubes into devices. In this section, manufacturing and printing methods will be investigated as well as the current state of CNT and nanotube composite thermal interface materials.

Integration Techniques

Due to their high growth temperatures CNTs are unable to be grown directly onto most devices. Attempts at low temperature growth have produced CNTs with low purity and alignment *[112]*. In addition, for applications such as thermal interfaces and electrical vias, the vertically alignment of the nanotubes is important *[25, 34]*. Procedures are continually being developed to meet the challenges of integrating CNTs into microsystems.

Conductive polymers *[15, 16, 19, 20, 23]* and solders *[25]* have been used as matrix materials for CNT composites. These techniques utilize a liquid matrix material to encompass the CNTs and the subsequent solidification to create the final composite. Challenges exist for incorporating randomly oriented and vertically aligned CNTs into such materials. Randomly oriented CNTs are grown using a free floating catalyst, and their lack of alignment can be attributed to the low spatial density of the catalyst during

synthesis. Difficulties arise in dispersing these nanotubes because of their affinity to clump *[113]* which may cause hotspots in the composite.

Transfer of vertically aligned nanotubes into a conductive adhesive relies on the ability of a matrix material to wet the CNTs *[113]* and the adhesion of the tubes to the host substrate. Vertically aligned tubes have been integrated into silver epoxy *[24]* and solder *[25]*. Dissolution of an SiO_2 sublayer beneath the nanotubes has also been shown to release the nanotube forest *[26]*.

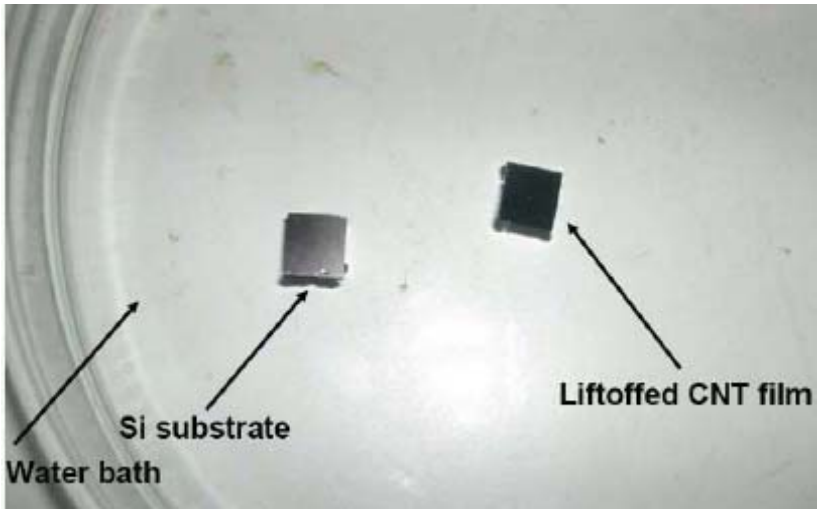

Figure 27. CNT film removed from growth surface using HF dissolution of SiO_2 sublayer *[26]*.

In this technique, the vertically aligned forest maintains its shape and alignment while suspended in a water bath. Transfer of the suspended structures to another surface has not proven viable for heat transfer applications because of the severe lack of adhesion.

Carbon nanotubes have also been transferred into polymer substrates such as polymethylmethacrylate (PMMA) and polydimethylsiloxane (PDMS) *[15, 16, 23]* using hot embossing techniques. These methods have shown the ability to consistently transfer aligned CNT patterns into substrates at varying depths. For these procedures, global

conductive heating and localized microwave heating of the polymer substrate to its glass transition temperature make it possible for the vertically aligned CNTs to penetrate. Vertically aligned CNT patterns were grown using thermal CVD onto an SiO_2 substrate. The tubes were then rested on the polymer substrate with the tips in contact with the plastic. The hot embossing technique described in *[15, 16]* used a global heating strategy to bring the PMMA to its glass transition temperature. With the application of 3 MPa of pressure, the tubes were embedded into the new substrate. Upon cooling, the polymer adhered to the individual or group of nanotubes with enough strength to separate the CNTs from the growth substrate. A localized heating method using a variable frequency microwave (VFM) is described in *[23]*. Again, vertically aligned CNT structures were placed tip-side down onto a polymer surface. Once in the VFM, the conductive silicon and CNT structures began to heat while the polycarbonate remained at room temperature. The low conductivity of the polymer helped to create an intense local heat at the tube/substrate interface. The temperature at this point could be maintained at a desired level by pulsing the microwave. Both embossing techniques allow the user to successfully transfer vertically aligned CNT structures into polymeric materials. However, the latter can operate much faster because of the quick localized heating provided by the VFM.

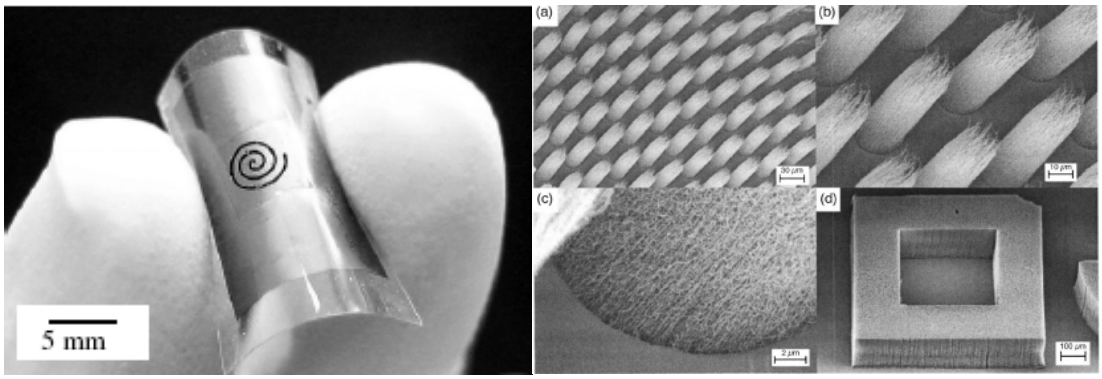

Figure 28. Transferred vertically aligned CNTs into flexible polymer substrate. The second (SEM) images show the vertical alignment being maintained after transfer *[16, 23]*.

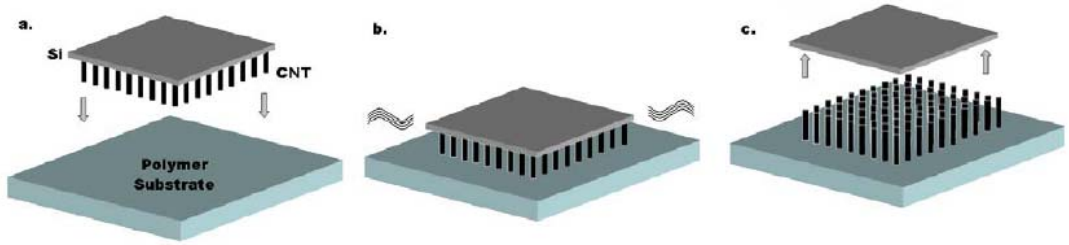

Figure 29. Schematic shows the hot embossing process in which (a) tubes are rested on the polymer, (b) system is heated locally or globally, and (c) growth chip is removed *[23]*.

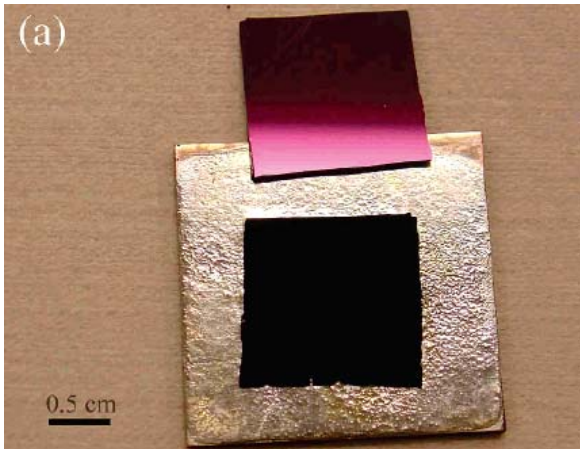

Figure 30 CNT array transferred into eutectic SnPb solder *[25]*.

Hot embossing is an attractive method of CNT transfer because of its simplicity. The use of expensive equipment and clean room facilities is also minimized which is favorable from a economic standpoint. The success of vertically aligned carbon nanotubes embedded into polymers as thermal interface materials will be investigated in the following section.

Transferring carbon nanotubes into solder has proven to be a significant challenge. As mentioned before, with solder one must contend with wettability issues which involve material chemistry and surface tensions. Zhu et al has demonstrated the ability to transfer vertically aligned CNTs into lead based solders. By using a water vapor etching step, they reported that the end caps of the CNTs were removed thereby facilitating capillary flow of the wetted solder into the CNT. The curved pentagonal structures in the end caps of the CNTs possess a larger strain than the unstrained bonds in the nanotube side walls. Therefore, the end caps are more prone to etching by the water vapor molecules *[25]*. The transfer they achieved, as shown in Figure 30, is complete. Thermal characterizations of these solder/CNT interfaces have not been published.

Thermal Interface Materials

A thermal interface materials (TIM) is any conductive material that bridges the gap between a heat producing element and a heat sink or heat spreader *[114]*. While being highly thermally conductive, TIMs must also be able to reduce the effects of thermal contact resistance between the mating surfaces. Surface roughness effects are the principal causes of thermal contact resistance *[42]*. This finite resistance value is quantified using the following equation

$$R_C = \frac{T_A - T_B}{q''_x} \tag{18}$$

where T_A and T_B are the two surface temperatures and q_x" is the heat flux through the system. The heat transfer being considered for this study is diffusive. The ability of a

thermal interface material to conform to the inherent roughness of the contact surfaces is paramount. In addition to conductivity and malleability, the strength of the interface must be considered. TIMs can experience a substantial amount of shear stress throughout the operation of a device because of the CTE mismatch between the joined surfaces. These stresses can cause significant problems such delamination and die cracking which can lead to electrical failure *[115]*. CNTs possess a negative coefficient of thermal expansion *[22]* which could be advantageous in TIM design.

As mentioned before, isotropic conductive adhesives (ICA) have been used in conjunction with CNTs to form thermal interface composites. Randomly dispersed CNTs have not shown considerable promise in improving the thermal conductivity of conductive adhesives *[113]*. Reasons for such performance include interface resistance between the individual CNTs and the polymer matrix and contact resistance between touching CNTs. A thermal resistance of 0.08 mm^2K/W was measured between a single wall carbon nanotube and sodium dodecyl sulphate (SDS) *[116]*. Vertically aligned CNTs have shown to be far more effective than randomly dispersed nanotubes at improving a composite's thermal conductivity *[19]*. However, the conductivity of these polymer/CNT matrices are in the range of 0.5-1.2 W/mK which is still below commercial TIMs.

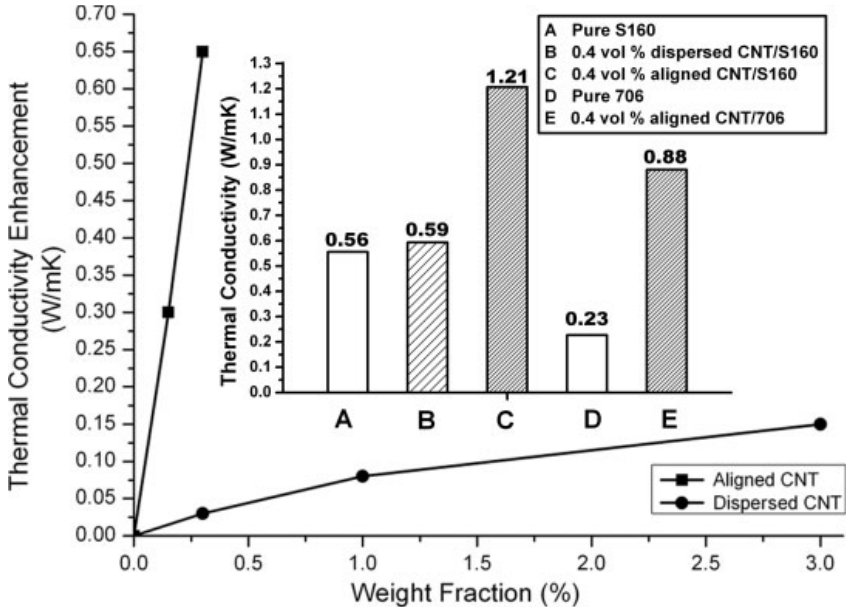

Figure 31. Thermal conductivity enhancement of polymers (Sylgard 160 and 706 single part vulcanized silicone elastomer) integrated with randomly dispersed and vertically aligned CNTs *[19]*.

Two routes have been forged in the development of CNT based thermal interface materials; wet and dry. Wet interfaces incorporate a polymer or phase change material with the vertically aligned CNT arrays. Dry interfaces do not incorporate any filler material into the interface. With regards to wet interfaces, CNTs have been introduced into several different polymeric materials such as S160 and silver filled thermoplastics *[18, 19]*. An injection molding process was used to create the CNT/S160 matrix. Thermal resistance measurements of these interfaces were greater than 100 mm^2K/W depending on the thickness. Resistance values lower by an order of magnitude have been achieved by several research groups using dry interfaces.

Current studies have shown that the total resistance of the vertically aligned CNT interface is dominated by the contact resistance between the CNTs and the mating surfaces *[117]*. Resistance values of 48 mm^2K/W were measured between the CNT and SiO_2/Si growth substrate with no applied pressure. Such high resistance values suggest poor contact with the growth substrate in the experiment. CNTs grown with excellent

adhesion have shown resistances as low as 1 mm^2K/W *[2]* between the CNTs and the growth surface. The Fisher group at Purdue University has performed extensive studies on thermal resistance of vertically aligned CNTs with applied pressure. Resistance measurements of 16 mm^2K/W have been recorded for interfaces with one side covered in vertically aligned CNTs *[118]*. However, interfaces with two sides of CNT growth have reduced that value by a factor of 4 *[2]*. Measurements for the Fisher group were performed using the photoacoustic method previously described. To achieve such low values of resistance, CNTs were grown onto either side of a thin sheet of copper foil. The contact resistance of the free ends of the tubes with the mating surfaces dominated the overall interface resistance. By applying pressure to the mating surfaces, the CNTs were able to conform to the imperfections in the surface, and the resistance of the interface was reduced *[1]*. The results shown in Figure 32 were evidence of the CNTs ability to conform to the mating surfaces.

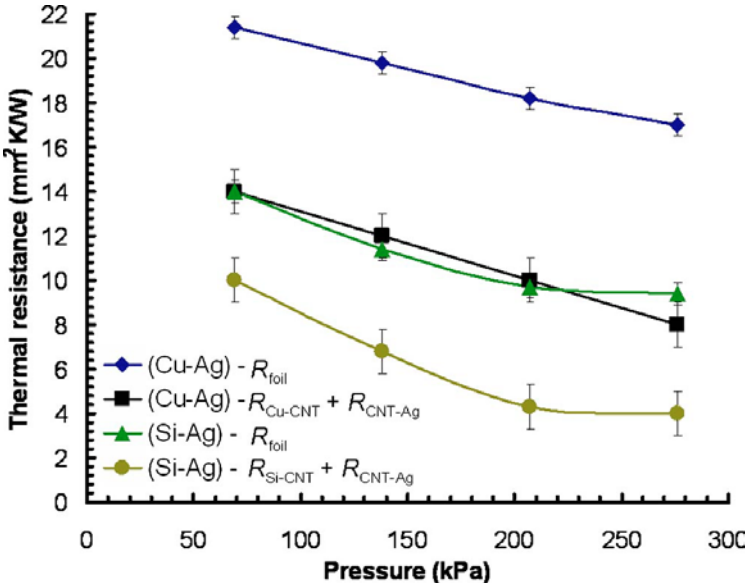

Figure 32. Decrease in thermal resistance with increasing pressure between various interfaces *[2]*.

Figure 32 is a great example of the ability of the CNTs to conform to the mating surfaces. The rougher copper surface elicited a higher thermal resistance however, it did not reach a bottoming level. Perhaps more pressure would induce the double sided CNT film to contact the deeper areas of the surface.

At the University of California, Berkeley, Majumdar et al have grown vertically aligned CNTs using thermal CVD and measured interface resistances around 11 mm^2K/W *[5]*. Measurements were taken using a laser thermo reflectance technique. For these experiments, a micron thick layer of indium was deposited on the tips of the nanotubes, and a glass slide was placed on top of that. The interface resistance of the CNTs with the growth substrate (Si) was measured to be ~ 1 mm^2K/W. However, the dominant resistance was the dry interface between the CNT/indium and the glass slide.

Finally, Dr. Goodson's group out of Stanford University has published data concerning the thermal resistance of metal coated vertically aligned CNTs. Resistance values of 12 mm^2K/W *[3, 4]* were measured which align closely with those from Berkeley and the one sided samples from Purdue. Goodson goes a step further to suggest that the metal coating (Al/Pd) on the vertically aligned CNTs only contacts the tallest nanotubes with in the array. Therefore, the majority of the conduction occurred through those tubes in contact with the metal coating as shown in Figure 33.

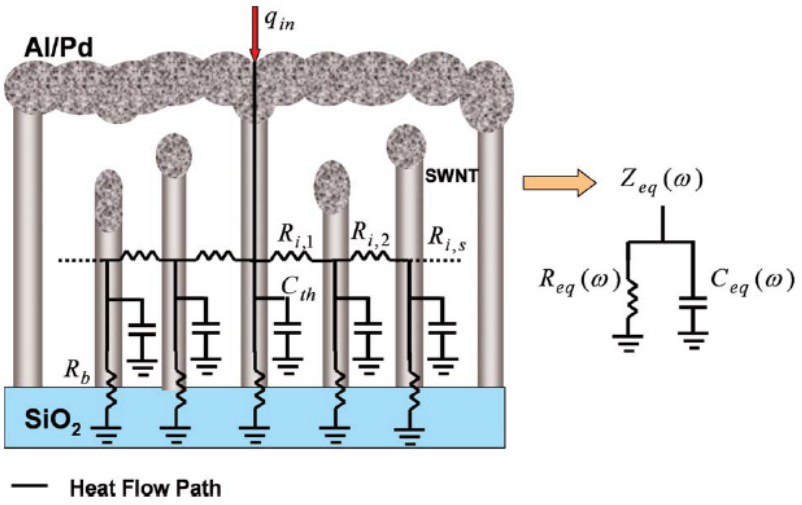

Figure 33. Thermal path for metal coated vertically aligned carbon nanotubes as hypothesized by Goodsen et al *[4]*.

In efforts to reduce the contact resistance between the CNT tips and joining surface, CNT arrays with thin metallization layers have been investigated. Recent studies in this realm have shown promising results. Layers of palladium and aluminum on CNT tips have yielded overall thermal resistances of 12 mm^2K/W *[3, 4]*. The fact that all of the CNTs are not in contact with the mating surface, and that there is minimal heat transfer longitudinally from tube to tube are explanations for not a more significant decrease in thermal resistance. An outline of the results obtained by the top research groups in this field is shown in Table 4.

Table 4. Summary of recent results for CNT thermal interface resistances.

Group	Location	R_{int} (mm^2K/W)	CNT Thickness (μm)	Applied Pressure	Filler Material	Ref.
Huang et. al.	Tsinghua University	110-400	100-500	-	S160	*[19]*
Fisher et. al	Purdue	20-37 4	7-13 50	0.445 MPa 0.275 MPa	- -	*[119]* *[2]*
Zhang et. al.	Hong Kong University of Science and Technology	15	30-70	0.1 MPa	-	*[6]*
Xu et. Al.	Nanoconduction Inc.	12-16	30	80 psi	-	*[118]*
Goodson et. al.	Standford	12	28	-	Al/Pd on CNT tips	*[3, 4]*
Majumdar et. al.	UC Berkeley	11	7	-	-	*[5]*

While the results obtained by the top research groups in this field have been intriguing, little progress has been made with regard to manufacturing of these interfaces. Limitations with regard to CNT adhesion and integration into microelectronic devices exist with each study. The success of carbon nanotubes as a thermal interface material hinges on its performance and the ability to integrate them into microelectronic devices in a safe reliable manner.

In summary, the structure of carbon nanotubes has prompted researchers to investigate their outstanding electrical, thermal, and mechanical properties. Challenges still exist with large scale production of high purity tubes with controllable structure and the procedures for integration into microsystems have yet to be refined. In this study, growth techniques for weakly adhered vertically aligned CNT arrays were investigated and a novel process for efficient CNT transfer was developed. Additionally, the thermal resistance of the transferred CNT arrays was characterized using a photoacoustic technique and through integration into a high powered LED system.

CHAPTER 4

CARBON NANOTUBE GROWTH AND TRANSFER

Introduction

For a thermal interface material to be effective it must have a low thermal resistance and be mechanically robust. The thermal resistance of the interface is composed of the resistance within the material and the contact resistance between the material and the mating surfaces. To improve the internal thermal resistance of the carbon nanotubes three factors must be optimized: CNT length, purity, and vertical alignment. Shorter CNTs with greater purity and alignment will yield the best results with regard to bulk thermal resistance. The contact resistance between the CNTs and the mating surfaces is predicated on the adhesion of the nanotubes to the joining surface. This can be controlled by growing CNTs with strong adhesion to the growth surface, or by transferring the CNTs to another surface by creating a substantial adhesive force.

The vertical alignment of the CNTs comes as a result of the density of catalyst particles on the substrate and the van der Waals forces between the tubes. High catalyst density will create a crowding effect with the CNTs and produce a vertical alignment. The alignment is important because thermal transport properties of carbon nanotubes is dominated down the axis of the CNT *[120]*. In this experiment vertically aligned carbon nanotubes were synthesized using a thermal chemical vapor deposition method. It was shown that the length and purity of the produced CNT arrays could be controlled by modulating the hydrocarbon soak time. The adhesion of the CNT arrays to the growth surface was able to be weakened using a water vapor etching step after the growth phase. Furthermore, carbon nanotubes grown with weak adhesion to the growth surface were able to be transferred to polyimide tape, and secured to other surfaces using a novel gold bonding method developed during this study. This technique capitalizes on the decreased

melting temperature of small gold particles that form on the tips of the CNTs. The bond created with the nanotubes and bonding surface was shown through tensile testing to be significantly more robust than other reports of CNT bonds.

Experimental Setup

CNT Growth

Vertically aligned carbon nanotubes were grown using a First Nano Easy Tube Furnace. The system incorporated four independent mass flow controllers for gas regulation, a resistive heating furnace with a temperature range in excess of 1000 ºC, and a crystal tube (1.5 inch diameter) with crystal loading tray. A simple exhaust system connected to the building exhaust line was set up to remove the reactants after passing over the sample. The process for growing CNTs with thermal CVD was straightforward. First, the temperature was elevated in an inert atmosphere (Argon) to the growth temperature. If the tube was not completely filled with an inert gas, the catalyst could prematurely react thus yielding no growth. At the growth temperature, the sample was allowed to soak to promote the formation of liquid catalyst particles. The longer this soak time, the larger the liquid catalyst particles. Next, the reactant gases (acetylene, methane, and hydrogen) were introduced at specific flow rates and the CNTs were grown. Finally, the temperature of the furnace was allowed to cool slowly while a steady flow of argon was sourced. Again, if the sample was removed from the furnace before it was allowed to fully cool, the CNTs could oxidize. Table 5 describes the foundation of the recipe used to grow the vertically aligned carbon nanotubes. By varying the flow rates of the hydrocarbons and the duration of the second soak step, CNTs with different lengths were produced.

Table 5. Recipe information for vertically aligned CNT growth on SiO_2.

Step Name	Temperature	Time (min)	Ar (sccm)	H_2 (sccm)	CH_4 (sccm)	C_2H_2 (sccm)
Ramp	25→800 ºC	12	500	0	0	0
Soak	800 ºC	10	500	0	0	0
Growth	800 ºC	1-60	0	500	1000	110
Cool	800→25 ºC	200	200	0	0	0

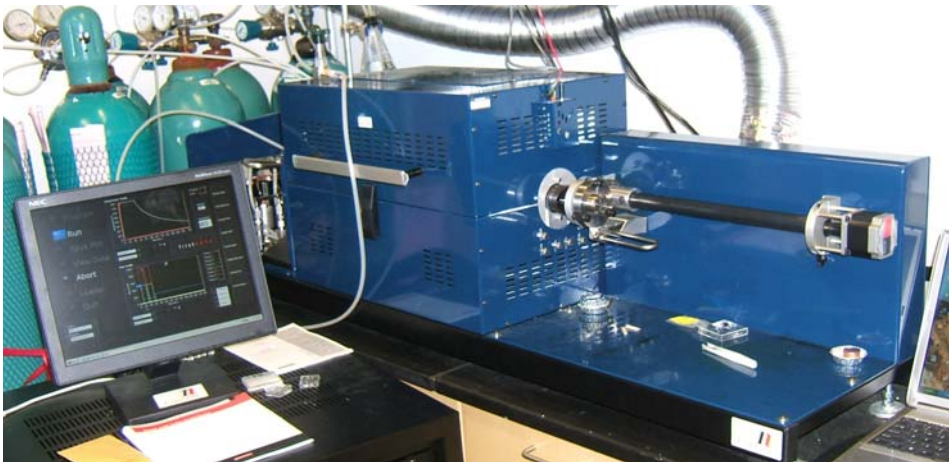

Figure 34. First Nano Easy Tube system used to grow carbon nanotubes with vertical alignments.

The catalyst and growth substrate were paramount to the success of the synthesis experiment. Silicon was used as a growth substrate because of its ability to withstand very high temperatures and its relatively low cost. Silicon dioxide (SiO_2) was deposited on top of the silicon using plasma enhanced chemical vapor deposition (PECVD). SiO_2 provided a diffusion barrier to prevent silicides from forming between the silicon and catalyst. The catalyst used for these experiments was 5 nm of thermally evaporated iron. The evaporation was performed using an electron beam deposition system from CVC. This catalyst thickness was chosen because it was thin enough to yield substantial CNT coverage. If the catalyst film were too thick, it would be too dense to allow tall CNT growth. Figure 35 shows the schematic of the substrate and catalyst used for this experiment.

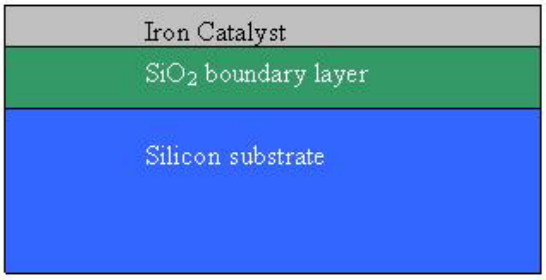

Figure 35. Schematic of substrate and catalyst used for CNT length measurements and transfer experiments.

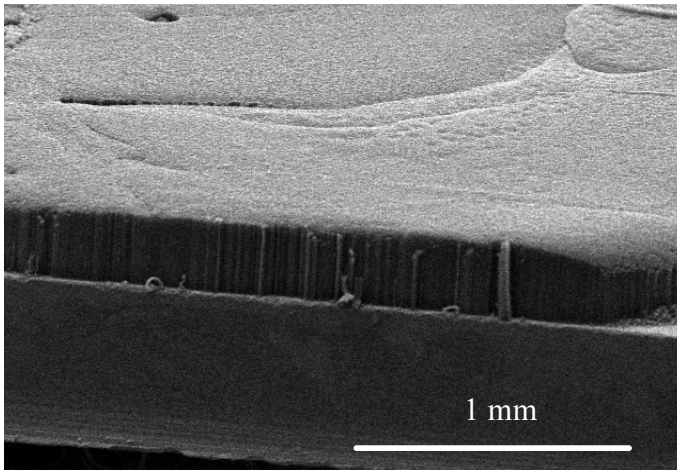

Figure 36. SEM image of vertically aligned CNTs produced with a five minute growth phase.

At a temperature of 800 ºC, a growth rate of approximately 45 μm/second was observed. As will be discussed in the Results section of this chapter, the growth of the CNTs was not constant the entire time. The lengths of the CNTs with relation to growth time followed an asymptotic curve leveling approaching 225 μm.

Water Assisted Etch

The adhesion of the carbon nanotubes to the substrate is a function of their adhesion to the catalyst particle as well as the catalyst particle itself to the substrate. It has been shown that introducing water vapor, as carried by an inert gas, after the growth

phase can help to reduce amorphous carbon within the array, etch the end caps of the nanotubes, and also etch away at the CNT/catalyst interface as shown in Figure 37 *[34]*.

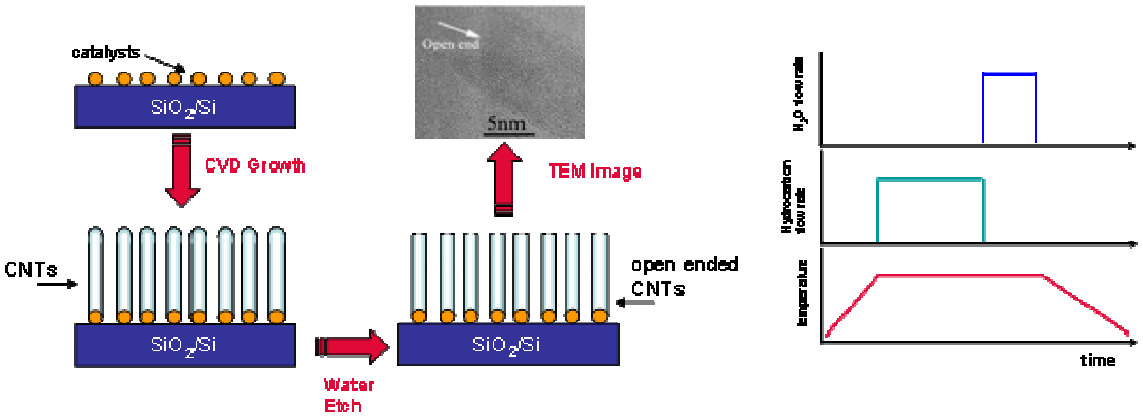

Figure 37. Schematic of procedure for water vapor etching of CNTs. The end caps and the interface between the catalyst particle and the nanotube are deteriorated.

A bubbler apparatus was created to interface with the existing tube furnace. Argon was used as the vapor carrier and the flow rate was controlled with an external mass flow controller. A regulating valve was placed downstream from the bubbler in order to prevent any contamination by the water during the growth phase. No air was allowed to enter the system because it would oxidize and destroy the nanotubes.

Figure 38. Bubbler apparatus used to introduce water vapor into the tube furnace.

The water vapor was introduced immediately after the CNT growth phase at the growth temperature of 800 ºC. This step lasted 5 minutes in which flow rates between 40 and 160 sccm were tested. Examinations of CNT length, purity, coverage, and adhesion were performed for each sample tested during this experiment.

Transfer Process

To effectively transfer vertically aligned carbon nanotubes two aspects were considered, host substrate adhesion and new bond strength. The host substrate adhesion was weakened by the water vapor etching step during synthesis. At times, the adhesion force of the CNTs to the growth substrate was so small that the CNT array would curl off but still maintain the shape of the chip.

In order for the new bond to be considered as a viable method of integration for CNT thermal interfaces, it must be created at low temperatures (< 300 ºC, similar to solder reflow temperatures) and it must possess a low thermal resistance. Processing

temperatures over 300 ºC could destroy the carbon nanotubes and may not suitable for some devices. This temperature limit ensured that any device that could be soldered to a printed circuit board (PCB) could also be bonded using the new method. The idea of gold welding has been used in wafer bonding processes for semiconductor manufacturing. However, understanding the melting point of gold (thermal conductivity ~ 320 W/mK) decreased with decreasing particle size *[121]* gave way to the idea of using a gold weld to transfer the CNT arrays. A thin layer of gold (500 nm) with a sublayer of titanium or chromium (50 nm) for adhesion was deposited on the tips of the CNTs using electron beam deposition. Since the layer of gold was so thin, a continuous film was not established, and small particles rested atop the CNT bundles.

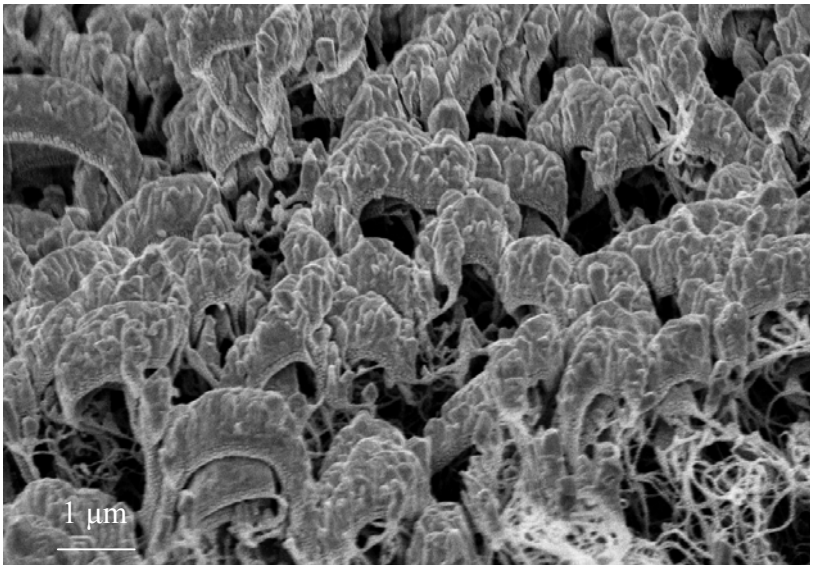

Figure 39. SEM image of gold particles on tops of CNTs.

The CNTs with gold tips were bonded to another substrate using a hot press at temperatures between 150 ºC and 200 ºC. This process is ideal for bonding to electronic materials such as copper and gold. In order to bond to other nonmetals, a thin film of copper or gold on the material surface may be required. The hot press was used to

maintain a constant temperature throughout the thickness of the system and to provide uniform pressure. However, only a small amount of pressure (not measurable with the press) was needed to create the bond. Light pressure was needed to assure that all the CNT tips would come into contact with the adjoining surface. Although the CNT were deformed under the pressure of the hot press, examination of the CNTs using an SEM after the bonding process revealed no permanent deformation. The applied pressure for this process was not optimized.

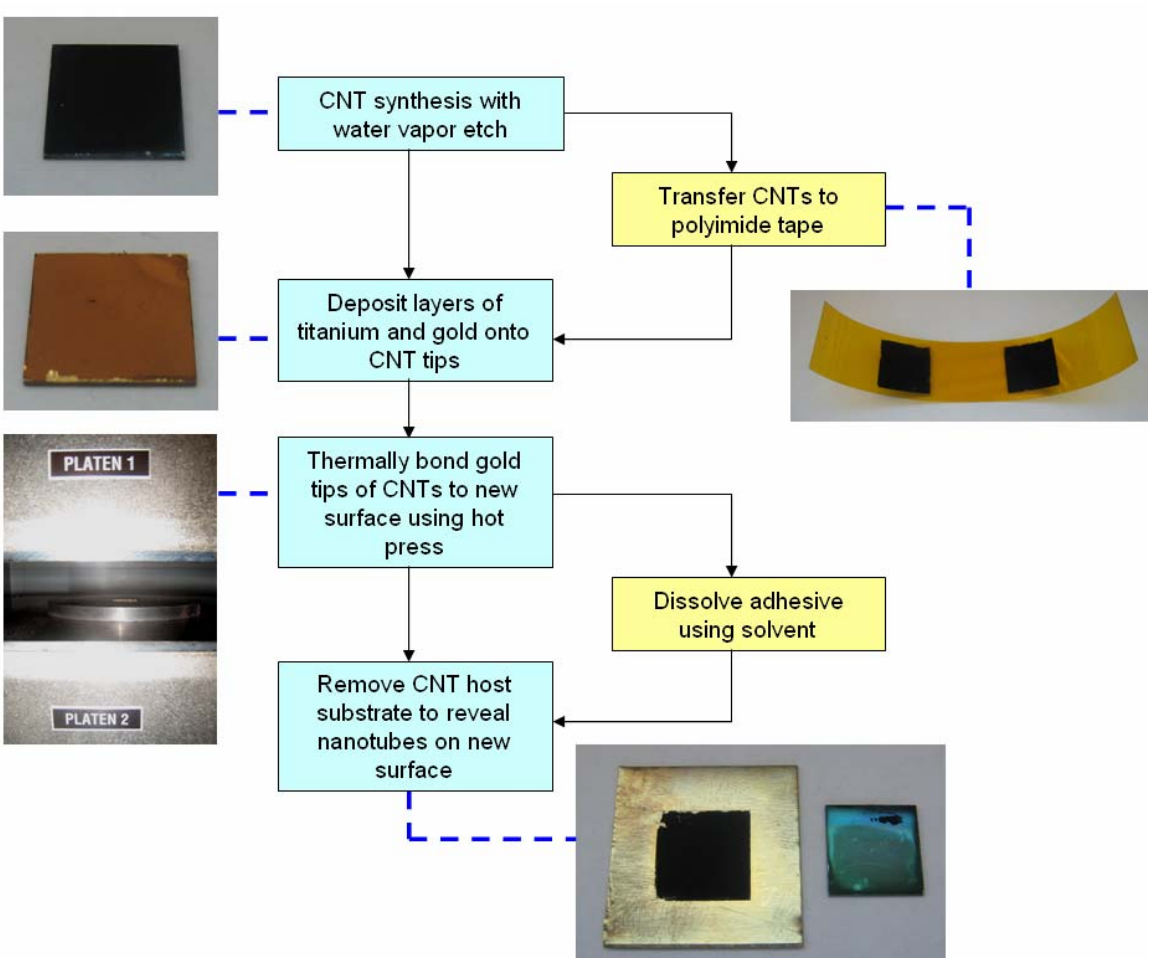

Figure 40. Flow chart for gold bonding transfer process of vertically aligned carbon nanotubes.

Results

CNT Length

The length of the CNT arrays was measured using a Hitachi 3500 SEM. Different CNT samples were created with varying growth times ranging from one minute to sixty minutes. A SiO_2 sublayer of 500 nm was employed to protect the 5 nm thick Fe catalyst film from diffusing into the silicon. The flow rates for the reactant gases given in Table 5 were used. Figure 41 shows the length of the CNT arrays as a function of growth time.

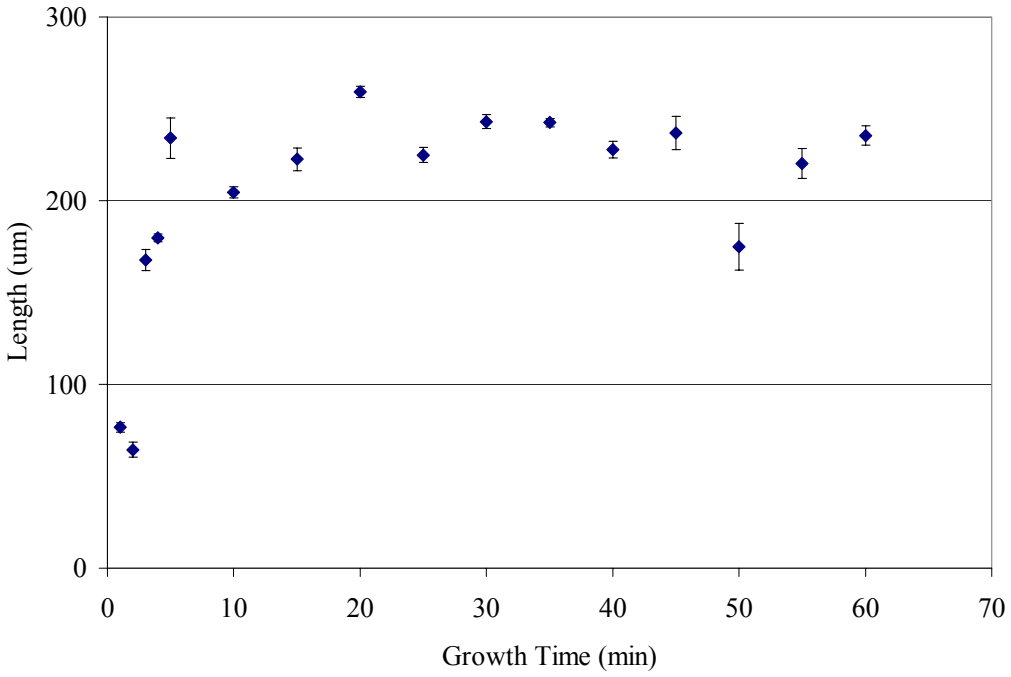

Figure 41. CNT length as a function of increasing growth time.

An asymptotic curve leveling out at approximately 225 μm was observed. The majority of CNT synthesis took place within the first 5 minutes of the hydrocarbon introduction. CNT growth was slowed significantly after five minutes because the CNT array at that point had become quite dense and the reactants were no longer able to reach

the catalyst particle. Since the growth of a carbon nanotube occurs at the catalyst, the rate of CNT growth is limited by the ability of the carbon gas to reach the catalyst. The idea of diffusion limited growth rate is outlined by Zhu et al *[34]*. Therefore, to maximize the efficiency of the process, growth times of five minutes were used for the water vapor etching experiments. The CNTs were etched by introducing water vapor molecules, carried by Argon, into the tube furnace after synthesis. The end caps of the CNTs are more susceptible to etching because of the highly strained pentagonal structure they posses *[25]*. By elevating the flow rate of water vapor, more of the individual tubes can be etched. Figure 42 shows the etching effect of the water vapor with increasing flow rates on the lengths of the CNT arrays.

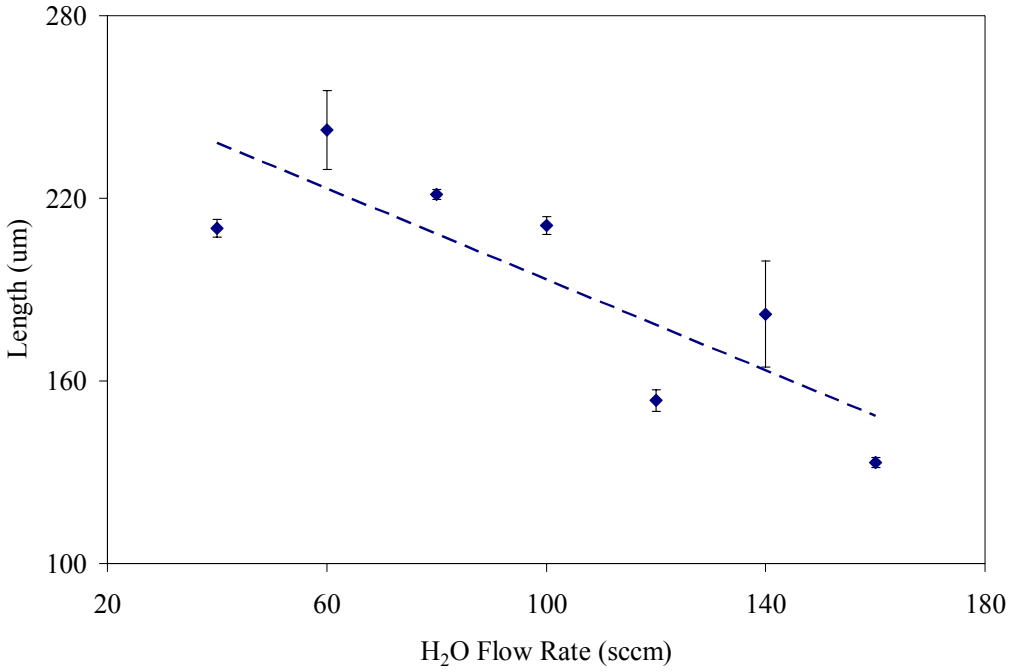

Figure 42. CNT length as a function of water vapor flow rate.

Raman Spectroscopy

Raman spectroscopy observes the inelastic scattering of photons with a surface which can be related to materials properties. Carbon nanotubes have been shown to possess a few Raman active modes. The *G*, or graphitic peak around 1560 cm^{-1} is an indicator of the graphitic nature of the CNTs *[122]*. Associated with the *G* peak is the *D*, or defect peak. The *D* peak, at approximately 1300 cm^{-1} is representative of the disorder present in the sample. The ratio of these two peaks is commonly used to assess the quality of CNTs. However, the ratio of the *D* peak with another peak, *G'*, at 2700 cm^{-1} has been suggested to be a more sensitive measurement of CNT purity *[123]*.

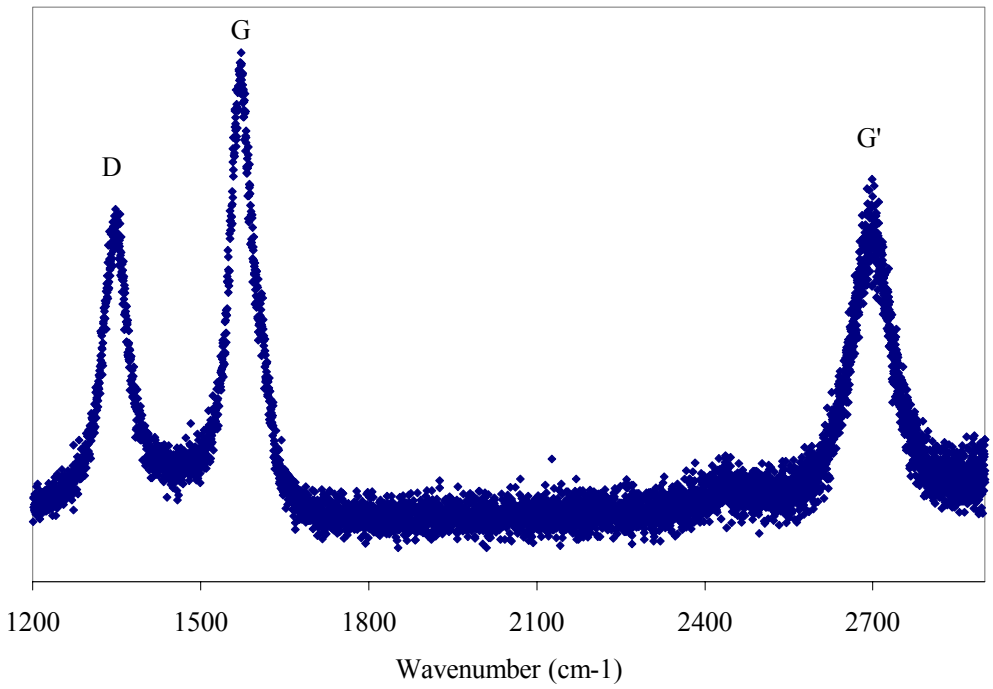

Figure 43. Raman spectra of vertically aligned carbon nanotubes with notations for the D, G, and G' peaks.

In this experiment the *G/D* and *G'/D* ratios were measured for CNT samples produced with varying growth times, and samples etched with different water vapor flow

rates. The Raman microscope used for this study utilized a 488nm wavelength laser as the energy source. The greater the intensity of the G and G' peaks with respect to the D peak suggests CNTs with greater purity. For this study, the Raman purity analysis was an assessment of defects and amorphous carbon present in the CNT arrays. Other assessments of purity (such as TGA or energy dispersive spectrometer, EDS) can include the presence of chemical functionalities and chemical particles. Figure 44 and Figure 45 show the trends of the *G/D* and *G'/D* ratios with increasing growth time and increasing water vapor flow rate, respectively.

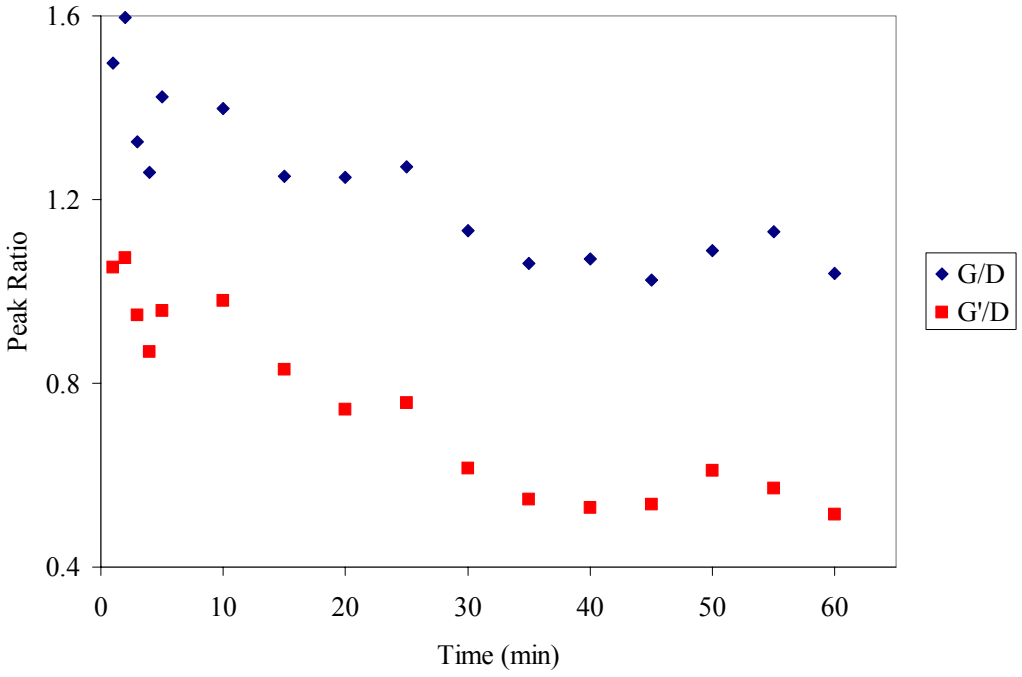

Figure 44. Raman peak ratios as a function of growth time.

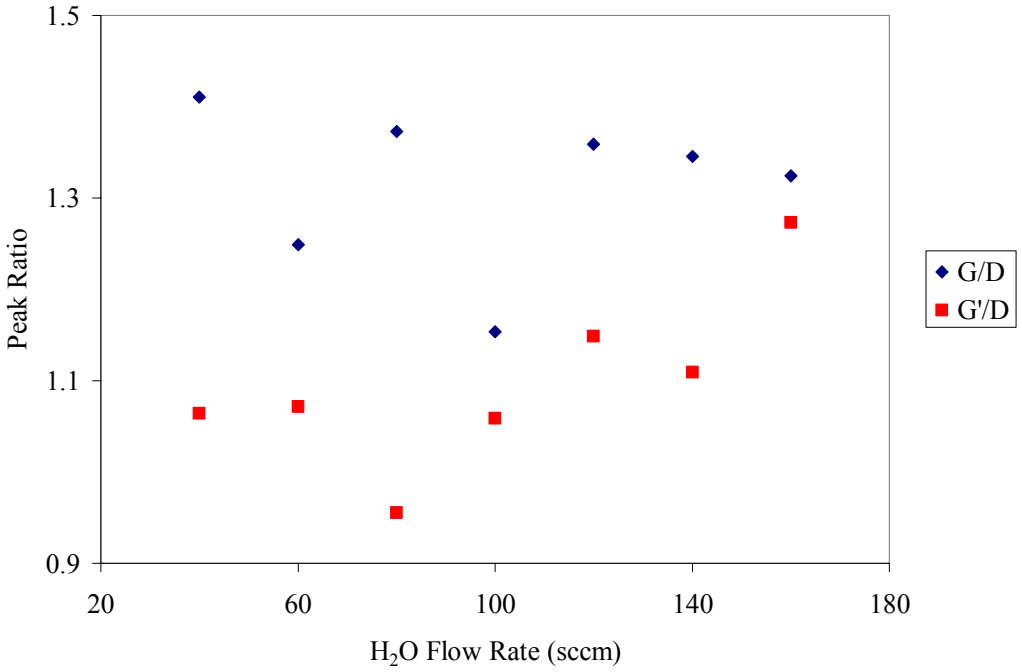

Figure 45. Raman peak ratios as a function of water vapor flow rate. Growth time for each sample was 5 minutes.

As growth time increased a noticeable decreasing trend with both ratios was observed. This was attributed to the build up amorphous carbon on the surface of the CNT arrays. At a certain point in the growth process the hydrocarbons were unable to reach the catalyst particle due to the increasing density of the CNT arrays. Therefore, the CNTs stopped growing, and amorphous carbon began to accumulate. The purifying effects of the water vapor etch step were inconclusive.

Transfer

To assess the effect of the water vapor etch step on the adhesion forces of the CNTs to the growth surface, samples with varying H_2O flow rates were prepared. CNTs grown for 5 minutes with a 5 nm thick iron catalyst were used. At higher water vapor flow rates, the coverage of the CNTs on the chip became less complete. For a quick assessment of transferability, polyimide tape was used to remove the vertically aligned

CNTs from the growth substrate. At each flow rate transfer was qualified as 'None', 'Partial', or 'Complete'. These ratings of transfer gathered using polyimide tape were verified using the gold weld transfer technique. Table 6 displays the assessments of the growth coverage and transferability of each sample at the different flow rates.

Table 6. Assessment of carbon nanotube coverage and transferability with varying flow rates of H_2O.

	Water Vapor Flow Rate (sccm)							
	0	40	60	80	100	120	140	160
CNT Coverage	Full	Full	Full	Full	Partial	Partial	Partial	Partial
Transfer	None	Partial	Partial	Complete	Complete	Complete	Complete	Complete

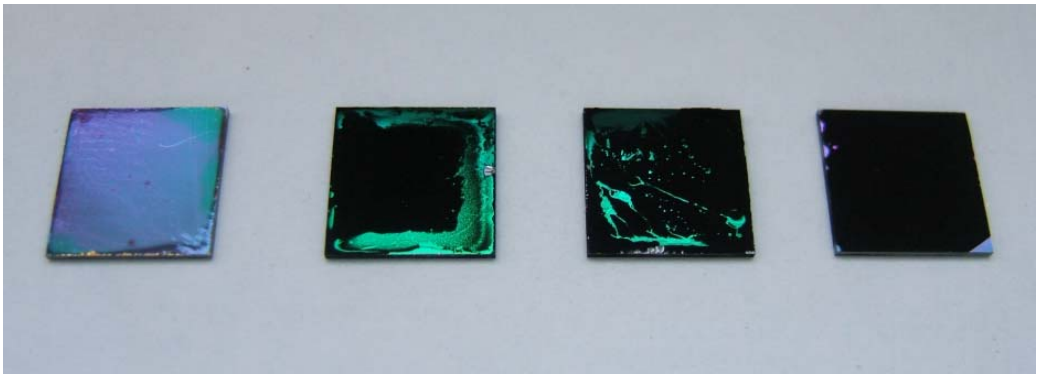

Figure 46. Examples of growth substrate after (from left to right) complete transfer, partial transfer, and no transfer using the gold bonding process.

Understanding the balance between transferability and CNT coverage, a flow rate of 80 sccm was selected for the remaining transfer experiments. With this method of production and transfer, CNTs were able to be adhered to any surface with a gold layer. Additionally, the direct transfer to copper with no gold or titanium layers on the copper surface was achieved.

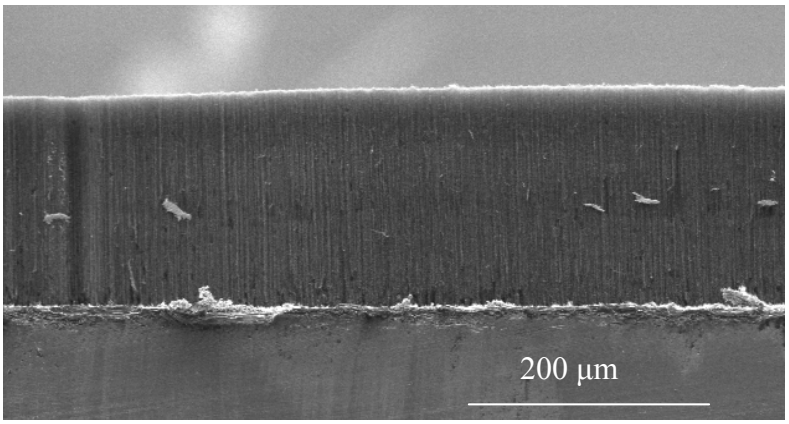

Figure 47. Cross section of CNTs transferred onto silicon using gold welding technique.

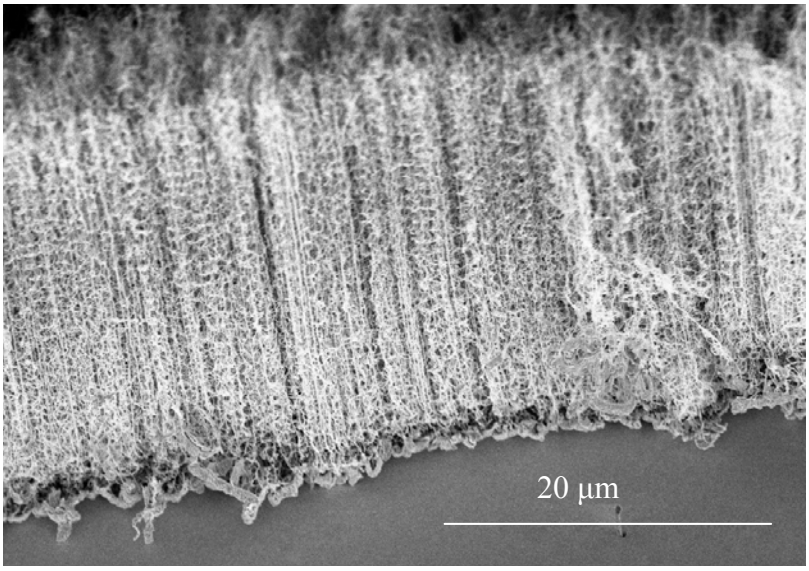

Figure 48. Close-up image of interface between CNTs and substrate using gold bonding technique.

In addition to direct transfer from growth substrate to another surface, a technique for transferring CNTs to and from polyimide tape was developed. Once attached to the tape, the tubes were coated with titanium and gold layers. The tube arrays were then bonded to another surface just like the direct transfer method. Upon the creation of the gold bond, the adhesive on the tape was dissolved using a solvent such as acetone.

By growing CNTs with such low adhesion, transfer into other thermal interface materials was possible. Transfer into Arctic Silver 5, a commonly used thermal adhesive, was accomplished without metallization of the CNT tips. The thermal epoxy was applied with an approximate thickness of 5 mils, and the silicon chip with loosely adhered CNTs was rested on top and applied a small amount of pressure. Upon the epoxy curing, the chip was removed leaving the vertically aligned nanotubes. CNT arrays were also able to be transferred into thin Sn/Bi solder layers. Metallization layers of Ti and Au were deposited on the CNT tips to promote wetting of the lead free solder surface. Sn/Bi solder paste from EFD Company was reflowed at 140 ºC and the CNT chip was rested on top and small amounts of pressure were applied. Once the system was cooled the chip was removed.

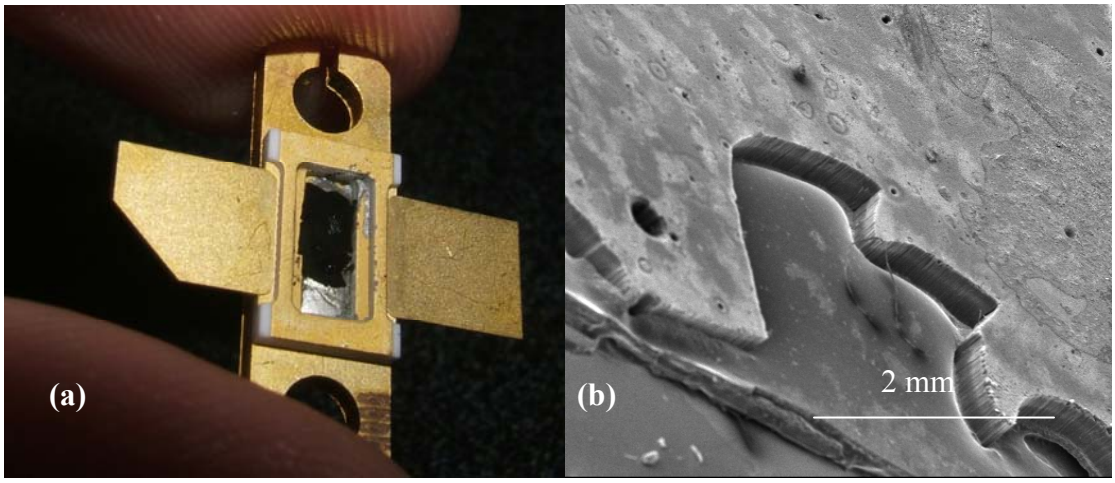

Figure 49. (a) Vertically aligned CNTs transferred into Sn/Bi solder in a small recessed area, (b) CNTs transferred into Arctic Silver thermal epoxy.

Uniformity of the thermal epoxy and solder paste were an issue. By applying pressure during bond formation, the fluids would spread thus causing irregularities with the film thickness.

Tensile Test

CNT arrays with an average length of approximately 30 μm were bonded to a copper sheet with a titanium and gold coating. Next, 50 nm of titanium and 500 nm of gold were deposited onto the exposed CNT tips. Finally, a silicon chip (1 cm^2) topped with thin films of titanium and gold (same thicknesses as before) was bonded to the tops of the CNTs. This test system was chosen to model a device (Si) bonded to a heat spreader (Cu).

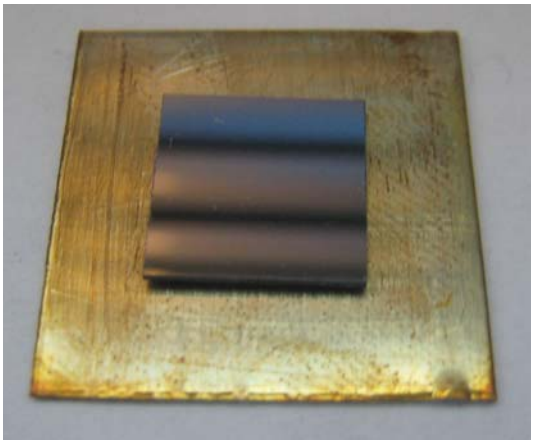

Figure 50. Tensile test sample before testing. Silicon chip bonded to CNTs that were transferred onto copper.

The tensile test was performed using an MTS Insight 2 electromechanical test system equipped with a 100 N load cell and compression platens. Both sides of the sample were attached to the platens using quick drying glue. Once the adhesive was completely set the top platen attached to the load cell pulled away at a constant rate of 3 mm/minute until fracture. Forces greater than 35 N were required to sever the bonds.

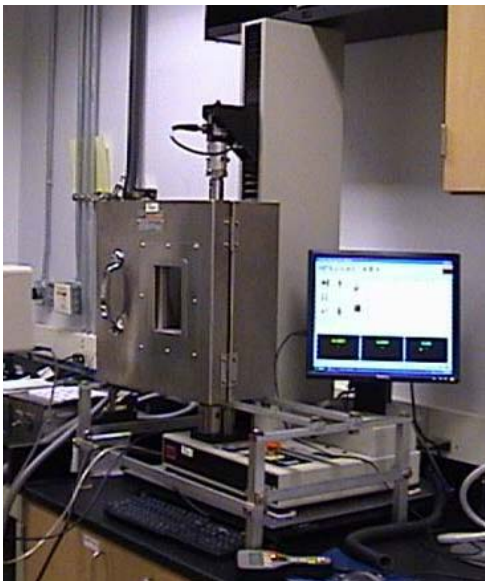

Figure 51. MTS Insight 2 electromechanical test system used to perform tensile tests.

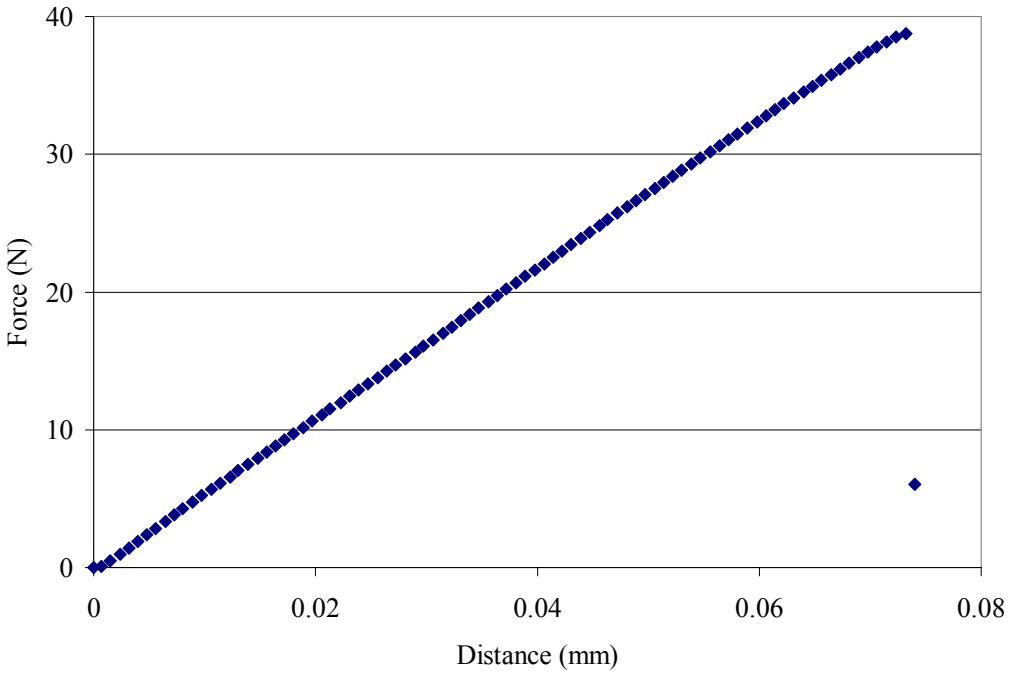

Figure 52. Tensile test results of CNT interface with gold bonding.

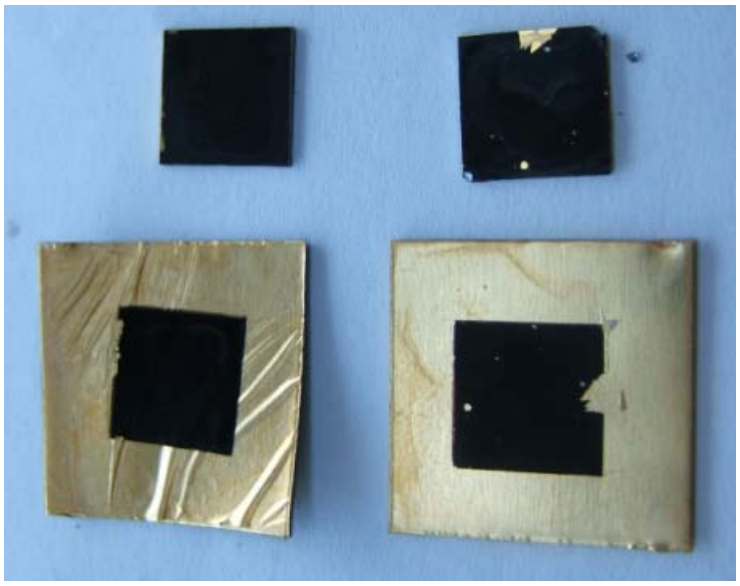

Figure 53. Severed bonds after tensile testing.

Upon examination of the copper sheet and silicon chip, CNTs were present on either side (Figure 53). This suggests that the CNTs were severed before the bond, and that a strong bond was produced on both sides of the interface. Other research groups have created similar bonds using an anodic bonding method. With this technique, the Fisher group out of Purdue has reported tensile strengths of 1.2 N. Their bonding method, like the one reported in this thesis, required a temperature of 200 ºC, but there was no mention of the ability to be performed at lower temperatures. Their measurement was recorded using a sample with a much smaller area (5.34 mm x 5.17 mm). Additionally, the area used by this group (bond affected area) was a modified surface area which accounted only for the points of contact between the tubes and substrate. To compare, the Fisher group recorded a bonding force of 4.35 N/cm^2 while our value was 35 N/cm^2. Moreover, the area used in our calculations reflects the size of the chip being bonded. Employing a "bond affected area" to our measurements would only widen the gap between us and the other group. The eight time increase in bond strength over a much larger area is evidence of a superior bonding method.

Conclusion

The ability to control the length of vertically aligned carbon nanotubes was accomplished by varying the growth time. Increasing growth time was shown to have an adverse effect on the purity of the CNT array due to the accumulation of amorphous carbon on the tubes. Introducing water vapor after the growth phase had little effect on the purity of the CNT arrays, but did weaken the adhesive force between the CNTs and the growth substrate. With such low adhesion, the vertically aligned CNT arrays were able to be transferred to other surfaces through a novel gold bonding method. These bonds exhibited substantial strength under a pure tensile load. The ability to transfer CNTs to materials not suited for CNT synthesis such as gold, copper, and diamond is attractive for thermal interface design. Also, the ability to first transfer to a polyimide adhesive then to another surface is desirable for storage purposes and manufacturing procedures using roll to roll processing.

CHAPTER 5

THERMAL RESISTANCE OF CARBON NANOTUBE THERMAL INTERFACES

Introduction

The thermal resistance of vertically aligned carbon nanotubes with differing levels of adhesion was measured using the photoacoustic method. Samples that were grown with low levels of adhesion demonstrated a dramatic increase in thermal resistance with applied pressure. This reaction to pressure was a consequence of the nanotubes becoming severed from their growth surface. Carbon nanotubes that were transferred using the novel gold bonding process described in the previous chapter showed a decrease in resistance with applied pressure. This proves that the bond created during transfer is of significant rigidity. The resistance values of the transferred CNT interfaces were on the level or less than the best published results to date.

CNT interfaces were also integrated into high brightness LED systems to investigate their cooling abilities. The junction temperature of the LED was found using the measured forward voltage of the device. Using the junction temperature the thermal interface resistance was calculated. Comparing the thermal interface resistance of a CNT interface and a lead free solder interface, it was shown that the CNT interface performed similarly. Finally, IR spectroscopy was used to measure the die temperature of LED with solder and CNT interfaces. The temperatures measured in this experiment were compared with junction temperatures found using the forward voltage technique. Comparatively, the two measurement techniques elicited similar results thereby validating the forward voltage measurement technique.

The experiments outlined in this chapter help to elucidate the promise of carbon nanotubes as a thermal interface material. Specifically, using the unique bonding process

developed in this study, the ability to integrate CNTs into many more devices with substantial adhesion and low thermal resistance can be accomplished.

Experimental Setup

Photoacoustic Measurement

Thermal resistance measurements were performed using a photoacoustic (PA) method developed by Prof. Xianfan Xu at Purdue University *[107]*. The PA technique is a straight forward noninvasive procedure for measuring thermal properties of solids. It has also been proven successful at obtaining thermal conductivity of thin films. A laser heating source was irradiated periodically on the sample surface and the acoustic response of the air above was measured. This response was subsequently related to the thermal properties of the sample. By fitting the phase shift and amplitude of the PA signals, thermal property data was obtained. For these experiments, a 1-D thermal model was assumed. Therefore, the thermal conductivity of the CNTs was assumed isotropic.

Each sample that was tested was topped with a 25 μm thick silver foil (99.998%, Alfa Aesar, Inc.) and coated with 80 nm of titanium via electron beam deposition. A reference measurement of silicon coated with the same Ti thickness was also prepared. The reference measurements were conducted at different pressures because, according to PA theory, phase shift is independent of pressure, while amplitude is proportional. Helium was used as the gas medium for the measurements, as opposed to air or nitrogen, because of its higher thermal conductivity, thus producing the best signal to noise ratio.

LED Junction Temperature Measurement

The junction temperature of a light emitting diode (LED) can be directly correlated to its forward voltage *[124]*. The change in voltage with respect to junction temperature was measured for each LED tested. To create a calibration, the backside temperature of the LED was measured using a thermocouple directly touching the surface

while the temperature of the junction was modulated using a hot plate. At a series of different temperatures a current pulse of 54 milliseconds was applied using a Keithley 2400 source meter. The voltage at each impulse was recorded and plotted. A series of measurements at each temperature for each different current were made to assure stability of the LED system and accuracy. Once the data were plotted, linear curves were fitted to each data set and the slope, *dT/dV,* was revealed. These trends had a remarkably linear nature, each of which possessed an R^2 correlation factor greater than 0.99. Each LED was calibrated to ensure accuracy when converting the voltage measurements to junction temperature. The slope, *dT/dV*, for each device was somewhat different at the various current settings.

Because the LED was moved from one set up to another, at the beginning of each experiment the voltage of the LED for each current setting at room temperature was measured in similar fashion to the calibration. With a data point of voltage (x_1) and temperature (y_1) and the slope (m) previously mentioned, the temperature of the LED could be found via the point slope linear equation $y = mx+b$.

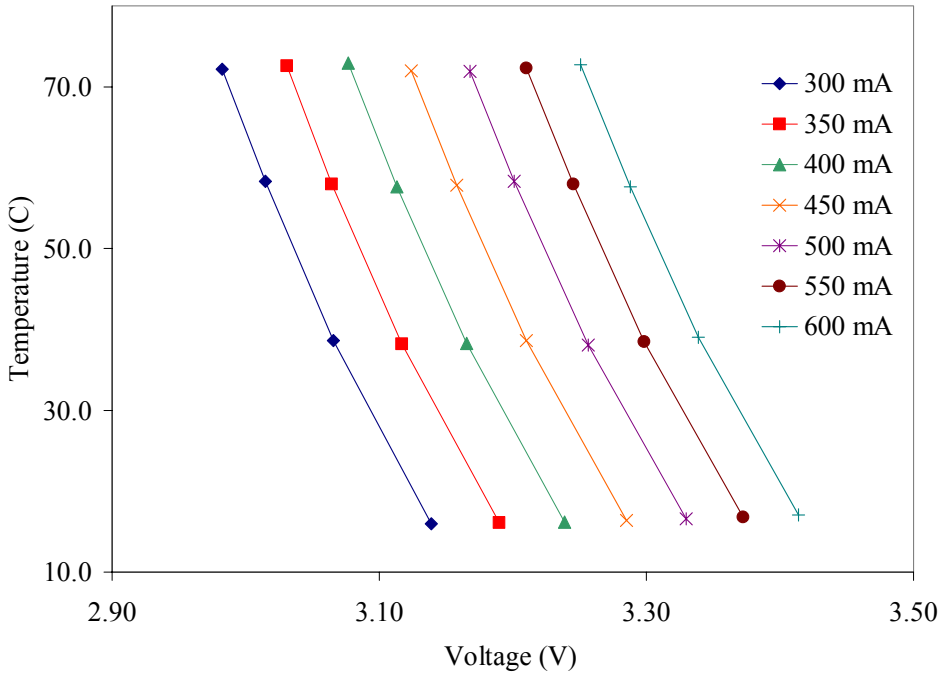

Figure 54. Calibration curves of LED for various currents.

To test the thermal interfaces, the calibrated LED was position with the TIM on a copper block with small hole through the middle. The hole allowed a thermocouple (diameter of 0.55 mm) to contact the backside of the LED/TIM system. The copper block was set on a thermoelectric cooler set below room temperature and fiberglass insulation was placed of over the LED. These two measures were taken to ensure the majority of the heat being generated by the LED would go through the TIM and thermocouple.

The resistance of the entire test system is shown in Figure 55. $T_{junction}$ is the junction temperature of the die which we measured via the forward voltage. The package resistance, $R_{package}$ is the thermal resistance of the layers between the die and the backside heat plate of the LED. $R_{contact\_1}$, $R_{interface}$, and $R_{contact\_2}$, cumulatively form the interface resistance of the TIM because each value is predicated on the TIM's material properties. The sum of these three resistance values will be called R_{TIM}, or the thermal interface resistance. Finally, R_{plate} is the resistance of the thin copper plate which was used to mount the different LED samples. Knowing the thickness of the copper plate (508 μm), the area of the LED (63 mm^2) and the thermal conductivity of copper (401 W/mK), R_{plate} is found to be 0.02 K/W. The temperature recorded by the thermocouple is designated as $T_{backside}$.

To get the package resistance of the LED, the same set up was used but with no interface material and the thermocouple applied directly to the back plate of the LED. Knowing the temperature from the forward voltage and the backside temperature of the LED from the thermocouple, the package resistance (K/W) was easily calculated (ΔT/power).

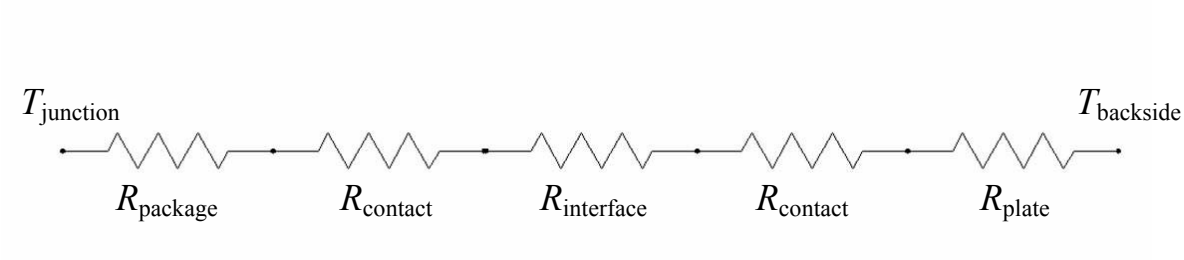

Figure 55. Thermal resistance network for LED junction temperature experiment.

Naturally, as pressure is applied to the interface, the thermal resistance will decrease. The size and geometry of the LED makes it difficult to apply direct vertical pressure. Therefore, a flat cord was wrapped around the set up and laid over the bulb of the LED. At the end of this cord, a reservoir was attached in which weights could be added. Knowing the mass and the area of the device, the applied pressure was easily derived.

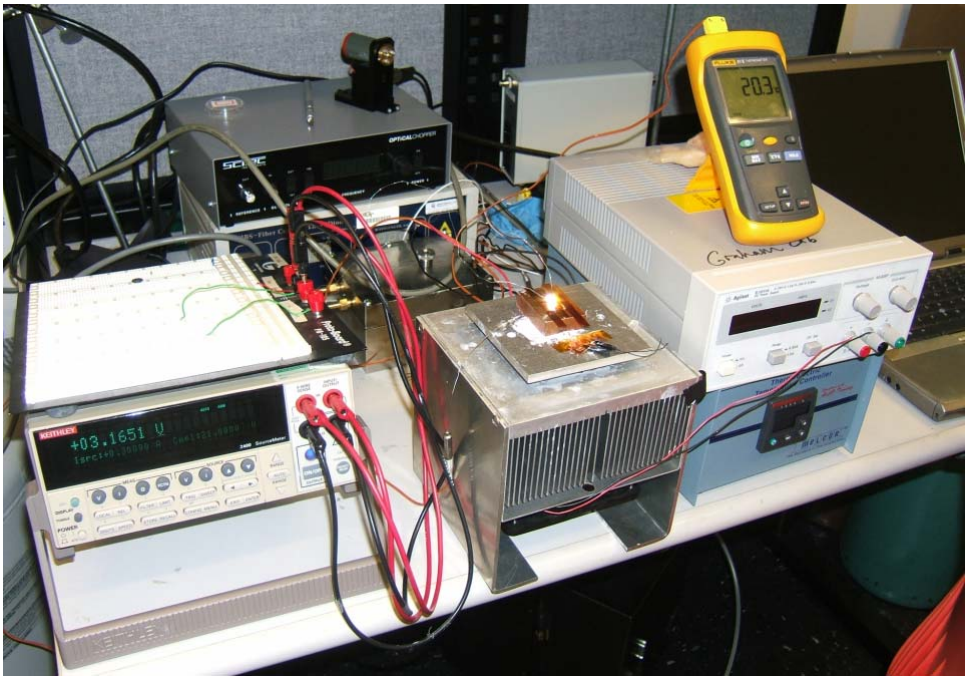

Figure 56. Experimental set up for LED thermal resistance measurements.

As a second form of die temperature measurement, infrared (IR) spectroscopy was used to validate the temperature measurements obtained through the forward voltage technique. In order to get a legitimate temperature measurement of the LED using IR, the bulb of the device had to be removed. The bulb prohibited the camera from focusing directly on the die. Additionally, the top of the LED must be in a clear line of sight with the camera, so no insulation on the top side could be used. The temperatures measured in these experiments could not be used to find the thermal resistances of the respective TIMs, but through direct comparison could offer a qualitative assessment as to which interface performed better.

Results

CNT Interface Resistance from PA Method

The interface resistance for several different vertically aligned CNT arrays was measured using the photoacoustic method at Purdue University. These measurements were taken at a series of applied pressures in hopes of observing a convergence in thermal resistance. Thermal resistance should decrease with increasing pressure because of the creation of more contact areas. Additionally, air within the interface is evacuated. However, thermal resistance may increase if the interface is not mechanically sound. The mechanical stability of vertically aligned CNT arrays is largely depended on their adhesion to the growth surface. In this experiment CNT samples were tested to observe the effect of CNT adhesion on thermal resistance.

The experimental control was CNTs grown on a SiO_2 substrate with an iron catalyst. These samples were synthesized with a one minute growth phase and had an average height of approximately 87 microns. The adhesion for samples such as these was qualified in previous experiments. Attempts at transferring CNTs grown in this matter

were unsuccessful. As previously mentioned, a silver foil was placed on top of the CNTs for this experiment.

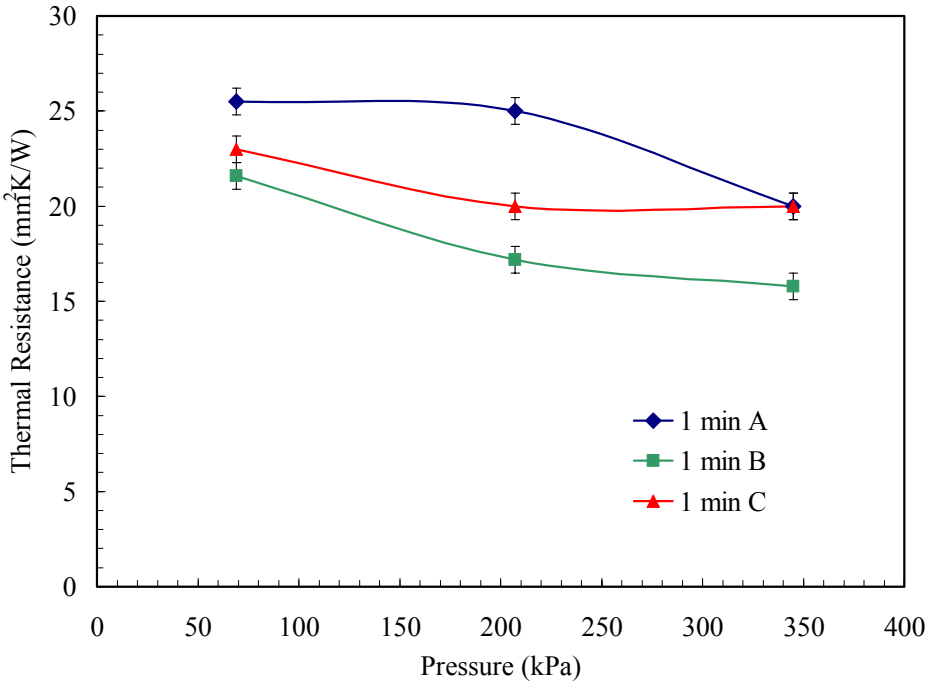

Figure 57. Thermal resistance of CNT array grown on SiO_2 with 5nm Fe catalyst for 1 minute.

For each of the three samples in this set, a convergence was not observed. After loading, inspection of the samples revealed some flaking and removal of the CNTs. The absence of convergence can be attributed to the lack of adhesion the CNTs had to the host substrate. The buckling of the CNTs can have detrimental effects on the thermal resistance. First, the axial alignment is lost thereby limiting the most efficient heat transfer mechanism of the tubes. Second, more contact points between the tubes are created causing more tube to tube contact resistance. Finally, air gaps are created by the non-uniform folding of nanotube bundles.

The effect of poor CNT adhesion on thermal interface resistance was exemplified with a test group of CNTs grown using the water vapor assisted etching technique. Introducing water vapor into the growth chamber after synthesis was shown to severely weaken the adhesion of the CNTs to the host surface. A water vapor flow rate of 80 sccm was used to weaken the CNT to substrate interaction. The nanotubes grown with substantially less adhesion, as expected, exhibited a worse thermal resistance response to applied pressure than the experimental control.

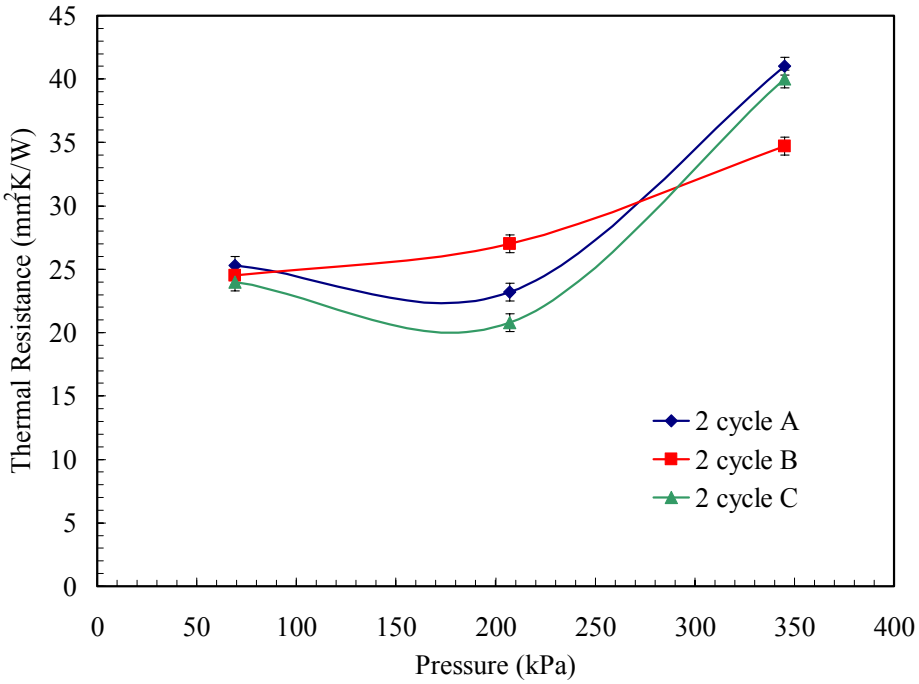

Figure 58. Thermal resistance of CNT arrays grown using the water vapor etching technique.

Interest exists in direct growth of vertically aligned CNTs onto heat spreading materials such as copper. Direct growth, with good adhesion, would allow package designers to forego CNT transfer procedures to the heat spreader. However, growth onto copper has significant challenges with regard to maintaining the integrity of the catalyst

particle. Unlike silicon, copper can more readily diffuse into the catalyst particle at high synthesis temperatures thereby rendering the catalyst ineffective. Boundary layers such as titanium and aluminum can be used to curb such effects.

Experiments were conducted in an effort to grown vertically aligned CNTs on thin copper surfaces. Although successful growth onto copper was achieved, it was not without the employment of several adhesion and boundary layers. A series of sublayers consisting of 20nm Ti, 20nm Al, 200nm SiO2 (evaporated), and 5nm Fe were deposited onto a 0.5 mm thick copper flashing. Vertically aligned CNT arrays were grown with comparable Raman peak ratios to that of the experimental control. Figure 59 shows SEM images of CNTs grown on copper.

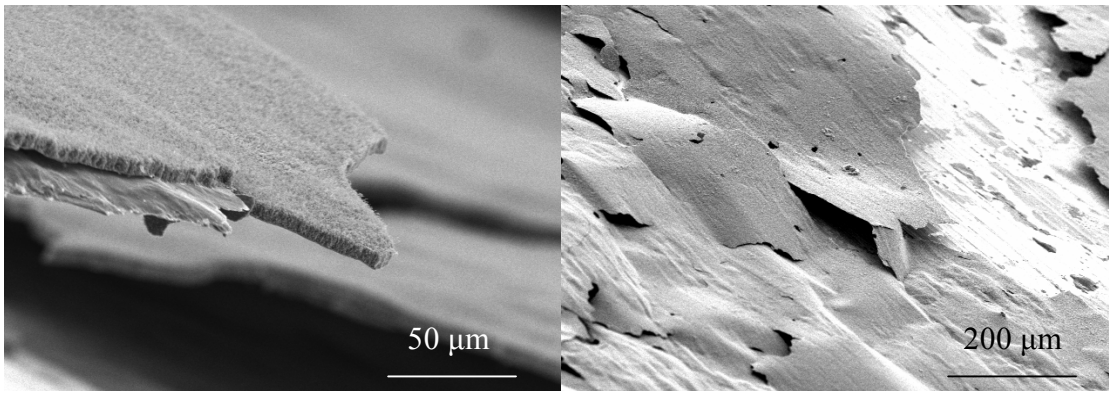

Figure 59. SEM images of CNTs grown onto copper surface.

Figure 60 shows the response of thermal resistance to applied pressure for CNTs grown on copper. Again, the rise in thermal resistance with increasing pressure is characteristic of poor adhesion. In this case, the increase in thermal resistance was exacerbated by both the nanotubes and sublayers pulling away from the copper surface. The SiO_2 sublayer was critical in achieving substantial vertically aligned growth. However, its brittleness was detrimental in maintaining quality contact with the copper surface during loading. The flaking and delamination of the CNTs is shown in Figure 59.

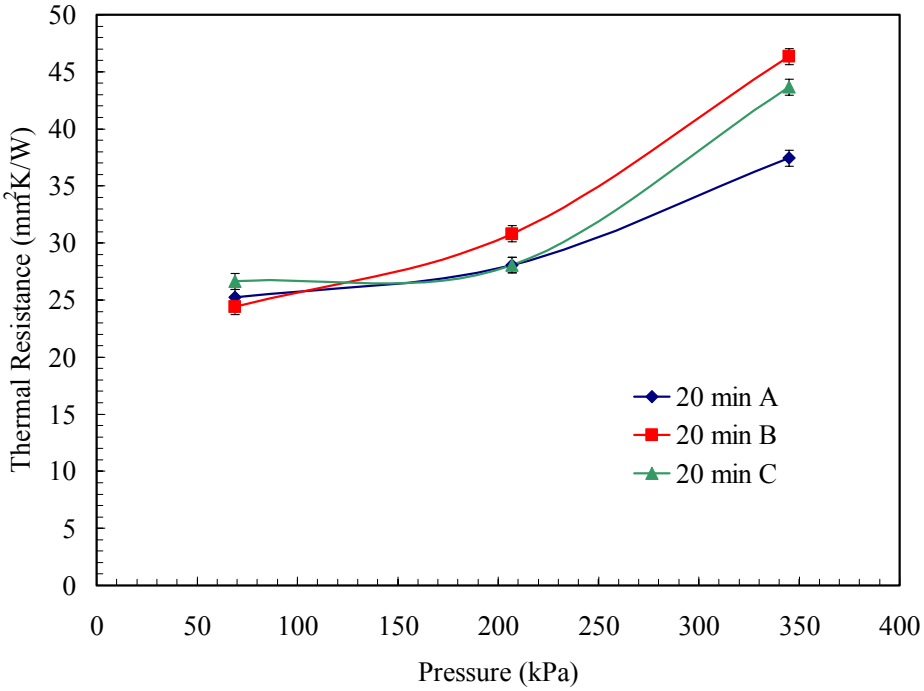

Figure 60. Thermal resistance as a function of applied pressure for CNTs grown on copper.

The previous two cases exemplify the need for increased adhesion between the CNTs and the substrate. This issue was addressed by using the gold bonding method to weld the CNTs to another surface. This process as described earlier has been shown to produce a significant adhesive force (> 35 N tensile force) between the CNT arrays and substrate. CNT arrays were synthesized using the water vapor etching technique for transferability. Titanium and gold layers were evaporated onto the CNT tips and then bonded to a silicon chip (it too with equal layers of titanium and gold). Each sample created for this test was examined to ensure complete transfer. Inspection of the bonded CNTs with a SEM revealed no structural damage to the alignment. Additionally, Raman spectroscopy data of the CNTs after bonding was in close agreement with pre-bonding scans.

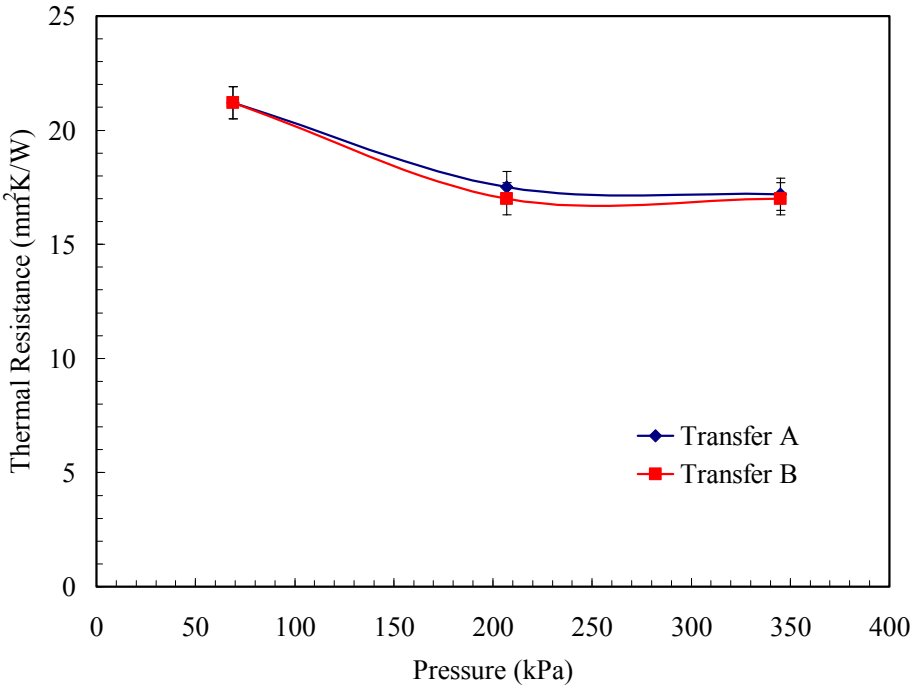

Figure 61. Thermal resistance as a function of applied pressure for transferred CNT interface.

Grown in an identical manner as the CNTs of Figure 58, the only meaningful difference between the two was the adhesion to the substrate. The post-pressure examination of the transferred samples revealed no flaking or lift-off, validating the claim of robust adhesion. These samples had CNT lengths greater than 125 microns which is considerably longer than the CNT thermal interfaces currently published. The resistance values of 17 mm^2K/W (Figure 61) achieved in this experiment were comparable to some of the best results by groups at Purdue and Stanford *[3, 4, 119]*.

A contact resistance that was not addressed in the creation of the previous test subjects was the interface between the silver foil, necessary for PA measurements, and the nanotube tips. Although the foil was pliable and could conform to the roughness of the CNT array, intimate contact was not established. For each of the next test samples, the silver foil was bonded to the tips of the CNTs. This was done in similar fashion as the transfer bonding. Titanium and gold layers were deposited on the tips of the CNTs

and the silver foil was placed on top then bonded. A small amount of pressure was required for this procedure to promote a high level of contact between the CNT tips and silver foil.

From the previous experiment (Figure 61), sample 'Transfer A' was redone with a bonded silver foil layer. The new sample consisted of a silicon chip with transferred CNTs (130μm) and a layer of silver foil bonded to the tops of the tubes. The thermal resistance of the new system with no applied pressure was reduced to 10 mm^2K/W. In comparison, the first sample with unbonded silver had a minimum resistance of 17 mm^2K/W with an applied pressure of 50 psi. The reduction in resistance by simply bonding the interface speaks volumes to the effectiveness of the procedure. Creating and maintaining real points of contacts through gold bonding only improved the thermal interfaces that were tested.

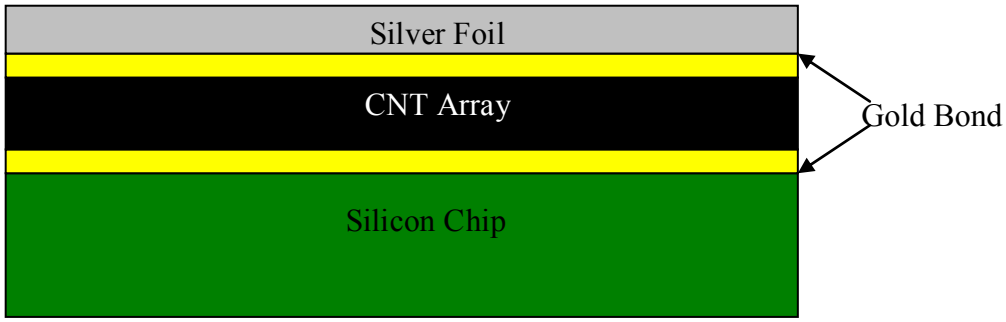

Figure 62. Schematic of transferred CNT array with silver foil bonded to the top.

Additionally, carbon nanotubes (~30μm) were directly bonded to a copper sheet. In this case, no gold was sputtered onto the copper. Again, silver foil was bonded to the tops of the transferred CNTs using the gold welding method. The thermal resistance of this system was measured to be ~10 mm^2K/W. The agreement of this sample with

'Transfer A' suggests the bond line thickness for CNT interfaces may have little importance under values of 150 μm.

Finally, samples of CNT arrays were grown onto silicon with a titanium adhesion layer of 30 nm and iron catalyst layer of 5nm. The thin film of titanium promoted a higher level of adhesion between the catalyst and substrate. With this catalyst and sublayer configuration, CNTs of approximately 10 to 15 microns in length were produced. As mentioned before, direct growth of CNTs onto heat spreading materials remains an attractive solution to many thermal management challenges. In this case, Si represented a heat spreading material. By bonding the silver foil to the exposed CNT tips average thermal resistances of 4.5 mm^2K/W with no applied pressure were achieved. This value is as low as the most recent published figures (Table 4). A reduction to 1.7 mm^2K/W was observed with a small applied pressure of 10 psi. The change in resistance indicated that some CNT tips remained unbonded to the silver foil. However, this resistance value is similar to some of the best published results to date.

The results of these experiments exemplify the success of the gold bonding transfer method in terms of increasing adhesion and lowing thermal contact resistance. Using this method, the CNT array is made more mechanically robust, and thermal contact resistance is significantly decreased. The thermal resistance values measured for transferred bonded CNT arrays was comparable with the thermal resistances of lead free solders. However, the thermal resistance of CNTs that were bonded, but not transferred, to the silver foil possessed a thermal resistance better than lead free solders, and better than any published results today.

CNT Interface Effect on LED Cooling

The junction temperatures of the LEDs were found by measuring the forward voltage at a certain current levels. The measured voltages were related to a linear calibration curve to obtain the temperature of the junction during operation. For this

experiment, LEDs were bonded with different thermal interfaces to copper stamps. The copper stamp helped facilitate transport of the test subject from location to location thereby increasing the efficiency and repeatability of the experiments.

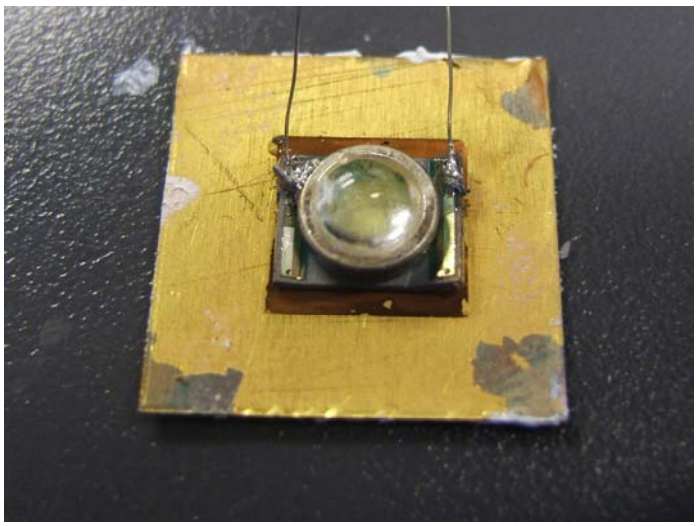

Figure 63. LED bonded to copper stamp with CNT thermal interface.

Two temperature measurements were needed during the experiment in order to calculate the thermal interface resistance; the junction temperature of the LED and the backside plate temperature. The backside plate temperature was recorded using a k-type thermocouple in direct contact with the back of the copper stamp. Using the thermal resistance network shown in Figure 55, the thermal interface resistance was obtained.

The package resistance of the LED was found by placing the device directly on the thermocouple with no interface or copper stamp between. The LED was allowed to reach steady state at a range of different currents at which time the forward voltage was recorded. The average package resistance was found to be 9.2 ºC/W. The manufacture reported LED package resistance, however, is 8 ºC/W. This discrepancy can be attributed to the uncertainty of the placement of the thermocouple on the backside of the

LED. Movement of the device on during the test was possible, although it was restrained.

Two interfaces were compared in this study, lead free solder (Sn/Bi) and bonded carbon nanotubes. Others were not as aggressively pursued because of the differences in manufacturing methods and probable applications. Both the solder bond and CNT bond were formed in temperatures of 150ºC. This manufacturing step could cause discrepancies in LED performance from device to device. Additionally, both bonds were mechanically sound unlike thermal greases. Finally, the CNT interfaces that were designed in this project are poised to compete directly with solder interfaces in device packaging applications, not with greases and PCMs in large scale heat sink systems.

For thermal interface resistance measurements a thermoelectric cooler was used to control the backside temperature. It was set to 14 ºC to promote conduction downward through the thermocouple. This, in conjunction with the top of the LED being insulated, limited the heat being lost through the bulb. The thermal resistances of the interface at different power levels for the solder and CNT interfaces are shown in Figure 64. The data for both interface materials are comparable.

The resistance measurements shown in Figure 64 include the LED package resistance. Being that these values are less than the previously measured or reported package resistance values, one cannot take this data at face value. Considerable effort was made to ensure the backside thermocouple was directly underneath the die of the device, and that it was in direct contact with the copper stamp. Deviations from the desired position would affect the thermal resistance measurements. Also, temperature fluctuations with the thermoelectric cooler complicate the backside temperature measurements. Furthermore, the thermal and mechanical stresses that were induced on the LEDs while creating the bond could have affected the individual device package resistance. The package resistance values measured in this study and those reported in the device literature were values based on a device that had not been bonded. The effects

on package resistance of the manufacturing steps taken to create the different bonds are unknown and should be investigated in future works. All things considered, the performance of the lead free solder and bonded CNT interfaces were similar and within the margin of error.

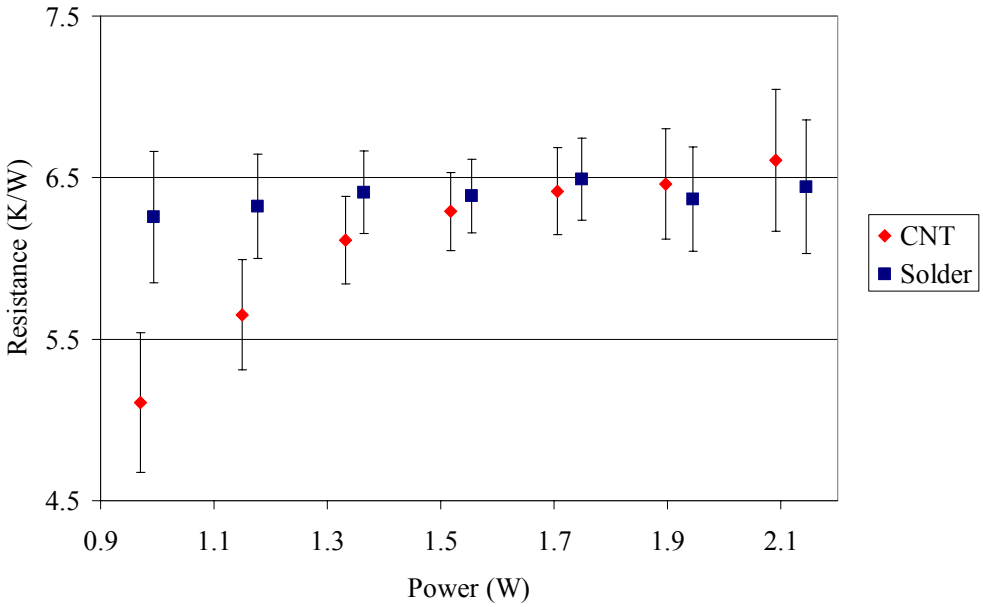

Figure 64. Thermal resistance measurements of CNT and lead free solder interfaces.

In an effort to eliminate some of the uncertainties in the last experiment, a direct comparison of interface performance was conducted by measuring die temperature. To test the validity of the junction temperature measurements, infrared (IR) temperature mapping was performed. For the best IR measurements, the LED systems were placed on a thermoelectric cooler maintained at 50 ºC. The camera was focused on the dormant LED to get a baseline reading. The LED was then powered up and allowed to reach steady state. An average temperature over the die area (1 mm^2) was recorded. The forward voltage experiments were performed under similar conditions. In each case, the

top side of the LED was uninsulated and the bulb was removed. Both precautions were taken to facilitate the IR experiments.

Differences in absolute temperature between the two measurements techniques can be attributed to differences in staging and ambient conditions. The backside temperature for the IR technique was controlled using the system's built in thermoelectric cooler while a hot plate was used in the forward voltage experiments. Additionally, since the bulb was not used and additional insulation was forgone atop the LED, the exposed die was suspect to ambient convective cooling. The effects of which are difficult to accurately quantify.

Comparing the performance of the thermal interface materials, the lead free solder consistently performed slightly better than the CNT interface. This can be attributed to a number of considerations. First, the solder in an isotropic material while the CNT interface is not. With interfaces spanning large areas, the ability to distribute heat uniformly in all directions is advantageous. Although the CNTs, in all likelihood, have a higher thermal conductivity axially, the limits transverse conductivity may have served as an equalizer to the less conductive solder. Second, the bond strength of the solder is significantly greater than the CNT interface. The lead free solder used in this study had a tensile strength of approximately 55 MPa, which is two orders of magnitude greater than CNT bonds. Delamination of the CNT interface was observed during testing of one of the LEDs which created a noticeable air gap between the device and the substrate. The result of this was an increase in die temperature of over 20 ºC. Special care was put forth in handling the LED systems to limit any external stresses on the interface. However, since movement from the hot press to the different test set-ups was inevitable, so too was the probability of bond delamination.

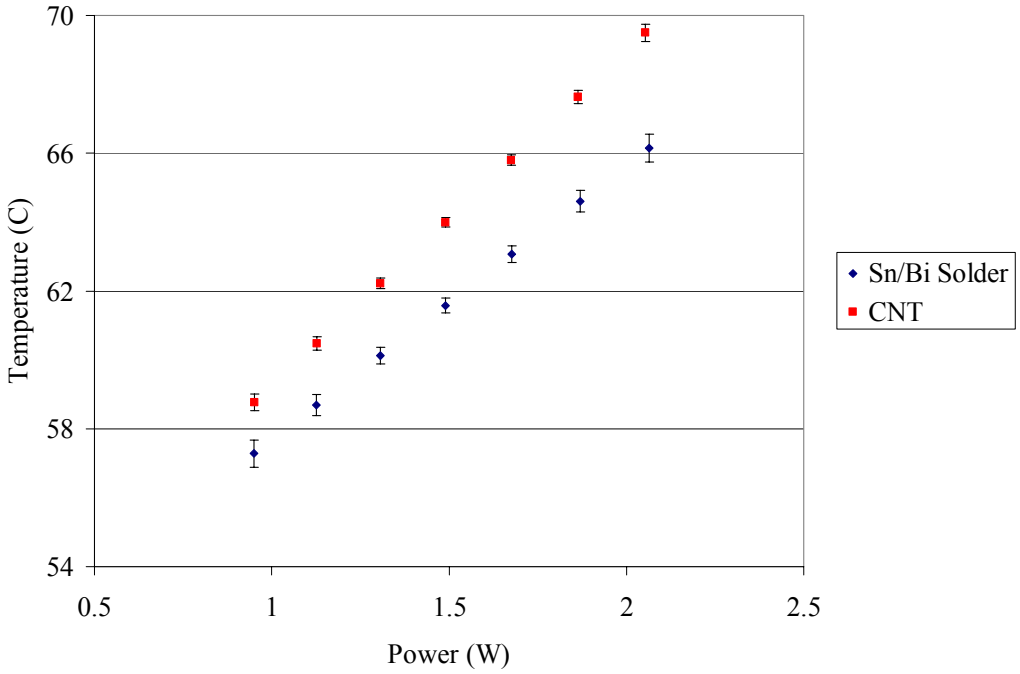

Figure 65. Die temperature of LED with solder and CNT interfaces measured using IR spectroscopy.

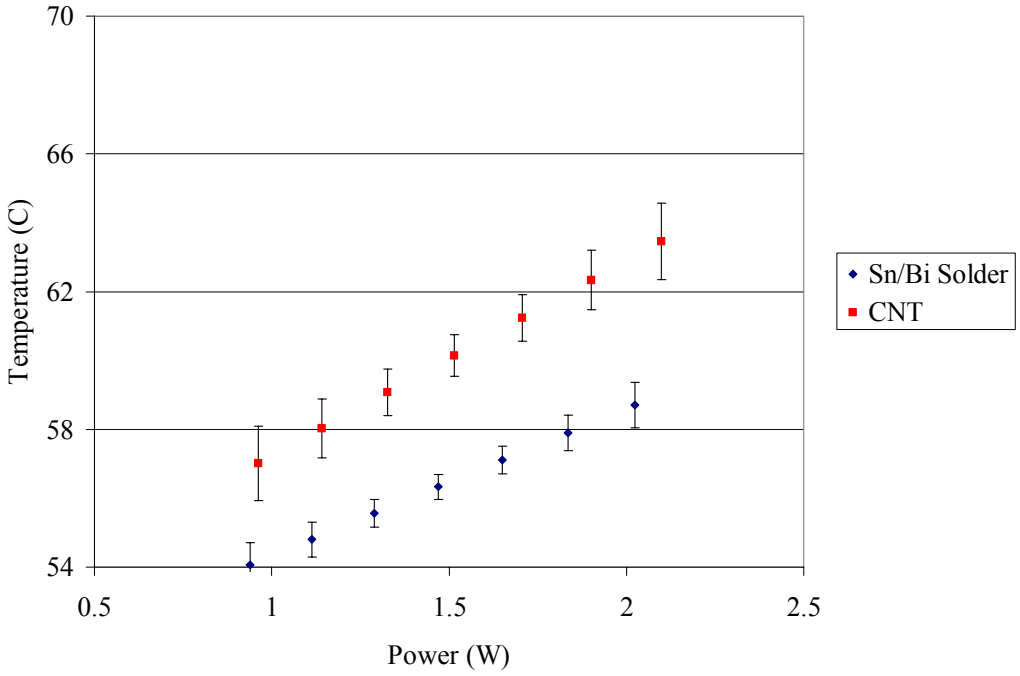

Figure 66. Junction temperature of LED with solder and CNT interfaces using forward voltage measurement technique.

In order to compare the two measurement techniques, the differences between the two interfaces in question were examined. The difference in trends, from the two measurement techniques, of junction temperature versus power for the CNT interface systems and solder interface systems were compared. In each case, the linear equation of the solder's performance was subtracted from the linear trend of the CNT's performance. By using the standard error of the measured temperature and power of the LED and an alpha value of 0.05, maximum and minimum likelihood bounds were fitted to the trends.

To compare the four different trends, the Bonferroni correction was used to determine the appropriate alpha value for each set of data. In this case, an alpha value of 0.05 was desired, and there were four sets of data, so for each set and alpha of 0.0125 was used. For each data set, the error was found using the following equation

$$Error = STrr \cdot t_{\alpha/4} \sqrt{\frac{1}{N} + \left(\frac{(x_i - \bar{x})^2}{\sum_{i=1}^{N} (x_i - \bar{x})^2} \right)} \tag{19}$$

where *STrr* is the standard error of the data, $t_{\alpha/4}$ is the t-statistic, *N* is the number of data points in the set, and *x* is the independent variable (power).

Because there is a consistent overlapping of bounds between the forward voltage measurement technique and IR spectroscopy measurement technique, it can be concluded that there was no meaningful difference between the two experiments.

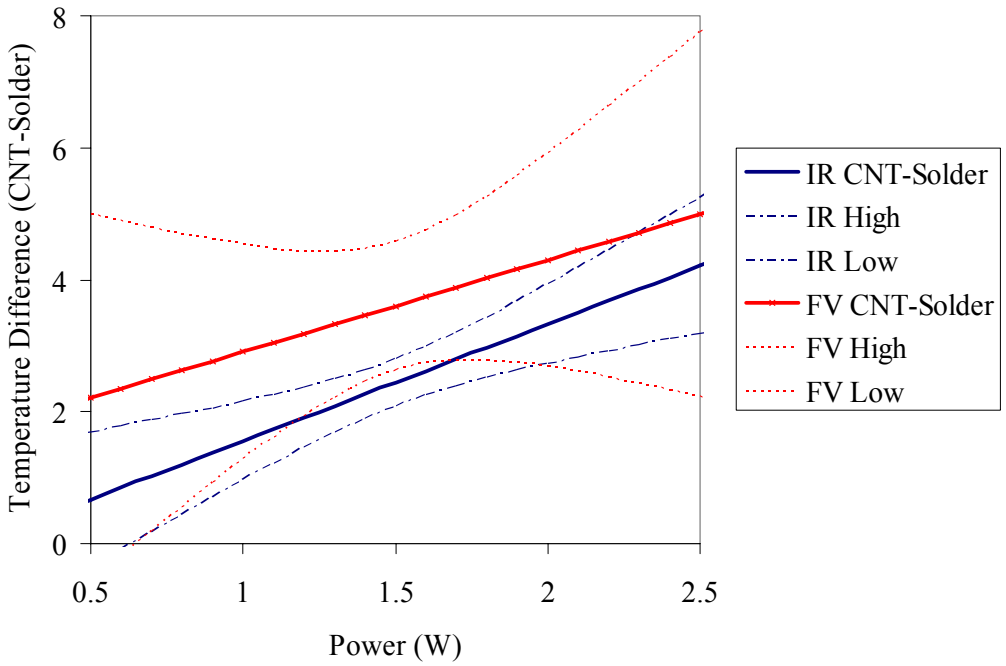

Figure 67. Comparison of forward voltage and IR temperature measurement techniques by relating the differences in trends of the CNT and solder interface performance.

Conclusion

Thermal resistance measurements of vertically aligned carbon nanotube arrays were performed using the photoacoustic method. It was shown that by increasing the adhesion of the CNTs to the substrate the thermal resistance was significantly reduced. Since growing CNTs directly onto a device is, at this point, difficult to do without causing damage, low temperature transfer is of critical importance. Using the novel transfer method of vertically aligned CNTs developed in this study, we were able to produce thermal interfaces with resistances as low or lower than any published results to this date. The applicability of CNT thermal interfaces was demonstrated by integrating them into LED cooling systems. The performance of the CNT interface was compared with the performance of a lead free solder interface. Using junction temperature data obtained via the measured forward voltage, it was revealed that the CNT thermal

interface had a comparable performance to the solder interface. However, in applications over large areas, such as the backside of the LEDs used in this study, the high axial thermal conductivity of the CNTs was somewhat negated by its low transverse conductivity. It can be concluded from this study that the possibility of using vertically aligned carbon nanotubes as a thermal interface material is real. The applications in which they are employed, however, are more appropriate in small scales.

CHAPTER 6

FUTURE WORK

It has been shown that arrays of vertically aligned carbon nanotubes can have comparable thermal performance to TIMs on the market today. Previous examinations of CNT thermal resistance have concluded that the contact resistance between the tubes and joining surfaces are the largest impedances. The novel technique created and explored in this study has proven to drastically cut down on CNT contact resistance. Additionally, this procedure has shown great promise as a viable transfer technique for vertically aligned CNTs that would be easily implemented in most laboratories.

To further assess the viability of CNTs as a solder replacement for thermal interfaces, the thermomechanical stresses must be explored. One of the drawbacks of solders, both as a TIM and as an electrical via, is their susceptibility to mechanical failure during cycling. Preliminary studies have shown that CNT interfaces can affect the stress levels in bonded silicon. In this examination, CNTs were transferred to copper with the gold bonding method, then a silicon chip was bonded to the top of the CNTs with the same process. Raman spectroscopy was used to evaluate the stress in the silicon with and without CNT interfaces. Initial results have suggested a reduction in stress for the system with the CNT interface. To conceptualize this, consider a rigid column (representing a solder connection) attached to a foundation and supporting a roof. When the foundation shifts, significant stress is seen in the column and in the roof because of the rigidity of the column and strong mechanical coupling. However, if the column was replaced with a rope, the roof would have more flexibility to translate. More research must be spent to understand the true pacifying capabilities of CNT interfaces.

Research focusing on the effects of stress on LED optical and electrical performance has been conducted. These studies have shown a 40% decrease in power

within 50 hours of operation under stress. The collective cooling and stress relieving effects of carbon nanotube thermal interface materials on LED performance should be investigated.

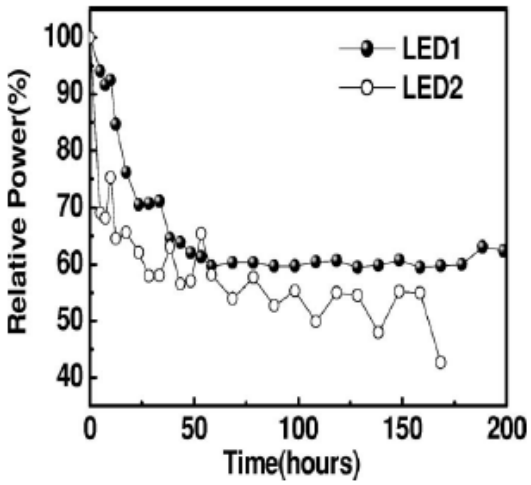

Figure 68. Decrease in power of two independent GaN LEDs operating with an applied stress *[125]*.

The viability of the CNT interfaces created in this study relies on the overall mechanical strength of the bond. It was shown that the bonded CNT interface could withstand over 0.35 MPa of tensile stress. However, the stress most critical in thermal interface materials is shear. An investigation into the shear strength of these interfaces must be conducted. In addition, procedures should be developed to increase the mechanical strength of the CNT interface.

The ability to scale up this technology for mass production must be investigated. Difficulties exist with large scale production of vertically aligned carbon nanotubes. Additionally, the ability to transfer patterns of CNTs to other surfaces with superior alignment should be perfected. Research in roll-to-roll processing for this method of CNT transfer will be of great value. Each of these areas of focus will help to define the

role of CNTs as a thermal interface material from both a performance and cost perspective.

Recent experiments at Georgia Tech using laser diffraction have proven the ability to ablate regions of vertically aligned CNTs to create large scale patterns. Using a high frequency laser pulse, patterned lines can be etched into CNT arrays as shown in Figure 69. Multiple ablations at different angles can reveal CNT towers. These structures could be used to penetrate viscous phase change materials to produce an effective thermal interface material.

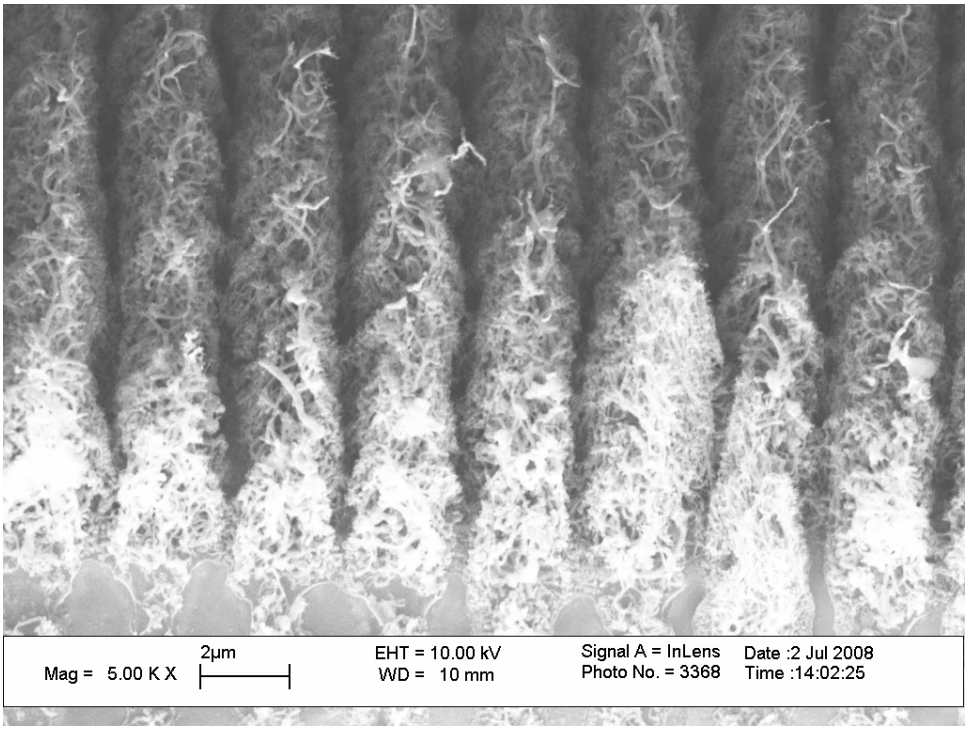

Figure 69. CNTs patterned using high frequency laser interference.

For instance, incorporation of the CNT interface with a phase change material such as paraffin could produce an excellent interface. As expected, when the device heats up to its operating temperature, the paraffin would be able to flow around the CNT to increase contact with the mating surface and reduce air pockets within the array.

Research must be conducted on the ability of the phase change materials to flow and fill in the gaps of these patterned CNT arrays.

Finally, chemical vapor deposition of polymeric materials could be an attractive solution for CNT integration. A vapor-based deposition procedure has been developed to synthesize a range of different polymers onto various substrates *[126]*. This particular form of deposition could be quite attractive for creating CNT/polymer thermal interface materials. Ideally, during the deposition, the reactant gasses for the polymer would infiltrate the vertically aligned CNT array and grow in a way that would reduce air voids and promote larger areas of contact between the two materials. This high level of contact and integration would be a significant advance in CNT/polymer thermal interface materials. Furthermore, the capability to remove the CNT/polymer composite from the host substrate by simply peeling the sheet from the surface is quite attractive for storage and handling concerns.

In conclusion, increasing demands in power and functionality for microelectronic devices make is necessary to develop innovative thermal management techniques. Carbon nanotubes have been investigated as a possible solder replacement for thermal interface materials because of their outstanding thermal properties. Issues with contact resistance and manufacturability have thus stalled their introduction into marketable microelectronic devices. In this study, a novel method to effectively transfer and bond vertically aligned CNTs with high mechanical strength and low thermal contact resistance was created. Results have shown a mechanical strength far superior to other research groups in the field, and thermal contact resistances several times lower than the top published results.

REFERENCES

[1] B. A. Cola, J. Xu, C. Cheng, X. Xu, T. S. Fisher, H. Hu, *Photoacoustic characterization of carbon nanotube array thermal interfaces*, *Journal of Applied Physics* **2007**, *101*, 054313.

[2] B. A. Cola, X. Xu, T. S. Fisher, *Increased real contact in thermal interfaces: A carbon nanotube/foil material*, *Applied Physics Letters* **2007**, *90*, 093513.

[3] M. Panzer, G. Zhang, D. Mann, X. Hu, E. Pop, H. Dai, K. E. Goodson, "Thermal properties of metal-coated vertically-aligned single wall nanotube films", San Diego, CA, United States, **2006**.

[4] M. A. Panzer, G. Zhang, D. Mann, X. Hu, E. Pop, H. Dai, K. E. Goodson, *Thermal Properties of Metal-Coated Vertically Aligned Single-Wall Nanotube Arrays*, *Journal of Heat Transfer* **2008**, *130*, 052401.

[5] T. Tong, Y. Zhao, L. Delzeit, A. Kashani, M. Meyyappan, A. Majumdar, *Dense vertically aligned multiwalled carbon nanotube arrays as thermal interface materials*, *IEEE Transactions on Components and Packaging Technologies* **2007**, *30*, 92.

[6] K. Zhang, M. M. F. Yuen, N. Wang, J. Y. Miao, D. G. W. Xiao, H. B. Fan, "Thermal interface material with aligned CNT and its application in HB-LED packaging", San Diego, CA, United States, **2006**.

[7] C.-P. Chiu, J. G. Maveety, Q. A. Tran, *Characterization of solder interfaces using laser flash metrology*, *Microelectronics Reliability* **2002**, *42*, 93.

[8] S. Iijima, *Helical microtubules of graphitic carbon*, *Nature* **1991**, *354*, 56.

[9] M. J. O'Connell, Ed. *Carbon Nanotubes: Properties and Applications*, CRC Press, Boca Raton, London, New York **2006**.

[10] *Carbon Nanotubes: Science and Applications*, CRC Press, Boca Raton, London, New York, Washington D.C. **2005**.

[11] J. Wei, *Challenges in cooling design of CPU packages for high-performance servers*, *Heat Transfer Engineering* **2008**, *29*, 178.

[12] X. Hu, L. Jiang, K. E. Goodson, "Thermal characterization of eutectic alloy thermal interface materials with void-like inclusions", San Jose, CA., United States, **2004**.

[13] G. Refai-Ahmed, Z. He, E. Heian, R. Vincent, T. Rude, D. Van Heerden, "Comparison of thermal performance of current high-end thermal interface materials", Vancouver, BC, United States, **2007**.

[14] M. Abtew, G. Selvaduray, *Lead-free Solders in Microelectronics*, *Materials Science and Engineering: R: Reports* **2000**, *27*, 95.

[15] A. Allen, A. Cannon, J. Lee, W. P. King, S. Graham, *Flexible microdevices based on carbon nanotubes*, *Journal of Micromechanics and Microengineering* **2006**, *16*, 2722.

[16] A. C. Allen, E. Sunden, A. Cannon, S. Graham, W. King, *Nanomaterial transfer using hot embossing for flexible electronic devices*, *Applied Physics Letters* **2006**, *88*.

[17] Y. Chai, J. Gong, K. Zhang, P. C. H. Chan, M. M. F. Yuen, *Flexible transfer of aligned carbon nanotube films for integration at lower temperature*, *Nanotechnology* **2007**, *18*, 355709.

[18] D. R. Hines, S. Mezhenny, M. Breban, E. D. Williams, V. W. Ballarotto, G. Esen, A. Southard, M. S. Fuhrer, *Nanotransfer printing of organic and carbon nanotube thin-film transistors on plastic substrates*, *Applied Physics Letters* **2005**, *86*, 163101.

[19] H. Huang, C. Liu, Y. Wu, S. Fan, *Aligned carbon nanotube composite films for thermal management*, *Advanced Materials* **2005**, *17*, 1652.

[20] H. Jiang, L. Zhu, K.-S. Moon, C. P. Wong, *Low temperature carbon nanotube film transfer via conductive polymer composites*, *Nanotechnology* **2007**, *18*, 125203.

[21] S. Li, Y. Yan, N. Liu, M. B. Chan-Park, Q. Zhang, *Transfer printing of submicrometer patterns of aligned carbon nanotubes onto functionalized electrodes*, *Small* **2007**, *3*, 616.

[22] S. M. L. Nai, M. Gupta, J. Wei, *Development of novel lead-free solder composites using carbon nanotube reinforcements*, *International Journal of Nanoscience* **2005**, *4*, 423.

[23] E. Sunden, J. K. Moon, C. P. Wong, W. P. King, S. Graham, *Microwave assisted patterning of vertically aligned carbon nanotubes onto polymer substrates*, *Journal of Vacuum Science & Technology B* **2006**, *24*, 1947.

[24] T. Wang, B. Carlberg, M. Jonsson, G.-H. Jeong, E. E. B. Campbell, J. Liu, *Low temperature transfer and formation of carbon nanotube arrays by imprinted conductive adhesive*, *Applied Physics Letters* **2007**, *91*, 093123.

[25] L. Zhu, Y. Sun, D. W. Hess, C.-P. Wong, *Well-aligned open-ended carbon nanotube architectures: An approach for device assembly*, *Nano Letters* **2006**, *6*, 243.

[26] Y. Chai, J. Gong, K. Zhang, P. C. H. Chan, M. M. F. Yuen, "Low temperature transfer of aligned carbon nanotube films using liftoff technique", Sparks, NV, United States, **2007**.

[27] D. G. Dresselhaus M.S., Avouris P., (eds.). *Carbon nanotubes : synthesis, structure, properties, and applications* Springer, Berlin ; New York **2001**.

[28] M. S. Dresselhaus, P. C. Eklund, *Phonons in carbon nanotubes*, *Advances in Physics* **2000**, *49*, 705.

[29] L. Delzeit, A. Cassell, D. Hash, M. Meyyappan, *Carbon nanotube growth by PECVD: A review*, *Plasma Sources Science and Technology* **2003**, *12*, 205.

[30] S. Inoue, T. Nakajima, Y. Kikuchi, *Synthesis of single-wall carbon nanotubes from alcohol using Fe/Co, Mo/Co, Rh/Pd catalysts*, *Chemical Physics Letters* **2005**, *406*, 184.

[31] H.-C. Kuan, C.-C. M. Ma, W.-P. Chang, S.-M. Yuen, H.-H. Wu, T.-M. Lee, *Synthesis, thermal, mechanical and rheological properties of multiwall carbon nanotube/waterborne polyurethane nanocomposite*, *Composites Science and Technology* **2005**, *65*, 1703.

[32] C. Laurent, A. Peigney, A. Rousset, *Synthesis of carbon nanotube Fe-Al2O3 nanocomposite powders by selective reduction of different Al1.8Fe0.2O3 solid solutions*, *Journal of Materials Chemistry* **1998**, *8*, 1263.

[33] G.-Y. Xiong, D. Z. Wang, Z. F. Ren, *Aligned millimeter-long carbon nanotube arrays grown on single crystal magnesia*, *Carbon* **2006**, *44*, 969.

[34] L. Zhu, Y. Xiu, D. W. Hess, C.-P. Wong, *Aligned carbon nanotube stacks by water-assisted selective etching*, *Nano Letters* **2005**, *5*, 2641.

[35] J. F. AuBuchon, L. H. Chen, A. I. Gapin, S. H. Jin, *Electric-field-guided growth of carbon nanotubes during DC plasma-enhanced CVD*, *Chemical Vapor Deposition* **2006**, *12*, 370.

[36] M. Cantoro, S. Hofmann, S. Pisana, V. Scardaci, A. Parvez, C. Ducati, A. C. Ferrari, A. M. Blackburn, K.-Y. Wang, J. Robertson, *Catalytic chemical vapor deposition of single-wall carbon nanotubes at low temperatures*, *Nano Letters* **2006**, *6*, 1107.

[37] V. Shanov, M. Schulz, Y. Yun, A. Gorton, University of Cincinnati **2005**.

[38] I. Knowledge, (Ed: S. W. Jones), **2008**.

[39] M. Berger, Nanowerk LLC, **2007**.

[40] P. Lall, M. Pecht, E. Hakim, *Influence of Temperature on Microelectronics and System Reliability*, CRC Press, **1997**.

[41] J. Senawiratne, Y. Li, M. Zhu, Y. Xia, W. Zhao, T. Detchprohm, A. Chatterjee, J. L. Plawsky, C. Wetzel, *Junction temperature measurements and thermal modeling of GaInN/GaN quantum well light-emitting diodes*, *Journal of Electronic Materials* **2008**, *37*, 607.

[42] F. P. Incropera, DeWitt, David P., *Fundamentals of Heat and Mass Transfer*, John Wiley & Sons, Inc., **2002**.

[43] M. M. Yovanovich, *Four decades of research on thermal contact, gap, and joint resistance in microelectronics*, *IEEE Transactions on Components and Packaging Technologies* **2005**, *28*, 182.

[44] M. Bahrami, J. R. Culham, M. M. Yovanovich, *Modeling Thermal Contact Resistance: A Scale Analysis Approach*, *Journal of Heat Transfer* **2004**, *126*, 896.

[45] Y. Aoyagi, C. K. Leong, D. D. L. Chung, *Polyol-based phase-change thermal interface materials*, *Journal of Electronic Materials* **2006**, *35*, 416.

[46] A. Dani, J. C. Matayabas Jr, P. Koning, "Thermal interface material technology advancements and challenges - An overview", San Francisco, CA, United States, **2005**.

[47] F. Sarvar, D. C. Whalley, P. P. Conway, "Thermal interface materials - A review of the state of the art", Dresden, Saxony, Germany, **2007**.

[48] M. H. Nurmawati, K. S. Siow, I. J. Rasiah, *Analysis of phase change material for use as thermal interface material*, *International Journal of Polymer Analysis and Characterization* **2004**, *9*, 213.

[49] R. S. Prasher, *Rheology based modeling and design of particle laden polymeric thermal interface materials*, *Ieee Transactions on Components and Packaging Technologies* **2005**, *28*, 230.

[50] S. A. Putnam, D. G. Cahill, B. J. Ash, L. S. Schadler, *High-precision thermal conductivity measurements as a probe of polymer/nanoparticle interfaces*, *Journal of Applied Physics* **2003**, *94*, 6785.

[51] J. P. Gwinn, R. L. Webb, *Performance and testing of thermal interface materials*, *Microelectronics Journal* **2003**, *34*, 215.

[52] C. G. Macris, T. R. Sanderson, R. G. Ebel, C. B. Leyerle, *Performance, Reliability, and Approaches Using a Low Melt Alloy as a Thermal Interface Material*, *Proceedings IMAPS* **2004**.

[53] T. Chellaih, G. Kumar, K. N. Prabhu, *Effect of thermal contact heat transfer on solidification of Pb-Sn and Pb-free solders*, *Materials and Design* **2007**, *28*, 1006.

[54] J. Calame, College Park, MD **2004**.

[55] A. Gowda, D. Esler, S. Tonapi, K. Nagarkar, K. Srihari, "Voids in thermal interface material layers and their effect on thermal performance", Singapore, **2004**.

[56] C. Deppisch, T. Fitzgerald, A. Raman, F. Hua, C. Zhang, P. Liu, M. Miller, *The material optimization and reliability characterization of an indium-solder thermal interface material for CPU packaging*, *JOM* **2006**, *58*, 67.

[57] N. Sobczak, A. Kudyba, R. Nowak, W. Radziwill, K. Pietrzak, *Factors affecting wettability and bond strength of solder joint couples*, *Pure and Applied Chemistry* **2007**, *79*, 1755.

[58] D. X. Xu, Y. P. Lei, Z. D. Xia, F. Guo, Y. W. Shi, *Experimental wettability study of lead-free solder on Cu substrates using varying flux and temperature*, *Journal of Electronic Materials* **2008**, *37*, 125.

[59] C. Y. Huang, C. Y. Huang, K. Srihari, A. J. McLenaghan, G. R. A. W. G. R. Westby, "Flux activity evaluation using the wetting balance", presented at *Electronics Manufacturing Technology Symposium, 1995. 'Manufacturing Technologies - Present and Future', Seventeenth IEEE/CPMT International*, **1995**.

[60] A. A. Loiseau, *Understanding carbon nanotubes : from basics to applications / A. Loiseau ... [et al.] (eds.)*. Vol. 677, Springer, Berlin ; New York **2006**.

[61] M. C. Hersam, *Progress towards monodisperse single-walled carbon nanotubes*, *Nat Nano* **2008**, *3*, 387.

[62] C. H. See, A. T. Harris, *A review of carbon nanotube synthesis via fluidized-bed chemical vapor deposition*, *Industrial and Engineering Chemistry Research* **2007**, *46*, 997.

[63] L. X. Zheng, M. J. O'Connell, S. K. Doorn, X. Z. Liao, Y. H. Zhao, E. A. Akhadov, M. A. Hoffbauer, B. J. Roop, Q. X. Jia, R. C. Dye, D. E. Peterson, S. M. Huang, J. Liu, Y. T. Zhu, *Ultralong single-wall carbon nanotubes*, *Nature Materials* **2004**, *3*, 673.

[64] J. Hone, M. Whitney, C. Piskoti, A. Zettl, *Thermal conductivity of single-walled carbon nanotubes*, *Physical Review B* **1999**, *59*, R2514.

[65] W. Yi, L. Lu, Z. Dian-lin, Z. W. Pan, S. S. Xie, *Linear specific heat of carbon nanotubes*, *Physical Review B* **1999**, *59*, R9015.

[66] D. J. Yang, Q. Zhang, G. Chen, S. F. Yoon, J. Ahn, S. G. Wang, Q. Zhou, Q. Wang, J. Q. Li, *Thermal conductivity of multiwalled carbon nanotubes*, *Physical Review B* **2002**, *66*, 165440.

[67] S. Maruyama, *A MOLECULAR DYNAMICS SIMULATION OF HEAT CONDUCTION OF A FINITE LENGTH SINGLE-WALLED CARBON NANOTUBE*, *Nanoscale and Microscale Thermophysical Engineering* **2003**, *7*, 41

[68] T. Borca-Tasciuc, M. Mazumder, Y. Son, S. K. Pal, L. S. Schadler, P. M. Ajayan, *Anisotropic thermal diffusivity characterization of aligned carbon nanotube-polymer composites*, *Journal of Nanoscience and Nanotechnology* **2007**, *7*, 1581.

[69] D. J. Yang, S. G. Wang, Q. Zhang, P. J. Sellin, G. Chen, *Thermal and electrical transport in multi-walled carbon nanotubes*, *Physics Letters A* **2004**, *329*, 207.

[70] J. W. Che, T. Cagin, W. A. Goddard, *Thermal conductivity of carbon nanotubes*, *Nanotechnology* **2000**, *11*, 65.

[71] H. Li, N. Zhao, C. He, C. Shi, X. Du, J. Li, *Thermogravimetric analysis and TEM characterization of the oxidation and defect sites of carbon nanotubes synthesized by CVD of methane*, *Materials Science and Engineering A* **2008**, *473*, 355.

[72] H. Kataura, Y. Kumazawa, Y. Maniwa, I. Umezu, S. Suzuki, Y. Ohtsuka, Y. Achiba, *Optical properties of single-wall carbon nanotubes*, *Synthetic Metals* **1999**, *103*, 2555.

[73] T. Durkop, S. A. Getty, E. Cobas, M. S. Fuhrer, *Extraordinary mobility in semiconducting carbon nanotubes*, *Nano Letters* **2004**, *4*, 35.

[74] Z. Yao, C. L. Kane, C. Dekker, *High-field electrical transport in single-wall carbon nanotubes*, *Physical Review Letters* **2000**, *84*, 2941.

[75] K. H. An, Y. H. Lee, *Electronic-structure engineering of carbon nanotubes*, *Nano* **2006**, *1*, 115.

[76] T. Rueckes, K. Kim, E. Joselevich, G. Y. Tseng, C.-L. Cheung, C. M. Lieber, *Carbon Nanotube-Based Nonvolatile Random Access Memory for Molecular Computing*, *Science* **2000**, *289*, 94.

[77] A. Garg, J. Han, S. B. Sinnott, *Interactions of Carbon-Nanotubule Proximal Probe Tips with Diamond and Graphene*, *Physical Review Letters* **1998**, *81*, 2260.

[78] J. P. Lu, *Elastic properties of carbon nanotubes and nanoropes*, *Physical Review Letters* **1997**, *79*, 1297.

[79] J. M. Gere, *Mechanics of Materials*, Brooks/Cole-Thomson Learning, Belmont, CA **2004**.

[80] P. Poncharal, Z. L. Wang, D. Ugarte, W. A. de Heer, *Electrostatic Deflections and Electromechanical Resonances of Carbon Nanotubes*, *Science* **1999**, *283*, 1513.

[81] E. W. Wong, P. E. Sheehan, C. M. Lieber, *Nanobeam Mechanics: Elasticity, Strength, and Toughness of Nanorods and Nanotubes*, *Science* **1997**, *277*, 1971.

[82] C. Tang, W. L. Guo, C. F. Chen, *Mechanism for superelongation of carbon nanotubes at high temperatures*, *Physical Review Letters* **2008**, *100*.

[83] D. A. Walters, L. M. Ericson, M. J. Casavant, J. Liu, D. T. Colbert, K. A. Smith, R. E. Smalley, *Elastic strain of freely suspended single-wall carbon nanotube ropes*, *Applied Physics Letters* **1999**, *74*, 3803.

[84] J. P. Salvetat, J. M. Bonard, N. H. Thomson, A. J. Kulik, L. Forró, W. Benoit, L. Zuppiroli, *Mechanical properties of carbon nanotubes*, *Applied Physics A: Materials Science & Processing* **1999**, *69*, 255.

[85] H. G. Chae, T. V. Sreekumar, T. Uchida, S. Kumar, *A comparison of reinforcement efficiency of various types of carbon nanotubes in poly acrylonitrile fiber*, *Polymer* **2005**, *46*, 10925.

[86] L. N. An, W. X. Xu, S. Rajagopalan, C. M. Wang, H. Wang, Y. Fan, L. G. Zhang, D. P. Jiang, J. Kapat, L. Chow, B. H. Guo, J. Liang, R. Vaidyanathan, *Carbon-nanotube-reinforeed polymer-derived ceramic composites*, *Advanced Materials* **2004**, *16*, 2036.

[87] F. Lupo, R. Kamalakaran, C. Scheu, N. Grobert, M. Ruhle, *Microstructural investigations on zirconium oxide-carbon nanotube composites synthesized by hydrothermal crystallization*, *Carbon* **2004**, *42*, 1995.

[88] J. W. Ning, J. J. Zhang, Y. B. Pan, J. K. Guo, *Fabrication and mechanical properties of SiO2 matrix composites reinforced by carbon nanotube*, *Materials Science and Engineering a-Structural Materials Properties Microstructure and Processing* **2003**, *357*, 392.

[89] E. Flahaut, A. Peigney, C. Laurent, C. Marliere, F. Chastel, A. Rousset, *Carbon nanotube-metal-oxide nanocomposites: Microstructure, electrical conductivity and mechanical properties*, *Acta Materialia* **2000**, *48*, 3803.

[90] T. Kuzumaki, O. Ujiie, H. Ichinose, K. Ito, *Mechanical characteristics and preparation of carbon nanotube fiber-reinforced Ti composite*, *Advanced Engineering Materials* **2000**, *2*, 416.

[91] K. W. Kolasinski, *Catalytic growth of nanowires: Vapor-liquid-solid, vapor-solid-solid, solution-liquid-solid and solid-liquid-solid growth*, *Current Opinion in Solid State & Materials Science* **2006**, *10*, 182.

[92] X. He, F. Wu, M. Zheng, *The synthesis of carbon nanoballs and its electrochemical performance*, *Diamond and Related Materials* **2007**, *16*, 311.

[93] S. Musso, S. Porro, M. Rovere, M. Giorcelli, A. Tagliaferro, *Fluid dynamic analysis of gas flow in a thermal-CVD system designed for growth of carbon nanotubes*, *Journal of Crystal Growth* **2008**, *310*, 477.

[94] A. M. Cassell, J. A. Raymakers, J. Kong, H. Dai, *Large Scale CVD Synthesis of Single-Walled Carbon Nanotubes*, *Journal of Physical Chemistry B* **1999**, *103*, 6484.

[95] C. P. Deck, K. Vecchio, *Growth mechanism of vapor phase CVD-grown multi-walled carbon nanotubes*, *Carbon* **2005**, *43*, 2608.

[96] Q. Fu, S. Huang, J. Liu, *Chemical vapor depositions of single-walled carbon nanotubes catalyzed by uniform Fe₂O₃ nanoclusters synthesized using diblock copolymer micelles*, *Journal of Physical Chemistry B* **2004**, *108*, 6124.

[97] S. Vetrivel, J. S. Do, M.-Y. Cheng, B.-J. Hwang, *Simple catalyst for the effective growth of carbon nanotubes by CVD*, *Journal of Physical Chemistry C* **2007**, *111*, 16211.

[98] L. Zhu, Y. Sun, J. Xu, Z. Zhang, D. W. Hess, C. P. Wong, "Aligned carbon nanotubes for electrical interconnect and thermal management", Lake Buena Vista, FL, United States, **2005**.

[99] M. A. Lieberman, A. J. Lichtenberg, *Principles of plasma discharges and materials processing*, Wiley, New York **1994**.

[100] N. A. Kiselev, A. P. Moravsky, A. B. Ormont, D. N. Zakharov, *SEM and HREM study of the internal structure of nanotube rich carbon arc cathodic deposits*, *Carbon* **1999**, *37*, 1093.

[101] J. L. Hutchison, N. A. Kiselev, E. P. Krinichnaya, A. V. Krestinin, R. O. Loutfy, A. P. Morawsky, V. E. Muradyan, E. D. Obraztsova, J. Sloan, S. V. Terekhov, D. N. Zakharov, *Double-walled carbon nanotubes fabricated by a hydrogen arc discharge method*, *Carbon* **2001**, *39*, 761.

[102] T. Guo, P. Nikolaev, A. G. Rinzler, D. Tomanek, D. T. Colbert, R. E. Smalley, *Self-assembly of tubular fullerenes*, *Journal of Physical Chemistry* **1995**, *99*, 10694.

[103] M. C. I. Siu, C. Bulik, *NATIONAL BUREAU OF STANDARDS LINE-HEAT-SOURCE GUARDED-HOT-PLATE APPARATUS*, *Review of Scientific Instruments* **1981**, *52*, 1709.

[104] A. Rosencwaig, A. Gersho, *THEORY OF THE PHOTOACOUSTIC EFFECT WITH SOLIDS*, *Journal of Applied Physics* **1976**, *47*, 64.

[105] A. G. Bell, *American Journal of Science* **1880**, *20*.

[106] A. Rosencwaig, G. Busse, *High-resolution photoacoustic thermal-wave microscopy*, *Applied Physics Letters* **1980**, *36*, 725.

[107] W. Xinwei, H. Hanping, X. Xianfan, *Photo-Acoustic Measurement of Thermal Conductivity of Thin Films and Bulk Materials*, *Journal of Heat Transfer* **2001**, *123*, 138.

[108] S. Shaikh, L. Li, K. Lafdi, J. Huie, *Thermal conductivity of an aligned carbon nanotube array*, *Carbon* **2007**, *45*, 2608.

[109] W. J. Parker, R. J. Jenkins, C. P. Butler, G. L. Abbott, *Flash Method of Determining Thermal Diffusivity, Heat Capacity, and Thermal Conductivity*, *Journal of Applied Physics* **1961**, *32*, 1679.

[110] S. Graham, in *George W. Woodruff School of Mechanical Engineering*, Vol. PhD, Georgia Institute of Technology, Atlanta **1999**, 255.

[111] N. Taketoshi, T. Baba, A. Ono, *Development of a thermal diffusivity measurement system for metal thin films using a picosecond thermoreflectance technique*, *Measurement Science & Technology* **2001**, *12*, 2064.

[112] Y. S. Min, E. J. Bae, B. S. Oh, D. Kang, W. Park, *Low-Temperature Growth of Single-Walled Carbon Nanotubes by Water Plasma Chemical Vapor Deposition*, *J. Am. Chem. Soc.* **2005**, *127*, 12498.

[113] S.-M. Yuen, M. Chen-Chi, H.-H. Wu, H.-C. Kuan, W.-J. Chen, S.-H. Liao, C.-W. Hsu, H.-L. Wu, *Preparation and thermal, electrical, and morphological*

properties of multiwalled carbon nanotube and epoxy composites, *Journal of Applied Polymer Science* **2007**, *103*, 1272.

[114] T. D. Yuan, H.-y. Pan, Y. Li, *Thermal Interface Material (TIM) Design Guidance for Flip Chip BGA Package Thermal Performace*, *CP-01020-1.0* **2004**.

[115] A. A. O. Tay, K. Y. Goh, *A study of delamination growth in the die-attach layer of plastic IC packages under hygrothermal loading during solder reflow*, *Ieee Transactions on Device and Materials Reliability* **2003**, *3*, 144.

[116] S. T. Huxtable, D. G. Cahill, S. Shenogin, L. Xue, R. Ozisik, P. Barone, M. Usrey, M. S. Strano, G. Siddons, M. Shim, P. Keblinski, *Interfacial heat flow in carbon nanotube suspensions*, *Nature Materials* **2003**, *2*, 731.

[117] Y. Son, S. K. Pal, T. Borca-Tasciuc, P. M. Ajayan, R. W. Siegel, *Thermal resistance of the native interface between vertically aligned multiwalled carbon nanotube arrays and their SiO[sub 2]/Si substrate*, *Journal of Applied Physics* **2008**, *103*, 024911.

[118] Y. Xu, Y. Zhang, E. Suhir, X. Wang, *Thermal properties of carbon nanotube array used for integrated circuit cooling*, *Journal of Applied Physics* **2006**, *100*, 074302.

[119] J. Xu, T. S. Fisher, *Enhanced thermal contact conductance using carbon nanotube array interfaces*, *IEEE Transactions on Components and Packaging Technologies* **2006**, *29*, 261.

[120] J. Lukes, H. Zhong, *Thermal Conductivity of Individual Single-Wall Carbon Nanotubes*, *Journal of Heat Transfer* **2007**, *129*, 705.

[121] C. Q. Sun, H. L. Bai, S. Li, B. K. Tay, E. Y. Jiang, *Size-effect on the electronic structure and the thermal stability of a gold nanosolid*, *Acta Materialia* **2004**, *52*, 501.

[122] M. A. P. A Jorio, A G Souza Filho, R Saito, G Dresselhaus and M S Dresselhaus, *Characterizing carbon nanotube samples with resonance Raman scattering*, *New Journal of Physics* **2003**, *5*, 17.

[123] R. A. DiLeo, B. J. Landi, R. P. Raffaelle, *Purity assessment of multiwalled carbon nanotubes by Raman spectroscopy*, *Journal of Applied Physics* **2007**, *101*, 064307.

[124] H. Hanping, W. Xinwei, X. Xianfan, *Generalized theory of the photoacoustic effect in a multilayer material*, *Journal of Applied Physics* **1999**, *86*, 3953.

[125] M. Meneghini, L. Trevisanello, C. Sanna, G. Mura, M. Vanzi, G. Meneghesso, E. Zanoni, *High temperature electro-optical degradation of InGaN/GaN HBLEDs*, *Microelectronics Reliability* **2007**, *47*, 1625.

[126] J. Lahann, *Vapor-based polymer coatings for potential biomedical applications*, *Polymer International* **2006**, *55*, 1361.